

DEVELOPMENT OF AN IN SITU SERS BASED METHOD FOR OBSERVATION OF
BIOFILM FORMATION



by
Seda Kelestemur

Submitted to Graduate School of Natural and Applied Sciences
in Partial Fulfillment of the Requirements
for the Degree of Doctor of Philosophy in
Biotechnology

Yeditepe University
2017

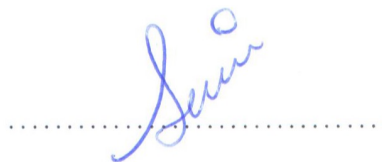
DEVELOPMENT OF AN IN SITU SERS BASED METHOD FOR OBSERVATION OF
BIOFILM FORMATION

APPROVED BY:

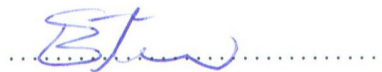
Prof. Dr. Mustafa ulha
(Thesis Supervisor)



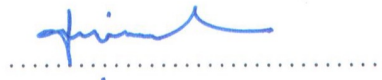
Prof. Dr. Aye Sesin Kocagöz



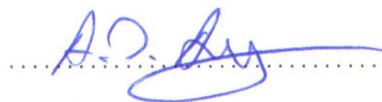
Prof. Dr. Ertuğrul Kılıç



Prof. Dr. Fatma Yeşim Ekinci



Assist. Prof. Dr. Ali Özhan Aytekin



DATE OF APPROVAL:/..../2017



*Dedicated to my father
with all my love...*

ACKNOWLEDGEMENTS

My PhD period is the most special chapter in my story with my gains and losses, which make me grow up in this life.

First, I would like to gratefully thank to my supervisor Prof. Dr. Mustafa Çulha for his support and most importantly for preparing me to academic life. I am also thankful to him for being a great role model for us in creating projects with novel ideas, showing the possibility of being successful without any dependence to anyone else and being a good group leader, who can manage crisis very successfully.

I am also grateful to my thesis monitoring committee members Prof. Dr. Ayşe Sesin Kocagöz and Prof. Dr. Fatma Yeşim Ekinci for their directive ideas throughout thesis work.

I would also like to acknowledge financial support of The Scientific and Technological Research Council of Turkey (TUBITAK) (Project no: 214Z129) during this thesis through the COST action BM1401 European Network on Raman-Based Applications for Clinical Diagnostics (Raman4clinics). Although I was not officially on the project, I had a chance to get involved starting from the development of the project idea.

I am very grateful for being a part of such a good research group and I would like to thank my lovely friends; Gamze Kuku for being very supportive and for helping me with proofreading of my thesis, Zehra Çobandede for her willingness to help, Sevda Mert for her contribution to during brainstormings and her help in statistical analysis, Hande Duru for her assistance and sincerity, Fatma Özen for sharing her knowledge about microbiology, Zeynep Işık, Merve Ercan and Hamide Özaydın for their lovely friendships. I will always miss our talks during lunchbreaks. I also thank to my friend Mine Altunbek, whom I worked together in the same project for long years without any disagreement. And thanks to Ertuğ Avcı, who is one of the person I met when I joined to this group. He was very helpful in every problem I dealt with in laboratory.

I owe you a big thank my husband Taha Keleştemur. You are always full of love, helpful, kind and understanding to me and you are my greatest supporter in this life. And how can I forget about my little Attila Sadri? He has grown up during my thesis project waiting me in front of the laboratory at almost every weekend with well-behaved.

My lovely mother Şermin Demir you deserve the biggest thanks for all your sacrifices. You raised your grandchild with full of love like you did to me. I am a mother now too and I can understand you very well as you said. Thank you my brother Yasin Demir for being one of my best friend who I can share everything with confidence. Although he is my little brother, I have been learning too much things from him with his deep knowledge.

I would also like to thank to my mother-in-law and father-in-law Fazilet Keleştemur and Fahrettin Keleştemur for their support, love and goodness.

My last words are special for my lovely father Sadri Demir, who I fell his absence more deeply in every sunshine. You will be my hero and role model until the end of my life with your personality and goodness. I dedicate my thesis to you and I believe that you can feel my thankfulness. I love you with all my heart.

ABSTRACT

DEVELOPMENT OF AN IN SITU SERS BASED METHOD FOR OBSERVATION OF BIOFILM FORMATION

A biofilm is an assembly composed of microbial cells and extracellular polymeric substances, which provides and supports microorganisms for attach themselves onto a surface irreversibly and protect them from environmental stress conditions. Monitoring the in situ molecular changes during a biofilm formation can provide valuable insights in the fields including medicine, biology and related industrial processes. The conventional molecular and microscopy techniques are time consuming due to cumbersome sample preparation steps and destructive nature. With the aim of better understanding biofilm formation and possibility of detection, in this study, biofilm formation of clinically important microorganisms, *Pseudomonas aeruginosa*, *Staphylococcus epidermidis* and *Candida albicans* were monitored by utilizing surface-enhanced Raman scattering (SERS).

Clinically relevant microorganisms threaten patient health often through biofilm formation on the surface of polymeric medical devices and implants. In this thesis work, the biofilm characteristics of the model microorganisms were identified on agar plates, 2D and 3D poly (methyl methacrylate) substrates and 3D glucose-gelatin scaffolds with the aim of understanding the influence of substrate type on biofilm formation process. The significant concentration changes on carbohydrates, lipids, proteins and genetic materials with increasing incubation time provided information about biofilm formation process. Moreover, the spectral data was attempted to confirm with confocal laser scanning microscopy and scanning electron microscopy analyses. The discrimination of microorganisms was also demonstrated from the SERS spectra using principle component analysis and linear discrimination analysis. A further step was taken in the way to clinical application of the approach by monitoring biofilm formation by using a multi-species sample. In summary, the results present a comprehensive evaluation of the applicability of SERS in clinically relevant biofilm formation with exciting outputs and opportunities.

ÖZET

BIYOFİLM OLUŞUMUNUN GÖZLENMESİ İÇİN YZRS TABANLI IN SITU BİR METOT GELİŞTİRİLMESİ

Biyofilm, mikrobiyal hücrelerden ve hücre dışı polimerik maddelerden oluşan bir bileşimdir. Hücre dışı polimerik maddeler, mikroorganizmaların bir yüzeye geri dönüşümsüz olarak bağlanmasını sağlar ve onları çevresel stres koşullarından korur. Biyofilm oluşumu sırasında moleküler değişikliklerin yerinde izlenmesi, tıp, biyoloji ve ilgili endüstri alanları için değerli bilgiler sağlayabilir. Geleneksel olarak kullanılan moleküler ve mikroskopik teknikler, örnek hazırlama aşamalarının zorluğu sebebi ile zaman alıcıdır ve örnek hazırlama sürecinde biyofilmin yaşayan kaotik sistemini bozmaktadır. Bu çalışmada, biyofilm oluşumunun daha iyi anlaşılması ve tespit edilmesi amacı için klinik olarak önemli mikroorganizmalar olan *Pseudomonas aeruginosa*, *Staphylococcus epidermidis* ve *Candida albicans*'ın biyofilm oluşumu yüzeyde zenginleştirilmiş Raman saçılması (YZRS) ile izlendi.

Klinik açıdan önemli olan mikroorganizmalar, polimerik medikal cihazlar ve implantlar gibi çeşitli yüzeyler üzerinde biyofilm oluşturarak hastaların sağlıklarını tehdit etmektedir. Bu tez çalışmasında model mikroorganizmaların agar plakalarda, 2D ve 3D poli (metil metakrilat) yüzeylerde ve 3D glikoz-jelatin yapı iskeleti üzerinde biyofilm oluşturma süreçleri belirlendi ve yüzey tipinin biyofilm oluşumuna etkisi gösterildi. Spektrumlarda artan inkübasyon süresi ile birlikte karbonhidrat, lipid, protein ve genetik materyallerdeki önemli konsantrasyon değişiklikleri belirlenerek mikroorganizmaların biyofilm oluşum süreci moleküler düzeyde aydınlatıldı. Ayrıca, elde edilen spektral bilgiler konfokal lazer taramalı mikroskobu ve taramalı elektron mikroskobu kullanılarak teyit edildi. Belirlenen inkübasyon sürelerinde biyofilm oluşturan mikroorganizmaların ayrılması, SERS spektrumları kullanılarak temel bileşen analizi ve doğrusal ayırma analizi ile gösterildi. Geliştirilen metodun klinik uygulamalarda kullanılabilmesi için çoklu tür içeren biyofilm örnekleri SERS ile analiz edildi. Sonuç olarak, elde edilen çıktılar SERS tekniğinin klinik önemi olan biyofilmin analizi için kullanılmasının kapsamlı bir araştırmasını ortaya koymaktadır.

TABLE OF CONTENTS

ACKNOWLEDGEMENTS	iv
ABSTRACT	vi
ÖZET	vii
LIST OF FIGURES	xi
LIST OF TABLES	xviii
LIST OF SYMBOLS/ABBREVIATIONS	xx
1. INTRODUCTION	1
1.1. Microorganisms	1
1.2. Microbial Growth	2
1.3. Historical Perspective and Formation of Biofilm	3
1.4. Clinically Relevant Microorganisms and Their Special Cases	6
1.4.1. Biofilm formation of <i>P. aeruginosa</i>	6
1.4.2. Biofilm formation of <i>S. epidermidis</i>	9
1.4.3. Biofilm formation of <i>C. albicans</i>	10
1.5. Biofilm Formation on Surfaces	12
1.6. Influence of Surface Properties on Biofilm Formation	14
1.7. Identification of Biofilm Composition	16
1.8. VIBRATIONAL SPECTROSCOPY	18
1.8.1. Electromagnetic Spectrum	18
1.9. Vibrational Motions of a Molecule	19
1.10. Theory of Infrared Spectroscopy	20
1.11. Theory of Raman Spectroscopy	21
1.12. Fundamental Differences of IR and Raman Spectroscopy	23
1.13. Surface Enhanced Raman Scattering (SERS)	24
1.14. Application of SERS in characterization of microorganisms and biofilms	28
2. OBJECTIVES OF THE STUDY	31

3. MATERIALS AND METHODS	32
3.1. Experimental Design	32
3.2. Chemicals	34
3.3. Microorganisms	34
3.4. Synthesis of Silver Nanoparticles	34
3.5. Preparation of 2D PMMA Substrates	34
3.6. Preparation of 3D PMMA Substrates	35
3.7. Preparation of 3D Glucose-Gelatin Scaffolds	36
3.8. Preparation of Microorganism Samples	36
3.9. Preparation of Microorganisms to Obtain the Background SERS Spectra	37
3.10. SERS Measurements	37
3.11. Data Preprocessing	38
3.12. Statistical Analysis.....	38
3.13. Ultraviolet-Visible Spectroscopy Analysis.....	38
3.14. Transmission Electron Microscopy Analysis	38
3.15. Scanning Electron Microscopy Analysis.....	39
3.16. Confocal Laser Scanning Microscopy Analysis.....	39
3.17. Fourier Transform Infrared Spectroscopy	39
4. RESULTS AND DISCUSSIONS	40
4.1. Characterization of Silver Nanoparticles.....	40
4.2. Characterization of Biofilm Substrates.....	40
4.2.1. Characterization of 2D PMMA Substrates	40
4.2.2. Characterization of 3D PMMA Substrates	42
4.2.3. Characterization of 3D Glucose-Gelatin Scaffolds.....	42
4.3. Background SERS Spectra of Silver Nanoparticles and Microorganisms	43
4.4. Biofilm Formation on Substrates.....	44

4.4.1. Agar Plates	44
4.4.2. 2D PMMA Substrates	58
4.4.3. 3D PMMA Substrates	69
4.4.4. 3D Glucose-Gelatin Scaffolds	79
4.5. Multi-Species Biofilm formation.....	91
4.6. Discrimination of Microorganisms in a Biofilm Structure.....	94
4.7. Reproducibility of SERS Measurements	97
5. CONCLUSIONS AND OUTLOOK	105
REFERENCES	109

LIST OF FIGURES

Figure 1.1. Schematic illustration of an eukaryote and a prokaryote cell and a prokaryotic Gram-positive and a Gram-negative cell	2
Figure 1.2. Microbial growth curve in a close system.....	3
Figure 1.3. The main morphologies of <i>C.albicans</i>	12
Figure 1.4. Biofilm formation phases in a smooth and a rough surface	15
Figure 1.5. The schematic diagram of electromagnetic spectrum	18
Figure 1.6. Possible vibrational modes of a polyatomic molecule	20
Figure 1.7. Raman spectrum of CCl_4	22
Figure 1.8. Schematic diagram of Rayleigh and Raman scattering processes.....	22
Figure 1.9. Representative image of a nonpolar and a polar molecule.....	23
Figure 1.10. Schematic illustration of surface plasmon resonance for a metal sphere.....	25
Figure 1.11. Colorful E-field enhancement contours of silver nanoparticle monomers with different shapes	27
Figure 1.12. Electric field contours for a 30 nm radius silver nanoparticle in vacuum.....	27

Figure 1.13. Comparison of electric field distributions of a single AuNP and nanoparticle dimer	28
Figure 3.1. Schematic diagram of the experimental design.....	32
Figure 3.2. A possible scenario for interaction of AgNPs with biofilm components.....	33
Figure 3.3. Experimental design of preparing a PMMA coated glass slide	35
Figure 3.4. Experimental design of preparing 3D PMMA substrates.....	36
Figure 4.1. The UV-Vis spectrum and TEM image of AgNPs.....	40
Figure 4.2. FT-IR spectra of PMMA and PMMA coated glass slide	41
Figure 4.3. Digital images and SEM images of PMMA coated glass slides	41
Figure 4.4. Digital image and SEM image of a 3D PMMA substrate	42
Figure 4.5. Digital image and SEM image of a 3D glucose-gelatin scaffold.	42
Figure 4.6. SERS spectra of AgNPs	43
Figure 4.7. SERS spectra of <i>P. aeruginosa</i> , <i>S. epidermidis</i> and <i>C. albicans</i>	44
Figure 4.8. SERS spectra of growth media; TSA, NA and SDA.....	46
Figure 4.9. SERS spectra of <i>P. aeruginosa</i> biofilm formation at different cultivation times between 4 and 120 h	48

Figure 4.10. SERS spectra of *S. epidermidis* biofilm formation at different cultivation times between 4 and 120 h.....49

Figure 4.11. SERS spectra of *C. albicans* biofilm formation at different cultivation times between 4 and 120 h50

Figure 4.12. SEM images of *P. aeruginosa* biofilm formation at different cultivation times between 4 and 120 h.52

Figure 4.13. SEM images of *S. epidermidis* biofilm formation at different cultivation times between 4 and 120 h53

Figure 4.14. SEM images of *C. albicans* biofilm formation at different cultivation times between 4 and 120 h54

Figure 4.15. CLSM images of *P. aeruginosa* biofilm formation at different cultivation times between 4 and 120 h.....55

Figure 4.16. CLSM images of *S. epidermidis* biofilm formation at different cultivation times between 4 and 120 h.....56

Figure 4.17. CLSM images of *C. albicans* biofilm formation at different cultivation times between 4 and 120 h57

Figure 4.18. SERS spectra of a 2D PMMA substrate.....58

Figure 4.19. SERS spectra of <i>P. aeruginosa</i> biofilm formation at different cultivation times between 4 and 120 h	59
Figure 4.20. SERS spectra of <i>S. epidermidis</i> biofilm formation at different cultivation times between 4 and 120 h.....	61
Figure 4.21. SERS spectra of <i>C. albicans</i> biofilm formation at different cultivation times between 4 and 120 h	62
Figure 4.22. SEM images of <i>P. aeruginosa</i> biofilm formation at different cultivation times between 4 and 120 h	63
Figure 4.23. SEM images of <i>S. epidermidis</i> biofilm formation at different cultivation times between 4 and 120 h. Scale bars are 10 μ m.....	64
Figure 4.24. SEM images of <i>C. albicans</i> biofilm formation at different cultivation times between 4 and 120 h	65
Figure 4.25. CLSM images of <i>P. aeruginosa</i> biofilm formation at different cultivation times between 4 and 120 h.....	66
Figure 4.26. CLSM images of <i>S. epidermidis</i> biofilm formation at different cultivation times between 4 and 120 h.....	67

Figure 4.27. CLSM images of <i>C. albicans</i> biofilm formation at different cultivation times between 4 and 120 h	68
Figure 4.28. SERS spectra of 3D PMMA substrates incubated with TSB, NB and SDB ...	69
Figure 4.29. SERS spectra of <i>P. aeruginosa</i> biofilm formation at different cultivation times between 4 and 120 h	70
Figure 4.30. SERS spectra of <i>S. epidermidis</i> biofilm formation at different cultivation times between 4 and 120 h.....	71
Figure 4.31. SERS spectra of <i>C. albicans</i> biofilm formation at different cultivation times between 4 and 120 h	72
Figure 4.32. SEM images of <i>P. aeruginosa</i> biofilm formation at different cultivation times between 4 and 120 h	73
Figure 4.33. SEM images of <i>S. epidermidis</i> biofilm formation at different cultivation times between 4 and 120 h	74
Figure 4.34. SEM images of <i>C. albicans</i> biofilm formation at different cultivation times between 4 and 120 h	75
Figure 4.35. CLSM images of <i>P. aeruginosa</i> biofilm formation at different cultivation times between 4 and 120 h.....	76

Figure 4.36. CLSM images of <i>S. epidermidis</i> biofilm formation at different cultivation times between 4 and 120 h.....	77
Figure 4.37. CLSM images of <i>C. albicans</i> biofilm formation at different cultivation times between 4 and 120 h	78
Figure 4.38. SERS spectra of glucose-gelatin scaffolds incubated with SDB, NB and TSB	79
Figure 4.39. SERS spectra of <i>P. aeruginosa</i> biofilm formation at different cultivation times between 4 and 120 h	81
Figure 4.40. SERS spectra of <i>S. epidermidis</i> biofilm formation at different cultivation times between 4 and 120 h.....	82
Figure 4.41. SERS spectra of <i>C. albicans</i> biofilm formation at different cultivation times between 4 and 120 h	83
Figure 4.42. SEM images of <i>P. aeruginosa</i> biofilm formation at different cultivation times between 4 and 120 h	85
Figure 4.43. SEM images of <i>S. epidermidis</i> biofilm formation at different cultivation times between 4 and 120 h	86

Figure 4.44. SEM images of <i>C. albicans</i> biofilm formation at different cultivation times between 4 and 120 h	87
Figure 4.45. CLSM images of <i>P. aeruginosa</i> biofilm formation at different cultivation times between 4 and 120 h.....	88
Figure 4.46. CLSM images of <i>S. epidermidis</i> biofilm formation at different cultivation times between 4 and 120 h.....	89
Figure 4.47. CLSM images of <i>C. albicans</i> biofilm formation at different cultivation times between 4 and 120 h	90
Figure 4.48. SERS spectra of multi-species, <i>P. aeruginosa</i> , <i>S. epidermidis</i> and <i>C. albicans</i> biofilm on agar plates at 48 h incubation time.....	92
Figure 4.49. SEM and CLSM images of the multi-species biofilm.....	93
Figure 4.50. PCA plot and PCs of biofilm formation on agar plates.....	95
Figure 4.51. PCA plot and PCs of biofilm formation on 2D PMMA substrates	95
Figure 4.52. PCA plot and PCs of biofilm formation on 3D PMMA substrates	96
Figure 4.53. PCA plot and PCs of biofilm formation on 3D glucose-gelatin scaffolds	96
Figure 4.54. PC-LDA plots of <i>C. albicans</i> , <i>P. aeruginosa</i> and <i>S. epidermidis</i>	97

LIST OF TABLES

Table 1.1. Degrees of freedom observed in a polyatomic molecule.....	19
Table 4.1. Tentative peak assignments list for SERS spectra.....	45
Table 4.2. CV values of SERS measurements of <i>P. aeruginosa</i> on agar plates.....	98
Table 4.3. CV values of SERS measurements of <i>S. epidermidis</i> on agar plates	99
Table 4.4. CV values of SERS measurements of <i>C. albicans</i> on agar plates	99
Table 4.5. CV values of SERS measurements of <i>P. aeruginosa</i> on 2D PMMA substrates	100
Table 4.6. CV values of SERS measurements of <i>S. epidermidis</i> on 2D PMMA substrates	100
Table 4.7. CV values of SERS measurements of <i>C. albicans</i> on 2D PMMA substrates ..	101
Table 4.8. CV values of SERS measurements of <i>P. aeruginosa</i> on 3D PMMA substrates	101
Table 4.9. CV values of SERS measurements of <i>S. epidermidis</i> on 3D PMMA substrates	102
Table 4.10. CV values of SERS measurements of <i>C. albicans</i> on 3D PMMA substrates	102

Table 4.11. CV values of SERS measurements of <i>P. aeruginosa</i> on 3D glucose-gelatin scaffolds	103
Table 4.12. CV values of SERS measurements of <i>S. epidermidis</i> on 3D glucose-gelatin scaffolds	103
Table 4.13. CV values of SERS measurements of <i>C. albicans</i> on 3D glucose-gelatin scaffolds	104

LIST OF SYMBOLS/ABBREVIATIONS

μl	Microliter
$^{\circ}\text{C}$	Degrees Celsius
Ag	Silver
Al	Aluminium
Au	Gold
C	Carbon
Cu	Copper
g	Gram
H	Hydrogen
h	Hour
kV	Kilovolt
Li	Lithium
min	Minute
ml	Milliliter
N	Nitrogen
O ₂	Oxygen
v	Volume
w	Weight
AAP	Accumulation-associated protein
ADI	Arginine deiminase operon
AFM	Atomic force microscopy
AgNO ₃	Silver nitrate
AgNPs	Silver nanoparticles
AuNPs	Gold nanoparticle
ATR	Attenuated Total Reflectance
CaF ₂	Calcium fluoride
<i>C. albicans</i>	<i>Candida albicans</i>

c-di-GMP	Cyclic diguanosine-5'-monophosphate
CLSM	Confocal Laser Scanning Microscopy
CV	Coefficient variants
ddH ₂ O	Double-distilled water
DNA	Deoxyribonucleic acid
eDNA	Extracellular DNA
EPS	Extracellular polymeric substances
ESI-MS	Electrospray ionization mass spectrometry
FT-IR	Fourier Transform Infrared Spectroscopy
LC	Liquid chromatography
LDA	Linear discrimination analysis
MALDI-MS	Matrix-assisted laser desorption ionization mass spectrometry
NA	Nutrient agar
NB	Nutrient broth
NIR	Near infrared region
NMR	Nuclear magnetic resonance
<i>P. aeruginosa</i>	<i>Pseudomonas aeruginosa</i>
PCA	Principal component analysis
PCR	Polymerase chain reaction
PCs	Principal components
PEI	Poly(ethylenimine)
PEO	Poly (ethylene oxide)
PIA	Polysaccharide intercellular adhesion
PMMA	Poly (methyl methacrylate)
PNSG	Poly-N-succinylglucosamine
pSBMA	Poly (sulfobetaine methacrylate)
RNA	Ribonucleic acid
<i>S. epidermidis</i>	<i>Staphylococcus epidermidis</i>
Sbp	Small basic protein
SDA	Sabouraud 2 per cent glucose agar
SDB	Sabouraud dextrose broth
SEM	Scanning electron microscopy
SERS	Surface-enhanced Raman scattering

sRNAs	Small RNAs
STXM	Scanning transmission X-ray microscopy
TEM	Transmission electron microscopy
TSA	Tryptic Soy Agar
TSB	Tryptic soy broth
UV-Vis	Ultraviolet-Visible



1. INTRODUCTION

1.1. MICROORGANISMS

Microorganisms are single-celled organisms including bacteria, fungi, viruses, protozoa and algae. They are the first entities in living system and they were discovered in 1665 by the renowned scientist Robert Hooke famous in biological studies for his microscopy investigations. In 1684, Antoni van Leeuwenhoek imaged the microorganisms by his simplest microscope. Microorganisms play an important role in the ecosystem and they are also used in many industrial application areas such as prevention of spoilage and providing safety in food, cleaning pollution and producing biofuels [1].

Prokaryotic cells have a simple structure; a cell wall, cytoplasmic membrane, cytoplasm, nucleoid, ribosome and plasmid but they do not have organelles. Archaea and bacteria are the two groups of prokaryotic cells. Their metabolic activities and protein synthesis take place in cytoplasm. Nucleoid is their genetic material, located in cytoplasm. Bacteria are divided into two groups according to their reactions with Gram stains, Gram-positive and Gram-negative. After treatment with the stain, based on their cell wall structures, Gram-positive bacteria appear purple-violet, whereas Gram-negative bacteria look pink [1]. Bacteria cell wall is composed of peptidoglycan, which is a polymer containing sugars and amino acids. Eukaryotes have their DNA in nucleus and their cellular structure is more complex than prokaryotes. Plant and animal cells, algae, fungi and protozoa are the eukaryotic cells. They have membrane-enclosed organelles in their cytoplasm such as nucleus, mitochondria, as well as chloroplasts in photosynthetic cells (Figure 1.1).

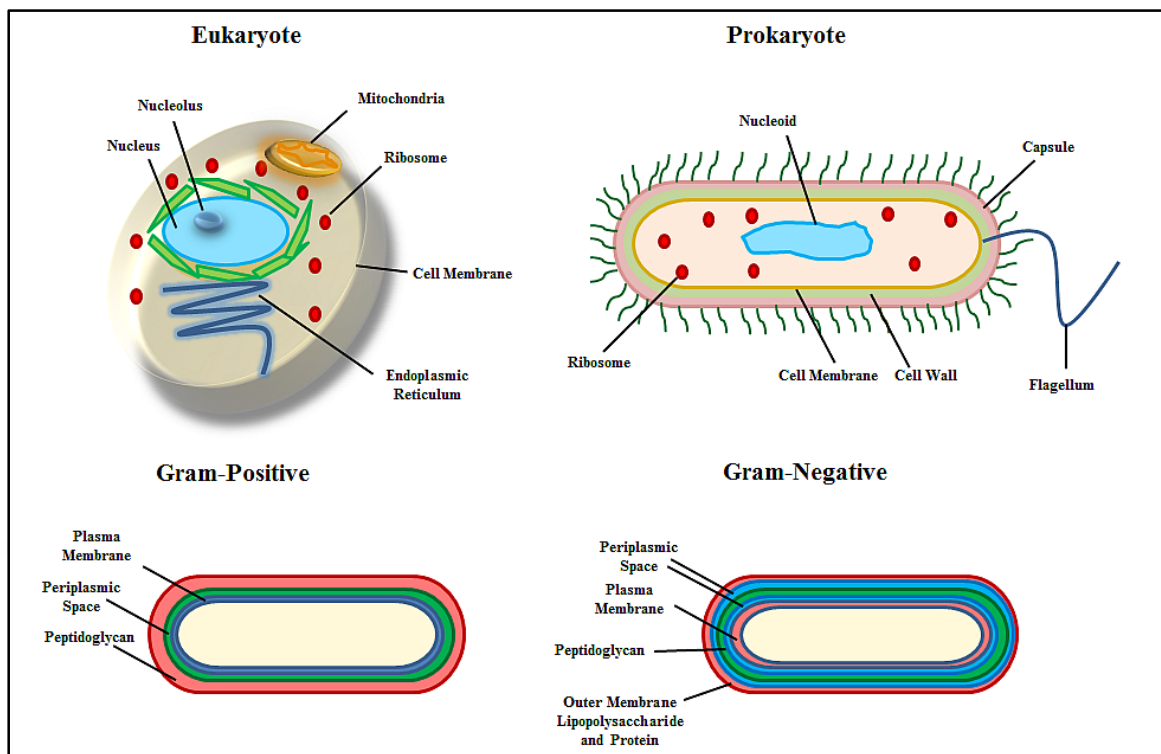


Figure 1.1. Schematic illustration of an eukaryote and a prokaryote cell and a prokaryotic Gram-positive and a Gram-negative cell.

1.2. MICROBIAL GROWTH

Suitable physical and chemical conditions should be established for growth of microorganisms. Temperature, moisture, pH level, oxygen and time are the most important parameters for proliferation. Nutrients in growth media must contain all the elements such as H, C, O₂ and N, which are necessary for the growth of microorganisms. The growth curve of microorganisms has four phases; lag phase, exponential (log) phase, stationary phase and death phase (Figure 1.2). In the lag phase an increase in cell number cannot be observed because microorganisms tend to adapt to the new environmental conditions, where they synthesize new enzymes to use different nutrients for adaptation. Finally, rapid cell division is observed with the end of lag phase. During the log phase, microorganisms begin to grow and divide at the maximum rate. In this phase, the metabolic activities of microorganisms are at their highest level. In the stationary phase population size is constant due to the limited amount of nutrient and soluble oxygen (aerobic organisms) and waste products produced by microorganisms. Eventually, the cell viability tends to

decrease and microorganisms go into death phase with decreasing nutrient and increasing toxic products [2].

Microorganisms can also form biofilms to resist external environmental conditions beside the natural growth cycle. The increase in gene expressions with the biofilm process provides formation of antibiotic resistance and phenotypic changes during colonization of microorganisms. At the same time, the cells can create mutualist life in a closer relationship with each other by forming biofilm shield for themselves with secreted polymeric substances. They can also survive from difficult environmental conditions by increasing their nutrient transport [3].

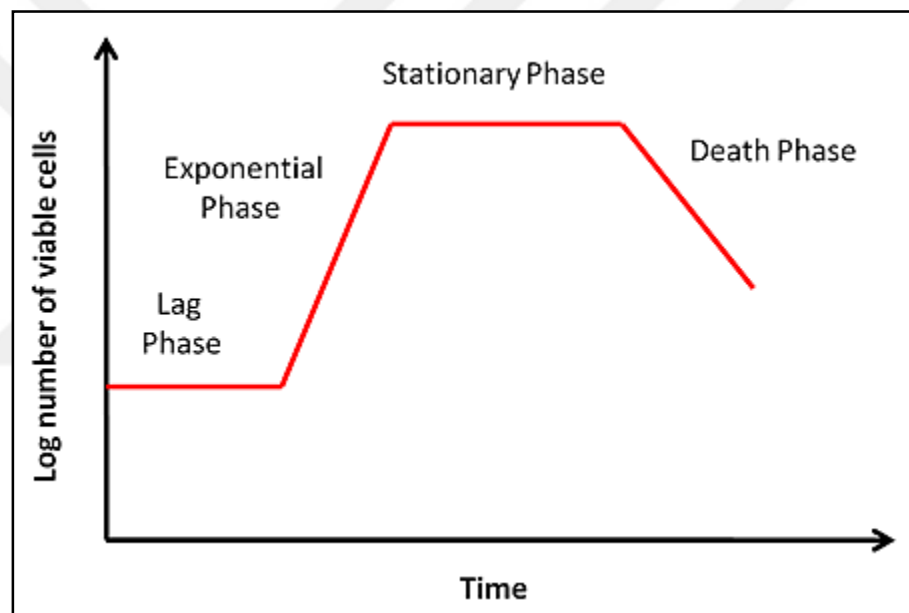


Figure 1.2. Microbial growth curve in a close system [2].

1.3. HISTORICAL PERSPECTIVE AND FORMATION OF BIOFILM

Biofilm is a complex system composed of microorganisms and extracellular polymeric substances (EPS) as a surrounding environment, where the cells adapt for a common life style and behave as a group for fighting with external conditions. Antonie van Leeuwenhoek noticed biofilm on tooth surfaces during his studies in seventeenth century [4]. Heukhelekian and Heller found that microbial growth was enhanced when they were attached to a surface [5]. Zobell assigned the two-step adhesion process of biofilm formation, reversible and irreversible, through investigating the biofilm on surrounding

seawater [6]. During 1960s and 1970s, the heterogenetic structure and chaotic environment of biofilm composition of different microorganisms and EPS were identified using scanning and transmission electron microscopy techniques [7, 8]. Eventually, in 1978 Costerton et al. put forward the theory of biofilm and described the mechanism of biofilm formation with the benefits, which microorganisms gain from this complex system [8]. Significant improvements have been made in the elucidation of biofilm structure with the use of confocal laser scanning microscopy (CLSM) [9]. Since then, biofilm formation has become an interesting study area and the biofilm model was revealed with the clarified microcolonies buried into the EPS matrix surrounded with water channels and is found to provide exchange of nutrients and metabolites between the microorganisms and the aqueous phase, and reduce toxic metabolites from environment [10, 11].

The formation of biofilms is an aggregation of microorganisms embedded in a matrix defined as EPS, which is formed of polysaccharides, lipids, proteins, genetic materials and humic-like substances. These substances are responsible of three-dimensional structure formation of biofilm architecture. The microorganisms also secrete enzymes to alter the content of EPS matrix for adaptation to the limited access to nutrients [12, 13]. The matrix ingredients provide hydrated and durable mushroom shape to the biofilm structure and increase the intercellular interaction and DNA exchange through preserving the microbial community from unfavorable conditions.

The composition of EPS also changes depending on the nature of microorganism. In a Gram-negative bacteria biofilm, the EPS consists of neutral and polyanionic polysaccharides, while in a Gram-positive bacteria biofilm, the EPS formation is cationic. On the other hand, the environmental conditions such as pH, temperature, oxygen and nitrogen levels, also the surface properties affect the composition of a biofilm [4, 14].

Biofilm formation is a complex process and it occurs in five stages according to Palmer and White [15];

- Compromising a surface attached film
- Motion of microorganism on the surface
- Adhesion
- Growth and division of microorganisms on the surface

- Biofilm cell assemble

The initial adhesion between the planktonic cells and the surface occurs reversibly. The microorganisms spread over the surface and flagellas and fimbriaes help to enhance the adhesion by expressing polymeric substances [9]. After the irreversible attachment of microorganisms on the surface, they maintain a common life with increase of the intercellular interaction and they start to grow and form aggregates. The maturation of biofilm composition is observed with the secretion of EPS. Heterogenic structure of biofilm consists of assembled microcolonies, polymeric substances and interstitial voids and channels, which are responsible for the nutrient supply and removal of toxic substances [16].

Biofilms increase genetic diversity by gene transfer during the biofilm formation process [17]. On the other hand, it is also known that antibiotic resistance of microcolonies occur by the up-regulation and down-regulation of a number of genes during biofilm maturation. The differentiation of gene expression is defined in biofilms of *Pseudomonas aeruginosa* (*P. aeruginosa*) with 0.5% up-regulated and 0.5% down-regulated genes [18]. An up-regulation in *algC* gene is observed during the attachment step of *P. aeruginosa* biofilm formation as well, which shows the responsibility of the gene for the adhesion process [19]. The significant increase in the expression of the *icaADBC*, *agrBDCA*, *aap*, and *atle* genes have been assigned to have a major role in medical device and skin colonization related pathogenesis of *Staphylococcus epidermidis* (*S. epidermidis*) [20]. In addition, *SarZ* is a key regulator gene for *S. epidermidis* biofilm and responsible for the virulence of this phenotype [21].

Biofilm formation of *Candida albicans* (*C. albicans*) can be explained in three main steps; attachment and spreading of planktonic cells on the surface, growth and aggregation of the cells and finally formation of pseudohyphae and hyphae concomitant during the maturation of biofilm. *KEMI*, *MDS3*, *NUP85* and *SUV3* are unconnected genes responsible for *C. albicans* biofilm formation through hyphal formation [22].

Quorum sensing is a chemical communication system for microorganisms. They produce chemical signals, called autoinducers, which diffuse across the cell membrane. When these signal molecules reach threshold concentration, they bind to the receptors on bacteria to lead the gene regulation [23]. Autoinducers differ depending on microorganism types; a

Gram-negative bacterium produce acylated homoserine lactones, a Gram-positive bacterium produce autoinducing peptides and also autoinducer-2. A furanosyl borate diester is produced by both a Gram-positive and a Gram-negative bacterium [24]. *C. albicans* is the first identified eukaryotic microorganism, which secreted quorum sensing molecules. Tyrosol is one of the main quorum sensing molecule secreted by *C. albicans* in the early and intermediate stages of biofilm formation. In addition, farnesol has a critical role in the assembly of yeast cells attached on a surface at later phases of biofilm process [25]. Quorum sensing is also essential for production of virulence factors and growth of biofilm. Microorganisms in biofilm formation provide high resistance to antimicrobial agents because EPS components act as a shield [17]. Compounds which suppress the quorum sensing processes are called quorum sensing inhibitors. They can inhibit; the signal molecule, signal production or the receptor. The antimicrobial resistance of the microorganisms in biofilm can be reduced by suppressing the biofilm formation by using quorum sensing inhibitors, so the therapy of the bacterial infections may be achievable with short-term usage of growth-inhibitory agents [24].

1.4. CLINICALLY RELEVANT MICROORGANISMS AND THEIR SPECIAL CASES

Clinical biofilm infections either do not respond to antibiotic treatments or recur after a long-term treatment. These infections risk patients with life-threatening diseases, especially in the intensive care units. Clinically relevant microorganisms tend to attach, form microcolonies and disperse on medical devices as well as on human skin and mucosa membranes. *P. aeruginosa*, *S. epidermidis* and *C. albicans* are clinically the most threatening microorganisms due to the difficulties in fighting with the infections they are responsible for.

1.4.1. Biofilm formation of *P. aeruginosa*

Being a Gram-negative bacterium, *P. aeruginosa* is an opportunistic pathogenic bacterium in clinic causing cystic fibrosis [26]. *P. aeruginosa* threatens human health through forming biofilm in patient's lung, which protects bacteria with a polymeric biofilm shell

against medical treatments [27]. These biofilms are also observed on indwelling medical devices and lenses [28].

Basically, *P. aeruginosa* biofilm formation can be examined in four main stages; attachment, motility, maturation and dispersion to the new host surfaces [29]. Although it is not obligatory in all cases, flagella and type IV pili play an important role in the adhesion process [30, 31]. The extracellular components are also very important during attachment such as cup fimbriae [32], Psl polysaccharide [33, 34] and extracellular DNA (eDNA) [35]. Motility is the stage, which the microorganisms grow into colonies and form the main shape of biofilm. Flagella provide the motility of *P. aeruginosa* and formation of mushroom shape in liquid media, while type IV pili is only responsible for the production of appendages on solid surfaces. Maturation of biofilm is observed with the formation of extracellular polymeric shell on the microorganisms during accumulation, which is involved in adhesion, inter-cellular and intra-cellular interactions and genetic diversity [33, 34, 36-38]. Polysaccharides, eDNA, proteins and lipids are the main ingredients of the extracellular matrix, which may change due to the environmental conditions [39]. Polysaccharides are very important in adhesion, growing into microcolonies and assembling of the microorganisms on the solid surface [40-43]. Furthermore, the type of secreted polysaccharides are the factors to determine the type and pathogenicity of *P. aeruginosa* biofilms. Alginate, Psl and Pel are the major polysaccharides detected in *P. aeruginosa* biofilm structure [44].

The phenotypes of *P. aeruginosa* can be investigated in two categories; non-mucoid and mucoid strains during evolution [45]. Mainly, alginate synthesis is observed in mucoid strains, which is formed of non-repetitive monomers of β -1,4 linked L-galuronic and D-mannuronic acids. Alginate production is very important during accumulation of biofilm because it protects microorganisms through eliminating the free radicals, which are produced by infected host cells in very dangerous clinical cases of cystic fibrosis. It also provides stability, preserve the architecture of the biofilm structure and supply water to the microorganisms based on its water binding property [16, 26, 46-48]. Psl is a polysaccharide composed of mannose and galactose that allows planktonic non-mucoid *P. aeruginosa* cells to adhere on solid surfaces and hold together with the polymeric ingredients as a scaffold [49, 50]. It is known that *P. aeruginosa* has an ability to form biofilm on air-liquid interface of the culture, where Pel, a glucose-rich polysaccharide, is

necessary for accumulation of biofilm [44]. The evolution of non-mucoid strains to mucoid cells is possible during the biofilm formation. However, this evolution does not increase the production of alginate, but alter the carbohydrate content of the matrix during the conversion [44].

eDNA is also essential in *P. aeruginosa* biofilm formation. It starts to produce eDNA in high levels from the initial stages of the formation, especially during proliferation to the formation of mushroom shape but the biofilm matrix contains low eDNA compared with other gradients at the maturation phase [51]. It is also demonstrated in a study that alginate and eDNA protects the microorganisms like a shell and prevent penetration of antibiotics [52].

The main roles of proteins in a biofilm matrix include; surface attachment, providing biofilm structure stability and enabling molecular interactions in the matrix [53]. CdrA is the most well-known protein, secreted by *P. aeruginosa*, has a carbohydrate-binding property and helps aggregation of the cells through binding with Psl polysaccharide [53]. Galactose specific lectin LecA and the fucose specific lectin LecB, cup fimbriae are the other proteins expressed in the beginning of adhesion process until proliferation [32, 54-56].

Rhamnolipids are composed of rhamnose and lipid moieties, which are bound with *O*-glycoside [57]. Rhamnolipids are generally produced in the maturation phase and it is important in formation of mushroom shape with motility [58, 59]. They also promote the dispersion of daughter cells [60].

Not only the polymeric substances but also the environmental conditions cause dispersion of the cells such as carbon source [12], nutrient availability [61], nitric oxide content [62], and lack of iron [63]. Recent studies demonstrated the importance of quorum sensing molecules on biofilm formation [38, 64]. In *P. aeruginosa* biofilms, quorum sensing signaling promote the expression of eDNA and rhamnolipids [35, 59, 60, 65]. In addition, beside the quorum sensing signals, it is demonstrated that secondary messenger cyclic diguanosine-5'-monophosphate (c-di-GMP) and small RNAs (sRNAs) are responsible for accumulation of biofilm formation through stimulating expression of EPS components [66, 67].

1.4.2. Biofilm formation of *S. epidermidis*

S. epidermidis, a Gram-positive bacterium, is a pathogenic microorganism causing nosocomial infections through forming biofilm on indwelling catheters and implanted devices. This bacterium also express coagulase, an enzyme that facilitates clot formation in blood, regulate biofilm formation on human skin and mucosa membranes. Although *S. epidermidis* secretes a few virulence factors, it has a superior ability to adhere on polymeric surfaces through protecting itself with an extracellular polymeric shell [68]. Primary adhesion of the microorganisms on the surface can occur in two main ways; direct attachment and binding with host-derived matrix proteins. The hydrophobic property of the surface is promoting the direct attachment process [69]. On the other hand, host-derived matrix proteins are playing an important role for the primary attachment. Fibrinogen-binding protein SdrG, Aas1 and Aas2 are the main identified matrix proteins covalently binding to the surface, which provide a very strong adhesion [70-73]. SdrH is one of the proteins binding on the surface with non-covalent interaction [74].

The proliferation of the adhered cells is observed in the second step of biofilm formation. Polymeric carbohydrates and proteins are responsible for the regulation of cell-cell interaction and formation of cell aggregates. Although their mechanisms are not identified clearly, it has been found that accumulation-associated protein (AAP), polysaccharide intercellular adhesion (PIA) and poly-N-succinylglucosamine (PNSG) are the defined polysaccharide and proteins that have a significant role on accumulation of intercellular adhesion [75-77]. Both PIA and PNSG are secreted from the same genetic locus *ica* consisting of *icaA*, *icaD*, *icaB* and *icaC* [78, 79]. It is also known that PIA has an additional role in controlling the hemagglutination activity, providing three-dimensional architecture of biofilm formation, blocking the neutrophils and increasing antibiotic resistance [80, 81]. Poly- γ -DL-glutamic acid is produced in PIA-dependent *S. epidermidis* biofilm to develop a resistance to the host immune system [82]. Proteinaceous factors (Bhp, Aap and Embp), teichoic acids and eDNA are also isolated from a mature *S. epidermidis* biofilm [83]. Protein expression is observed significantly increased throughout all the regulation steps of biofilm formation. A fibrillary protein Aap and Bhp are specific proteins responsible for initial adhesion and have a role during early maturation phase [84].

The *S. epidermidis bhp* gene is responsible for the production of a protein, which is responsible for accumulation of biofilm formation in PIA deficiency [85].

Development of a survival mechanism during biofilm formation is the main purpose of microorganisms during maturation of biofilm formation. Arginine deiminase operon (ADI) is up-regulated during maturation phase to survive under external conditions and regulate amino acid metabolism [86, 87].

1.4.3. Biofilm formation of *C. albicans*

C. albicans is also a very pathogenic fungus causing life-threatening infections related with the indwelling medical devices. The biofilm formation process of *C. albicans* can be inspected in three major phases; early phase occurs in the first 12 hours, intermediate phase can be observed between 12-30 hours and maturation phase approximately observed between 38-72 hours [88].

The composition of EPS excreted during biofilm formation changes based on environmental conditions such as nutrient availability, temperature and pH [89]. In general, the main components of the biofilm matrix are polysaccharides, proteins, lipids and nucleic acid and *Zap1* is responsible for the regulation of the matrix [90]. Polysaccharides constitute approximately one-fourth of the *C. albicans* biofilm matrix including arabinose, mannose, glucose, and xylose [91]. The mannan polysaccharides are mostly identified in structure of α -1,2 and α -1,6 branched and also in linear β -1,6 glucans form, which can also be found as a highly-branched structure in cell wall. In addition, β -1,3 glucan is evenly distributed throughout the whole matrix [91, 92]. Protein richness of the matrix is very high, about half of the matrix, and proteins have an important role in regulation of the biofilm process. Glycoproteins, heat shock proteins and secretion-signal-less proteins are the main clarified proteins [91]. The main regulator of biofilm formation is *Bcr1* and activates the cell wall proteins Als1, Als3, and Hwp1 all of which are responsible for adhesion in the beginning of the biofilm formation [88, 93, 94]. Nearly 15% of the biofilm matrix are detected to be formed of lipids containing glycerolipids and sphingolipids. Oleic and linoleic acids, glycerolipids. palmitoleic, palmitic, stearic, and myristic acids are the main fatty acids produced by *C. albicans* and also ergosterol is

identified as a sterol [91]. eDNA is also defined as a main component of biofilm composition responsible for the structure formation [95].

Biofilm matrix components have important roles for adhesion, colonization, assembly and also, they provide mechanical strength to biofilm structure. It is demonstrated that β -1,3 glucan and eDNA are involved in development of antibiotic resistance of *C. albicans* [89, 96, 97]. Glucans have a special role to block neutrophil attacks at the same time [98]. After maturation of biofilm formation, the cells tend to release and disperse on new host surfaces with expression of the regulators *Nrg1* and *Ume6*, the molecular chaperon Hsp90 and the cell wall protein YWP1 [99-103].

The heterogenic composition of *C. albicans* biofilm includes several cell types according to morphological alterations. Morphological change is related with virulence and observed in many pathogenic fungus species. The proper morphologies of fungus can be clarified in main four types; planktonic yeast cells, pseudohyphae, true hyphae and chlamydo spores as seen in Figure 1.3 schematically [104]. In pseudohyphal morphology, yeast cells are attached end-to-end longitudinally and observed in an ellipsoidal shape. Conversely, in true hyphae, the cells are arranged in parallel with the pores on their septum that provide cell-cell interaction [105, 106]. There are main differences between pseudohyphae and hyphae in their life cycles. The first obvious difference is observed in the forms of division. In pseudohyphae and planktonic cells, the division occurs across the mother-bud neck area, while in true hyphae, it takes place in the germ tubes. Furthermore, the hyphal filaments are not branched as pseudohyphae because the germ tube formation is observed before the G1/S transition, different from the general cell cycle, and also the hyphal cells remain stable in the G1 phase until the amount of their cytoplasmic mass is ready for the second cycle of division [106-109]. The last form of the coevolution that is observed after hyphal formation is chlamydo spores. This formation is rarely encountered in clinic infections with its oversize compared to the other forms of *C. albicans* under nutrient shortage [110-112]. It is known that hyphal formation enhances the virulence of *C. albicans*. The filament formation help the cells to penetrate and branch in and between the host cells. It can proliferate very easily on the host surface by damaging the macrophages and neutrophils [113-115].

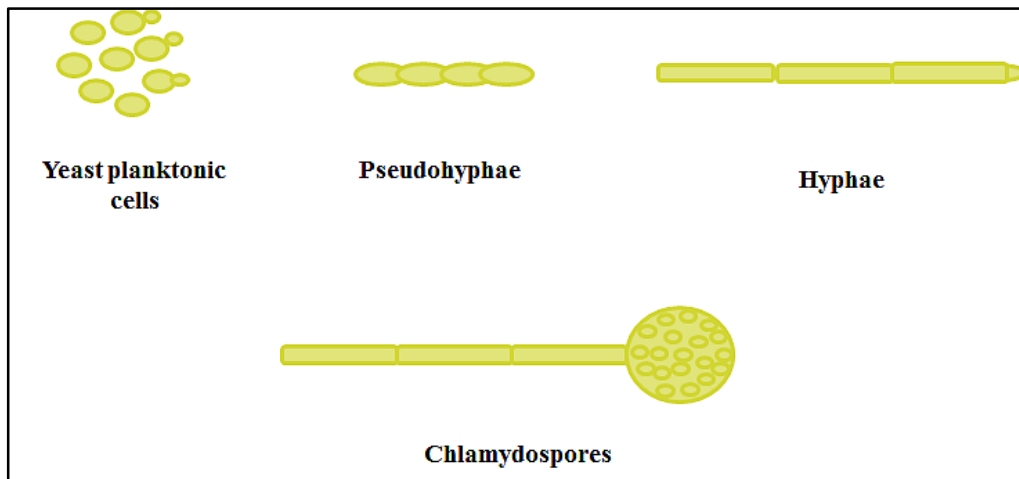


Figure 1.3. The main morphologies of *C. albicans*.

Identifying the relationship between filament formation and virulence is a very interesting research area. Although it is demonstrated that there are many genes playing role in both the morphology and virulence process such as *HGCI*, secreted aspartyl proteinase (*SAP*) gene family (*SAP4*, *SAP5*, and *SAP6*), *SOD5* and *HYR*, there are several genes responsible for virulence but are not related with coevolution, which can be listed as *ALS3* and *HWP1* [116-120]. *UME6* is defined as a specific gene regulating pseudohyphal and hyphal formations, which is not secreted during cell growth. Pseudohyphal formation is observed in low expression of *UME6*, while hyphal cells are commonly identified in high expression of *UME6*, which demonstrate that the morphological differences not only depend on the environmental conditions [121]. It may be suitable to make the inference that pseudohyphal forms show low virulence, while hyphal forms are more pathogenic. The most important point is that although pseudohyphal seems as an intermediate cell between planktonic cell and hyphae, it conserves its morphology during the evolution and observed correlated with low expression of virulence genes so we can also conclude that these two forms can be two alternative states [104].

1.5. BIOFILM FORMATION ON SURFACES

Biofilms can be formed by microorganisms on several surfaces such as aquatic systems, living tissues and medical devices. Marine ecosystem is very important in terms of hosting many different life forms. This ecosystem can provide all the necessary conditions for microorganisms to form biofilms. The microorganism communities can easily attach and

proliferate on the solid surfaces as microcolony aggregates [122]. Biofilm diversity depends on nutrient availability, salinity and temperature of the aquatic environment, light and intracellular interaction between species as well as predation [123]. The marine biofilms increase formation of larvae from sessile invertebrates through providing nutritious surfaces, which are coated with EPS [123]. On the other hand, these biofilms cause serious contamination and economic problems in fishery and maritime, oil and gas extraction and water industries, which is defined as biofouling. The waste products of microorganisms and polymeric films on the surfaces decrease the operation efficiency of vessels in marine industry and prevent the flow on the oil and gas pipelines. Industrial biological pollution causes very serious financial losses, thus has led to the implementation of yield increasing studies. Biofilms in aquatic environment also contaminate the water bodies and disrupt the ecological balance [124].

Living-tissue biofilms could be identified with the development of microscopy techniques and they were defined as one of the main effect of human infections [125]. The term of 'mucosal biofilm' was first introduced to the literature by Garth Ehrlich and his friends [126, 127]. Pulmonary infection is one of the most common infection originating from biofilms and *P. aeruginosa* cause cystic fibrosis [128]. Living-tissue biofilms can also be observed on ear and nose mucosa, throat, urinary tract and vaginal mucosa, which appear as chronic otitis, chronic tonsillitis, cholesteatomas, sinusitis and urethritis [129-133].

Medical devices are very suitable environments for biofilm formation by microorganisms. The medical device-related biofilms can be formed of single-species or multi-species of microorganisms depending on the location where the devices are placed in the body and the duration time. These biofilms are observed commonly on prosthetic heart valves, central venous catheters, urinary catheters, contact lenses, intrauterine devices and dental unit water lines [134]. The biofilms observed on implanted prosthetic heart valves or surrounding tissue are one of the main factor caused serious infections in patients [135]. It is defined that the microorganisms can easily attach and colonized on the sewing cuff fabrics of these valves [136]. *Streptococci*, *enterococci*, *Staphylococcus aureus* (*S. aureus*), Gram-negative *coccobacilli* and fungi biofilms are generally identified in these valves [137]. The devices interacting with the circulating blood in the body provide suitable attachment surface surrounded with proteins and proper colonization area with the nutrient richness. Central venous catheter is one of such devices and *S. epidermidis*, *S. aureus*,

P. aeruginosa and *C. albicans* are common microorganisms that attach and disperse on these devices [138, 139]. Single-species biofilm formation of *P. aeruginosa*, *S. epidermidis*, *C. albicans*, *Enterococcus faecalis* and *Escherichia coli* is observed in urinary catheters, which are made of silicon and latex with and open or closed system. Open systems are always a potential for microorganism localization and infections occur in as soon as four days [140]. The raw materials used in the production of medical devices have also a decisive influence on biofilm formation. Poly (methyl methacrylate) (PMMA) is used in production of hard contact lenses and the microorganisms have a great interest to attach on these hydrophobic surfaces [141]. The biofilm of several microorganisms such as *S. epidermidis*, *S. aureus*, *C. albicans* were defined on intrauterine devices composed of polyethylene [142, 143]. However, dental unit water lines are not implanted devices, the tubings that are responsible for the water supply cause infections through biofilm formation [134].

1.6. INFLUENCE OF SURFACE PROPERTIES ON BIOFILM FORMATION

Biofilm formation on solid surfaces such as medical devices and aquatic systems cause significant health and economic problems as mentioned above. The ideal conditions for the attachment process and proliferation of microorganisms are the interface between the aqueous media and the host surface [134]. The characteristics of the solid surface are the determining factors for the attachment step of the biofilm formation such as surface charge, surface energy, topography and roughness, and the chemical property of the surface [144]. The microorganisms produce extracellular substances depending on the physicochemical properties of the solid surface [145]. Electrostatic interaction between a microorganism and a surface is the first demonstrated factor affecting the attachment. Most of the bacteria in the environment are negatively charged and they can attach and assemble on a positively charged surface easily [146, 147]. Negatively charged surfaces prevent the interaction and then flagella and pili take the control and provide adhesion of microorganisms [148]. However, in static biofilm systems, the dead cells coat the solid surface area and block the electrostatic interaction. Thus, surface charge becomes a less important factor for adhesion [144].

The surface energy has an important role in adhesion of microorganisms. It is demonstrated that low-energy hydrophobic surfaces are much more preferred compared to high-energy hydrophilic surfaces [149]. In addition, the attachment occurs very quickly on low-energy surfaces [150]. On the other hand, metallic and glass surfaces reduce the attachment efficiency of microorganisms due to the surface tension [151]. In addition, the attachment of microorganisms on a non-polar surface can be also promoted with higher surface tension of bacteria cell wall than the aqueous media [152]. Different from the other bacteria, *S. epidermidis* is also widely forms biofilm on hydrophilic human skin and mucosa membranes [153].

Surface topography influence the adhesion of microorganisms. Roughness of a surface provide a large surface area for initial attachment and assembly of the microorganisms during the growth phase [154]. The representative image of biofilm formation on a smooth and rough surface is given in Figure 1.4.

The alteration in surface chemistry of the substrate is a good strategy to control the biofilm formation [154]. The charge, surface energy and topography of the surface can be changed with modifications to obtain smart surfaces to reduce bacterial attachment [144].

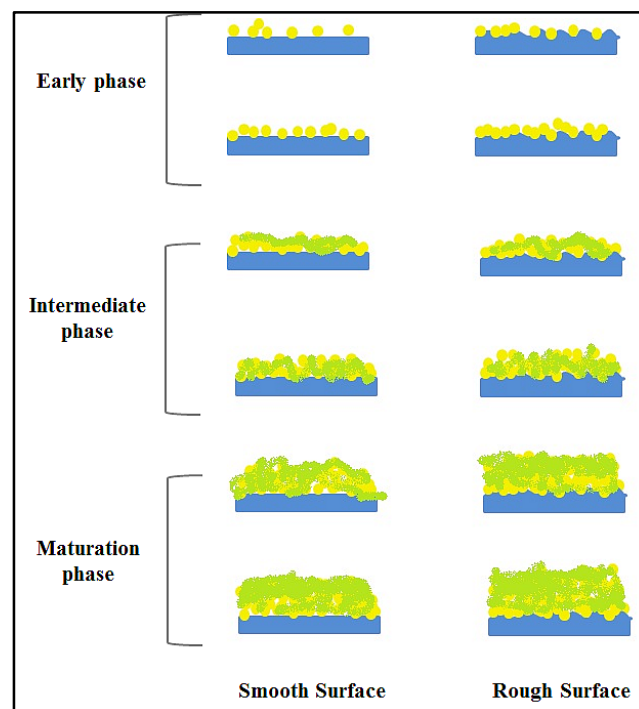


Figure 1.4. Biofilm formation phases in a smooth and a rough surface.

Epstein et. al. produced a smart surface with Teflon membranes recently, which reduced bacterial attachment significantly [155]. Many polymers are also used to prevent the attachment such as dextran, [156] poly(ethylene oxide) (PEO), [157] poly (ethylenimine) (PEI) [158, 159] and poly (sulfobetaine methacrylate) (pSBMA) [160].

1.7. IDENTIFICATION OF BIOFILM COMPOSITION

Identification of biofilm composition is very important to clarify the interaction between environment and microbial growth and also for understanding the molecular dynamics of biofilm's own chaotic system. Biofilm analysis can be performed with microscopic, spectroscopic and molecular techniques [161]. Improvements in analytical techniques have greatly contributed to the elucidation of the biofilm structure.

Microscopy is one of the pioneering techniques used to analyze the biofilm structure. CLSM gave the opportunity to monitor the biofilm structure and dynamics during the accumulation stage [162, 163]. Characterization of the three-dimensional architecture of biofilm composition is possible by using specific fluorescent dyes [164]. Combinations of the microscopy techniques allow obtaining detailed information as demonstrated in a study of Strathmann et al., where they combined epifluorescence microscopy with CLSM and monitored carbohydrate distribution in extracellular matrix [165]. On the other hand, in these techniques, sample preparation steps are exhaustive. Specific dyes use for staining the sample brings additional costs. The assembly of a biofilm structure on a solid surface can be examined with scanning electron microscopy (SEM) and transmission electron microscopy (TEM) after a fixation procedure, which disturb the living system of a biofilm. Although the distribution of the cells and the polymeric matrix can be monitored excellently, these microscopy techniques are not able to monitor living biofilm structure [166]. The other important microscopy technique is scanning transmission X-ray microscopy (STXM), which is extensively used in mapping biofilm composition without using a probe and also with reduced radiation damage on sample. STXM is used to monitor not only the polymeric substances but also allowed to view metal distribution but errors in reference spectra and absorption saturation limits use of the technique [161]. Atomic force microscopy (AFM) is the most general technique used to get information from the depth of the surface topography, this feature allows to display the distribution of

the polymers [167]. However, low scanning speed is the main disadvantage of the technique that is time consuming in characterization of large areas of a heterogenic biofilm structure. Lawrence et al. showed the power of combining the STXM, CLSM and TEM techniques to obtain detailed information about the biofilm structure [168].

Nuclear magnetic resonance (NMR) is a very advantageous technique to obtain structural information from the substances in a biofilm matrix [169-171]. Although the technique gives opportunity to acquire information *in situ* from a biofilm, it is not suitable for characterization high molecular weight molecules and also interpretation of the obtained data can be very complex [172]. Separating EPS from the biofilm matrix is another most preferred method for characterization of the components. Extraction with centrifugation or using chemical additives, solid phase extraction with liquid chromatography (LC) and field-flow fractionation as new approaches are the main techniques used in several studies [173]. Identification of biofilm-associated genes of a microorganism can be carried out using molecular techniques as well as analytical techniques. Combination of the widely used molecular techniques, gel electrophoresis and polymerase chain reaction (PCR), with microscopic and spectroscopic techniques allowed to reveal gene regulation profile during biofilm formation [174-177]. Understanding the polysaccharide, protein and lipid profile in a biofilm can be also achieved by separating the matrix with a chromatography column and identification with a sensitive and high technology mass spectroscopy methods such as matrix-assisted laser desorption ionization mass spectrometry (MALDI-MS), electrospray ionization mass spectrometry (ESI-MS) or nano-ESI-MS, ESI-tandem MS, ESI-MS-MS and LC-MS-MS [178-180]. However, MS based techniques are destructive, expensive and time consuming.

In addition to the techniques mentioned above, the vibrational spectroscopic techniques are used to get information about the biofilm structure in molecular level. Infrared and Raman spectroscopies are vibrational spectroscopy techniques used as complementary to each other to acquire spectral information from the biofilm structure. Although infrared spectroscopy (IR) is widely used for characterization of biofilm, the interference from water limits its use in hydrated biofilm composition [181-183]. The spectral –OH band attributed to water suppress the other characteristic bands of the ingredients in a biofilm [184]. On the other hand, Raman spectroscopy is a preferable technique for detection and identification of planktonic cells and chaotic biofilm structure. Besides this, the technique

has advantages such as easy sample preparation and limited influence from water and is widely used in biofilm characterization [185-189]. One of the main handicap limits the usage of Raman is obtaining weak signals. It is known that using high laser power and long exposure time can enhance the scattering but it can damage the molecules. The discovery of enhancement effect of metals revealed surface-enhanced Raman scattering (SERS) that brings new approaches for characterization biological and non-biological molecules without any weak scattering problem [206-207].

1.8. VIBRATIONAL SPECTROSCOPY

1.8.1. Electromagnetic Spectrum

Spectroscopy can be basically defined as the field of study where interaction of the electromagnetic radiation with matter is studied [190]. The schematic diagram in Figure 1.5 shows the representative energy absorption with frequency. The longer wavelength has lower energy and cause molecular rotation and vibrations as observed in microwave and infrared regions, while shorter wavelengths such as Ultraviolet-Visible (UV-Vis) and X-ray, the most energetic regions, elevate the electron to higher energy states and remove the electron from the orbit of an atom.

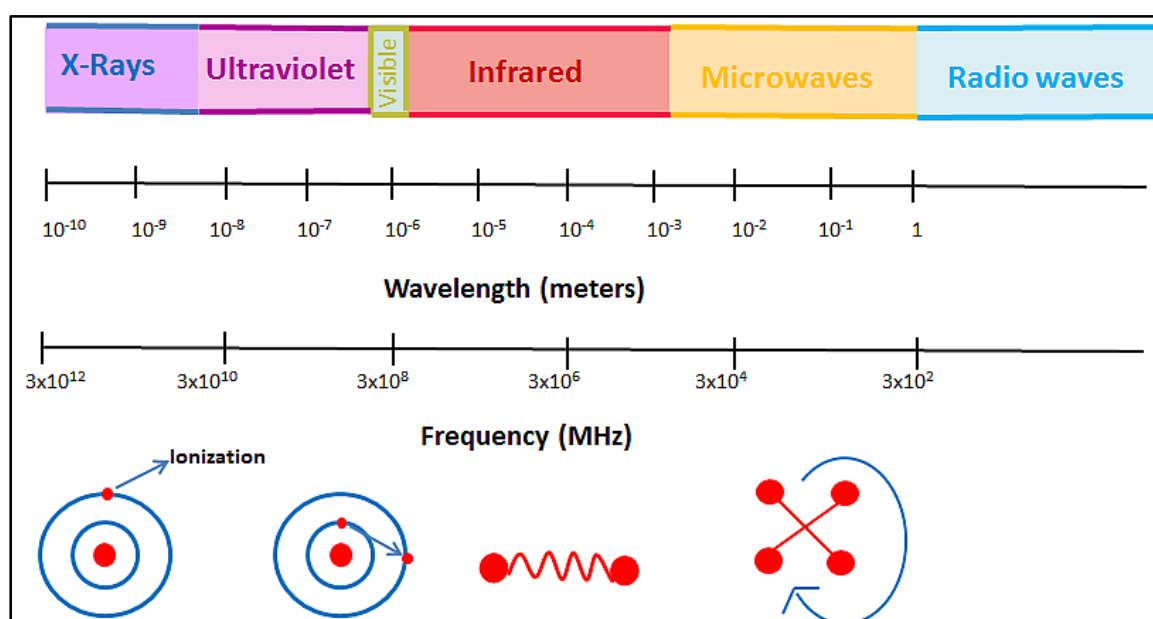


Figure 1.5. The schematic diagram of electromagnetic spectrum.

IR and Raman spectroscopy are the two complementary techniques based on the vibrations of atoms. IR is a vibrational technique based on absorption of the incident light, while Raman spectroscopy is correlated with the inelastic scattering of photons [191]. IR and Raman spectroscopy are used to identify and characterize the chemical structure of a sample, which has a fingerprint feature [192].

1.9. VIBRATIONAL MOTIONS OF A MOLECULE

Number of atoms in a molecule is the decisive factor for the vibrational freedom. The motions of atoms in a molecule are dependent on each other due to their connection. In a diatomic molecule, the vibrational freedom can be calculated as one, while in polyatomic molecules with N atoms display $3N$ degrees of freedom, which is shown in the table adapted from Stuart et. al at Table 1.1 [193].

Table 1.1. Degrees of freedom observed in a polyatomic molecule.

Degrees of Freedom	Linear	Non-linear
Translational	3	3
Rotational	2	3
Vibrational	$3N-5$	$3N-6$
Total	$3N$	$3N$

Vibrations can cause alterations in both bond length and bond angle and these motions are known as stretching and bending, respectively. Stretching can be observed as symmetrically and asymmetrically, while bending types can be listed as in-plane bending vibrations; deformation, rocking and out-of-plane; wagging and twisting as seen in Figure 1.6.

Vibrational spectroscopy can be used in characterization complex biological molecules such as lipids, proteins and nucleic acids. Most significant vibrations observed in lipids are

CH₂ and CH₃ symmetric and asymmetric stretching, CH₂ bending, asymmetric deformation of CH₃, and C=O stretching. Also, PO₂⁻ symmetric stretching is observed in phospholipid groups. C=O stretching, C–N stretching, N–H stretching, O–C–N bending and C–N torsion are the much intense vibrations related with the amide groups of proteins. Nucleic acids contains sugar, base and phosphate groups and vibrations in purine and pyrimidine bases, between a base and the sugar groups and also in sugar-phosphate chain are the most observed intense modes [193].

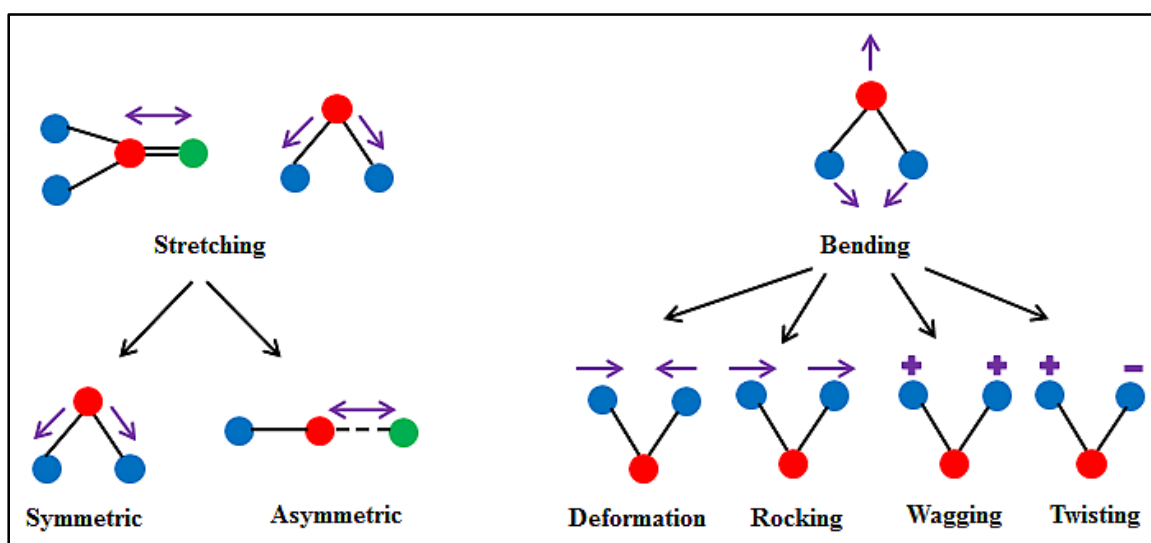


Figure 1.6. Possible vibrational modes of a polyatomic molecule.

1.10. THEORY OF INFRARED SPECTROSCOPY

The principle of IR spectroscopy is based on absorption of a radiation, which cause dipole moment change in a molecule during the vibrational motion. The energy can be absorbed when the fields of dipole moment and electromagnetic radiation comes in resonance, which then results in the vibrational fluctuations of a molecule. The structure of a molecule can be easily elucidated by the help of the spectra obtained from IR measurements. The bands observed in the spectrum indicate group frequencies of specific parts of the molecule. The region of IR is classified as near IR, mid IR and far IR. The absorptions in mid-infrared region are observed between 4000–400 cm⁻¹. It is known that each band in the spectrum represent band deformation, stretching or bending motions. The combinations and overtones of the stretching bands are observed in the near-infrared area between 13000-4000 cm⁻¹. Although the far-infrared region 400-100 cm⁻¹ gives limited information

about the molecular structure compared to the other regions, the heavy atom and crystal lattice vibrations can be observed clearly [193].

1.11. THEORY OF RAMAN SPECTROSCOPY

As mentioned earlier, spectroscopy is the study of interactions between light and material. The photons can be absorbed or scattered by the molecule or they can pass through the molecule. The Raman scattering process is based on an inelastic collision between photons and molecules [194]. When a ray of light interacts with a molecule, the electric field of the light influences the electron cloud of a bond and a dipole moment is induced on the bond. Scattering is associated with re-emission of light while the bond returns its initial condition after the instantaneous disruptions present on the distribution of electrons around the bond. Bond activity upon scattering depends on the distribution tendency of electrons which called “bond polarizability”. The polarization instead of change in dipole moment is essential for observing a Raman shift at scattered light [195]. The theory of scattering with change of light frequency was first suggested by Smekal in 1923 [196]. The difference in visible region wavenumbers of scattering and incident radiation was observed by Raman and Krishan and then Landsberg and Mandelsam in 1928 [197, 198]. In Figure 1.7, a representative spectrum of CCl_4 is given, where difference in wavenumbers upon interaction with the incident light were plotted. The difference of wavenumbers depends on the chemical structure of a molecule, which is responsible for scattering. There are three types of scattered light; Stokes scattering, anti-Stokes scattering and Rayleigh scattering. The wavenumber difference of Rayleigh scattering is the same with the wavenumber difference of incident radiation and the intensity of Rayleigh scattering is higher than the intensities of other scattering photons. Stokes radiation occurs at longer wavenumber and at lower energy but anti-Stokes radiation occurs at shorter wavenumber and at higher energy according to Rayleigh. [195].

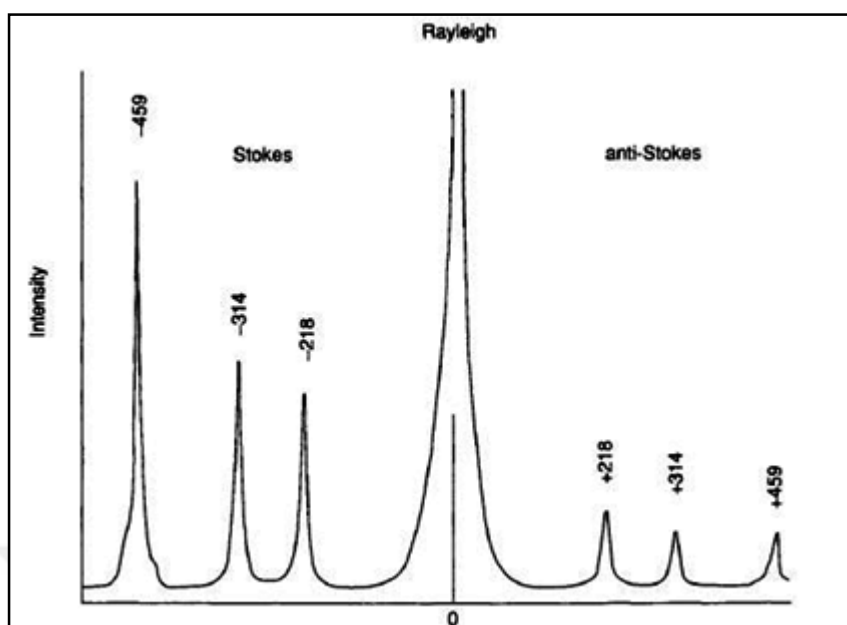


Figure 1.7. Raman spectrum of CCl_4 (488 nm excitation) [199].

Generally, molecules prefer to be present in the lowest energy vibrational state (Figure 1.8). The Rayleigh scattering has high intensity and it is the most preferable scattering process by molecules. There is no energy change in Rayleigh scattering; the molecule turns back to the vibrational state again. When the molecule absorbs energy at vibrational state (m), some of the photon's energy is absorbed by the molecule's electrons and the molecule turns back to the vibrational state (n). This is called Stokes scattering. Some molecules prefer to be present in the vibrational state (n) due to their thermal energy, in anti-Stokes scattering a part of the energy is transferred to the photon and molecule turns to vibrational state (m), losing energy [194].

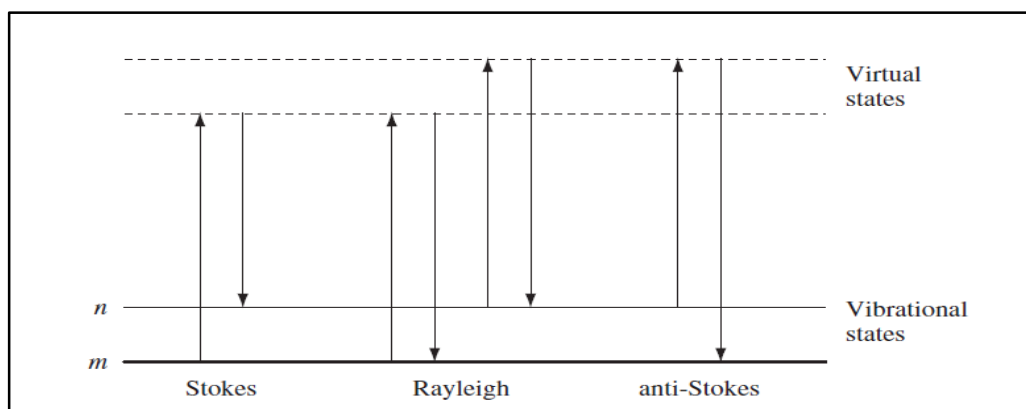


Figure 1.8. Schematic diagram of Rayleigh and Raman scattering processes.

1.12. FUNDAMENTAL DIFFERENCES OF IR AND RAMAN SPECTROSCOPY

There are some fundamental differences between IR and Raman spectroscopy. A vibrational fluctuation occurs in the infrared absorbing molecule, which have a net dipole moment. However, in scattering, the electrons, which are scattered around a molecular bond, undergo a sudden and inflexible deterioration, and then the beam re-emits in every direction as the bond returns to its normal state. The molecule is temporarily polarized while it is degraded; thus, creating a sudden dipole effect that disappears with relaxation and re-emission. The efficiency of a bond's scattering depends on the tendency of the electrons to decay from their normal position, which is referred to as being "polarizable". The increase in electron density causes an increase in bond strength and a decrease in bond length, resulting in a decrease in the ability to be polarized. Different from IR, there is a need for "polarity change", not dipole moment change, in order for Raman shift to occur in the scattered light [195]. Figure 1.9 shows two different molecules; the first molecule is nonpolar, which is symmetric and the dipole moment vectors quench each other, while the second molecule is in asymmetric structure with a net dipole moment, making the molecule polar [200, 201]. Raman and IR spectra complement each other, each defining a separate set of molecular vibrations. There are also vibrations that are active both in Raman and IR. In such cases, peaks appear at the same energies in both spectra.

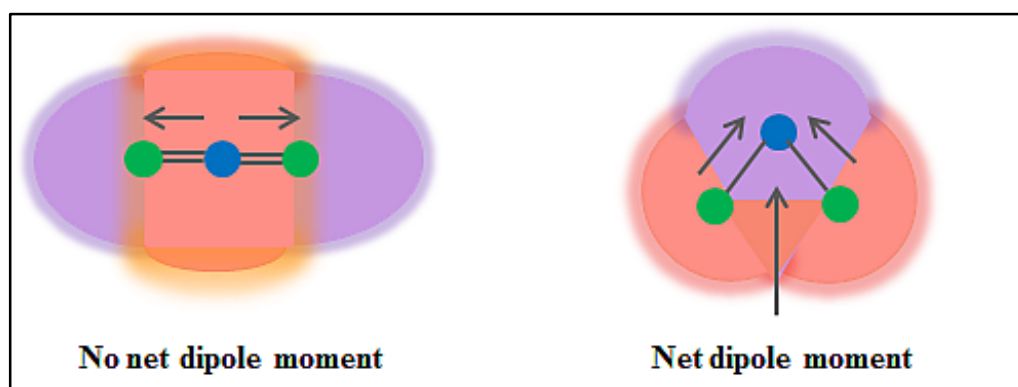


Figure 1.9. Representative image of a nonpolar and a polar molecule

1.13. SURFACE ENHANCED RAMAN SCATTERING (SERS)

Raman spectroscopy can be used to identify the molecules according to their characteristic 'fingerprinting bands'. The changes in wavelenghts depends on the polarizability of the molceule related with their spesific chemical structures. Thus, aromatic molecules cause much intense scattering according to aliphatic molecules. Raman scattering is rather weak and it's typical cross section is lower than the fluorescence has. Although Raman technique has advantages of easy sample preparation and minimal interference from water, weak scattering phenomenon was the major disadvantage and require sensitive detectors and higher power lasers sources. The adventure of SERS began 40 years ago with using silver-electrode substrate for pyridine measurements and has developed in line with the progress of the surface chemistry and sensor production up to day [202-205]. The discovery of the enhancement effect of a noble metal surface on Raman scattering brought a new breath to the technique. The enhancement effect was first reported by Fleischman et al., where they used a roughened silver-electrode surface for pyridine measurement. A significant shift on the wavenumber and the intensity of the peaks due to the alteration of the electrode potential was observed, which revealed the theory of adsorption of the pyridine on the roughened surface [206]. Fleischmann and McQuillan stated that the enhancement effect primarily related with surface roughness and this hypothesis seemed reasonable at first because the amount of adsorbed pyridine increased with increasing surface area. Meanwhile the study of Fleischmann and McQuillan was published, Van Duyne and Jeanmaire were working on enhancing the weak Raman signals with using pyridine adsorbed on an electrode surface but they found the signal intensity as 25 counts, while it was reported around 500-1000 counts in Fleischmann study. Van Duyne and McQuillan repeated the experiments of the Fleischmann's study by increasing the roughness of the electrode surface but they discovered a contrary result that the Raman signals increased with the decreasing surface roughness. They calculated the surface enhancement factor by proportioning the intensity of the molecule on the surface to that of the free molecule. Their study that was published in 1977, included an explanation of the enhancement of Raman signals with "electromagnetic effect"; which claimed that an electromagnetic field occurs on the metal surface as a result of induction of conductive electron of the metal to oscillate [207]. Whereas Albrecht and Creighton hypothesized the second SERS theory; "chemical effect" and published their study in 1977. They explained

that the charge transfer between metal surface and the molecule affects the polarizability of the molecule, which caused resonance Raman scattering [202]. Since then, electromagnetic and chemical enhancement mechanisms are accepted by the scientific community and the technique is named as surface-enhanced Raman scattering (SERS) [208]. It is now clear that the effectiveness of the electromagnetic enhancement is much more than the charge transfer effect, which is related to the chemical structure of the adsorbed molecule on the active metal surface.

Silver and gold colloidal nanoparticles has been widely used as SERS substrates since the discovery of the enhancement effect of the rough electrode surface and then the discovery supported with the better explanation of the plasmonic properties of the metals.

Plasmonics is the study of interactions of light with oscillating electron system of metals. When electromagnetic component of light interacts with the metal, the conductive electrons on metal surface begin to oscillate, these oscillating electrons are known as surface plasmons and first in 1978, Moskovits explained the relationship between surface plasmon and enhanced Raman scattering [209, 210]. Localized surface plasmon resonance (LSPR) and propagating plasmon, which are called as surface plasmon polaritons (SPP), are the types of surface plasmon resonance. In LSPR, a coherent oscillation occurs when oscillations of conducting band electrons of metal surface and frequency of light come into resonance as seen in Figure 1.10.

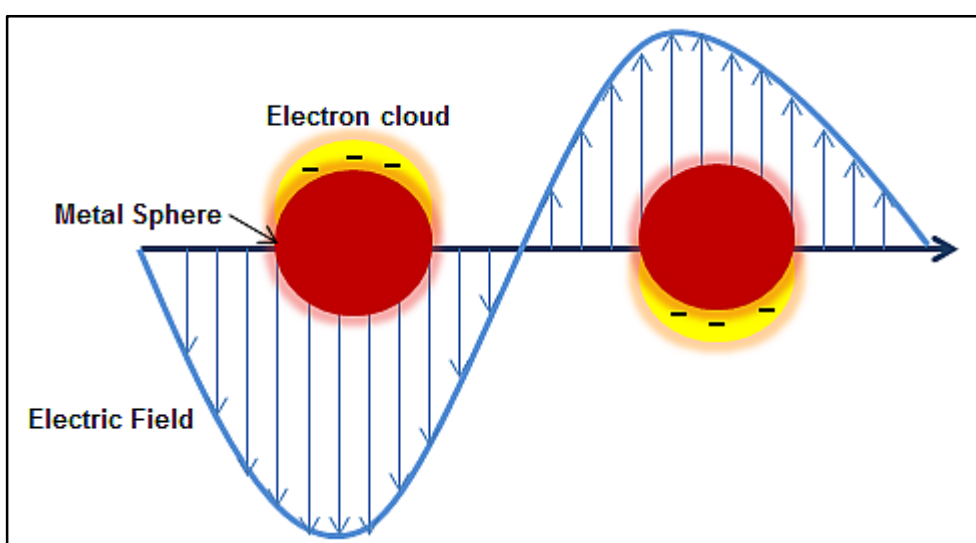


Figure 1.10. Schematic illustration of surface plasmon resonance for a metal sphere.

SPP is a surface electromagnetic wave between interface of a metallic film and dielectric due to coherent charge oscillation [211]. Localized surface plasmons are formed around 10-200 nm sized AuNPs and AgNPs and the size of the electromagnetic field around the nanoparticles is approximately a few nanometers, which is called 'hot spot' [212, 213]. Surface plasmons can be changed by modifying the shape, size and assembly of nanoparticles [214]. Electromagnetic fields of nanoparticles vary due to their geometries and the size of active field increase at sharp edges of metal nanoparticles as seen in Figure 1.11. Geometries with sharp edges such as triangular, rod and oval display an efficient electromagnetic field compared to spherical nanoparticles as shown in Figure 1.12 [215]. It has to be noted that although the electric field of angular nanoparticles is more effective, their synthesis procedures are much more difficult than the spherical ones. The number and peak position of LSPR modes can change depends on the size of nanoparticles. When the size of nanoparticles increase, it enhances the scattering of light and a red shift occurs in the peak position and also a significant band width broadening is observed [216]. Nanoparticle clusters enhance the electromagnetic field formed by a single nanoparticle. A strong electromagnetic coupling occurs between the nanoparticles in the clusters and these coupling can be explained by plasmonic hybridization. A comparison of electric fields of a single and dimer nanoparticle can be seen in Figure 1.13 [217, 218].

SERS is one of the application areas of plasmonic nanostructures. Metal nanoparticles; Ag, Au, Cu, Li and Al support surface plasmon activity due to their dielectric function in the UV/Vis and near infrared region (NIR) [219, 220]. Unlike other metal nanoparticles, AgNPs support surface plasmon activity in the region of 300-1200 nm. Furthermore, electrical and thermal conductivity of silver is higher than other metals, which is related with the electron density [214].

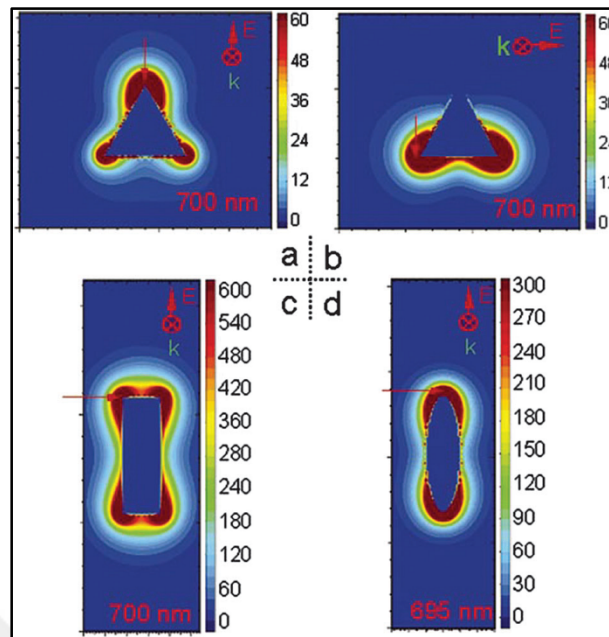


Figure 1.11. Colorful E-field enhancement contours of silver nanoparticle monomers with different shapes: (a) and (b) a triangular prism polarized along the two different primary symmetry axes; (c) and (d) rod and spheroid polarized along their long axes. The arrows show the maximum of the E-field [221]

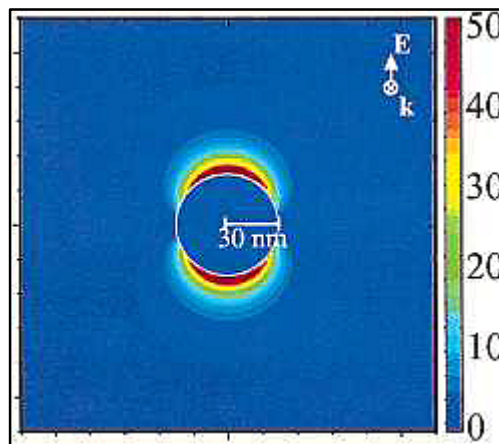


Figure 1.12. Electric field contours for a 30 nm radius silver nanoparticle in vacuum. The excitation light is in resonance with the plasmon oscillations [222].

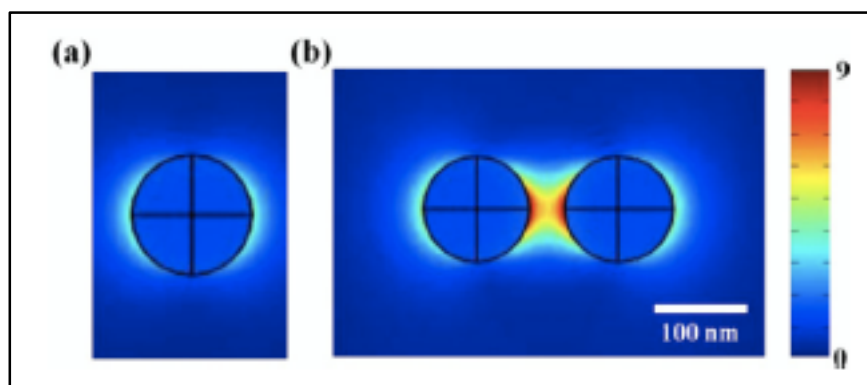


Figure 1.13. Comparison of electric field distributions of (a) a single AuNP and (b) nanoparticle dimer [223].

1.14. APPLICATION OF SERS IN CHARACTERIZATION OF MICROORGANISMS AND BIOFILMS

Identification and detection of microorganisms are very important in clinics inset but the complex nature of microbial world complicates the process. SERS is also studied as an alternative technique to the conventional techniques. Initially, Holt and Cotton characterized bacteria by utilizing SERS in 1988, where they identified the cell membrane with using a silver electrode as a SERS substrate [224]. Then, the whole bacterial cells were characterized by Efrima et. al in 1998 [225]. Zeiri et al. used silver and gold nanoparticles (AuNP) as substrates for detection of microorganisms using SERS [226, 227]. Premasiri et al. used AuNPs coated SiO₂ SERS substrates by sol-gel method for characterization of bacteria [228]. According to several studies, the potential of using SERS technique is promising compared to other conventional detection methods [229] and AgNP and AuNP colloidal suspensions are the most suitable SERS substrates. However, there is a major problem in the utilization of SERS in the field, which is the reproducibility and quality of the obtained SERS spectra. This problem occurs because of the heterogeneous mixture of metal colloid as well as the sample. New approaches were developed by our group to solve reproducibility problem of SERS. Bacteria and nanoparticles were assembled onto a glass slide by convective assembly and concentrated AgNPs were used to improve reproducibility and also layer-by-layer coating approach were applied for identification of a single bacterial cell [230-232].

While the use of SERS in bacteria detection is an attractive research field, the uncertainty in molecular origins of the SERS signals from the spectrum limited its applications. In general, it was accepted that the main spectral pattern of a microorganism exhibit the SERS signals attributed to outer cell wall components [189, 233-239]. There are conflicting assignments in the literature about the band observed at around 730 cm^{-1} , which is the strongest band of the SERS spectrum of a bacterium. In several studies, it was indicated that this peak is attributed to the main components of a peptidoglycan; glycosidic ring or C–N stretching mode of N-acetyl-D-glucosamine or N-acetylmuramic acid [76, 240]. One of our previous study, we found that the spectral features on a SERS spectrum of a bacteria could not be originating from peptidoglycan structure but could be originated from nucleic acids and metabolites attach on the surface of microorganisms' cell wall during sample preparation steps [241]. In a very recent study, it was demonstrated that the bands on the SERS spectra of bacteria mainly belong to the purine bases in the extracellular matrix, which occur with the nucleotide degradation under stress conditions [242].

Although SERS is a useful technique to identify biofilm composition, published studies in this area are limited at the moment. Ivleva et al. demonstrated characterization of biofilm matrix by SERS, where they used hydroxylamine hydrochloride-reduced AgNPs to obtain reproducible SERS spectra and this was the first study of biofilm characterization by SERS [187]. In another study, quorum sensing molecule N-acyl homoserine lactones were determined by SERS [189]. A multispecies heterotrophic biofilm was characterized and imaged by utilizing SERS with silver colloidal NP-based substrate. Raman spectroscopy and SERS techniques were compared in the same study and the better suitability of SERS was demonstrated [187]. Ramya et al. characterized algae and bacteria biofilms which were grown on titanium surface by micro-SERS [243]. Observing differentiation of the composition during biofilm formation is very important for understanding the behavior of microorganisms during the process. With this approach, Chao et. al observed the differentiation stages of the biofilm composition by obtaining SERS spectra at specific cultivation periods [185]. Biofilm formation were also monitored *in situ* by our group with using chitosan coated AgNPs as a SERS substrate [186]. Chitosan layer prevented dissolution of Ag ions and act as a biological semipermeable barrier in complex biological systems. A possibility of a more detailed examination of the biofilm structure by

combining spectroscopic methods has been shown in a different study, where they used confocal Raman spectroscopy and matrix-assisted laser desorption ionization mass spectrometry for identification EPS components in biofilm matrix of *P. aeruginosa* [244].

The response of the biofilm-forming microorganisms to the antibiotic treatment can also be determined by SERS through comparing the spectral changes during the process as demonstrated in a study published by our group [245]. Biofouling is one of the major problem in water industry as mentioned above, and SERS has started to be used in recent studies both in the biofouling detection in water membranes, in monitoring the response of microorganisms to cleaning agents as well as in the identification of interspecies interactions in dual-species biofilm [246]. Clinically important microorganisms, *P. aeruginosa* is known as one of the most important clinic pathogenic bacteria, leading to lethal, irreversible infections. For this reason, in recent years, there has been an increase in research studies about understanding the biofilm processes of *P. aeruginosa*, determination of the quorum sensing molecules and their biomarkers by using SERS [247, 248]. In our recent published study, we also aimed to apply SERS to the clinical investigations, and we used *P. aeruginosa*, *S. epidermidis* and *C. albicans* and identified the molecular changes in the biofilm formation with SERS and at the same time we demonstrated the discrimination of these microorganisms with a multivariate statistical method, Principal Component Analysis (PCA) according to significant differences in the spectral patterns [188].

2. OBJECTIVES OF THE STUDY

Pathogenic microorganisms form biofilms on different types of surfaces in environment and human body, which alter their metabolic activities during adaptation on the host surface. Identifying the metabolic activities of the clinically relevant microorganisms, *P. aeruginosa*, *S. epidermidis* and *C. albicans*, on surfaces with different chemical structure is one of the key point of this study. Showing the applicability of SERS, instead of microbiological techniques, in biofilm detection in clinics was the pivotal aim of this study.

To compare the biofilm processes of pathogenic model microorganisms; the microorganisms were incubated on various surfaces such as agar plates, 2-dimensional (2D) and 3-dimensional (3D) poly (methyl methacrylate) (PMMA) substrates and 3D glucose-gelatin scaffolds. The purpose of using agar plates was to monitor the behavior of microorganisms in their natural environment, PMMA was preferred because it is one of the widely used polymer in medical devices and implants. Also, the glucose-gelatin scaffolds were used as representative substrates that can mimic the substrates present in the environment as energy sources, which microorganisms can use extensively. At the same time, the importance of the effect of physicochemical properties of substrates on biofilm formation were aimed to be demonstrated with this study using 2D and 3D surfaces.

At a clinical setting, biofilms do not always consist of a single-species of microorganism. Therefore, discriminating microorganism species in a chaotic biofilm structure was the main goal to show the efficiency of the SERS technique. For this purpose, discrimination of microorganisms was aimed not only in a single-species biofilm but also in a multi-species biofilm to show the power of the technique with its easy and fast analysis approach.

3. MATERIALS AND METHODS

3.1. EXPERIMENTAL DESIGN

The experimental design is given in Figure 3.1. Briefly, the microorganisms were inoculated on agar plates, 2D PMMA glass slides, 3D PMMA substrates and 3D glucose-gelatin scaffolds after subculturing. 10 μ l of AgNPs were added on the biofilm samples and SERS measurements were performed after AgNPs get in contact with biofilm components. The details of the experimental steps are given below.

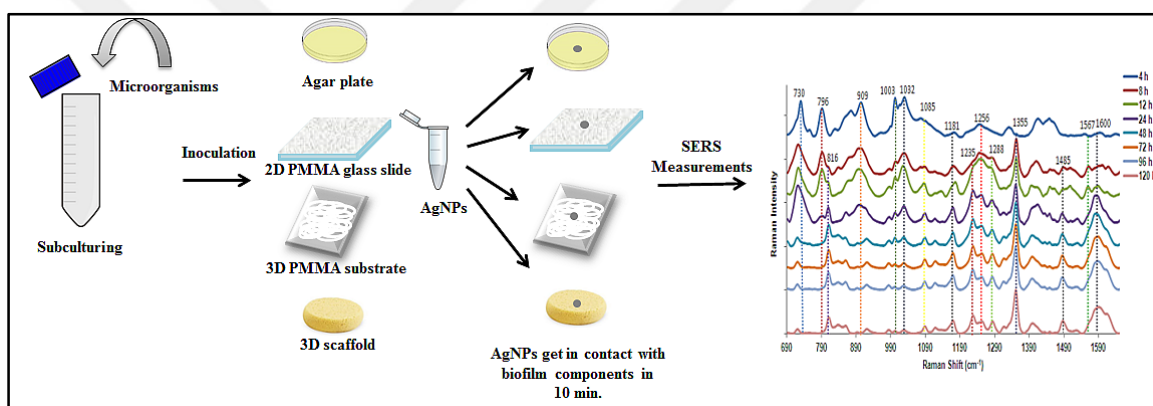


Figure 3.1. Schematic diagram of the experimental design.

SERS spectra originate from very close vicinity of AgNPs or molecular species stick to their surfaces. Thus, it is important to understand the interaction possibilities between AgNPs in the colloidal suspension and the biofilm components. As seen on Figure 3.2, a 10 μ L of AgNP colloidal suspension is added onto the biofilms started to form. As soon as the droplet of suspension is added, depending on the surface hydrophobicity/hydrophilicity, the droplet spreads and the water in the droplet is adsorbed by the underlying biofilm. The dynamics in the droplet during this process determines the interaction of AgNPs and their aggregates with the soluble biofilm components diffuses into the colloidal suspension during spreading. In addition, the preferential interaction of the molecular species with AgNPs can be a factor defining the strength of the interaction between them. Certain species might have increased affinity for AgNPs surfaces. At early incubation times of biofilm formation, we could say that AgNPs get in contact both with

purine bases secreted by the microbial cells and the biological components secreted as an extracellular matrix. However, extracellular matrix coated the surface of microbial cells at the maturation phases of biofilm formation, which prevent the interaction of AgNPs with early metabolites around the cells and AgNPs interacted with the biofilm components. The possible situation is that the AgNPs may be mostly interacted with diffusible components into the silver colloid (Figure 3.2 a) and when the droplet get dried, the AgNPs aggregated on the biofilm with the components on their surfaces (Figure 3.2 b). An electromagnetic field occur around the plasmonic AgNPs and this active hot spot areas increase when the AgNPs form clusters especially during drying on the biofilm sample. The SERS signals not only obtained from the molecules on the surface of AgNPs but also, they may obtained from the molecules, which are in an interaction with the electromagnetic field. The diffusion of proteins, carbohydrates and genetic materials from biofilm sample into the colloidal droplet is possible, but diffusion can not be possible for lipids and other water-insoluble components. However, specific peaks of water-insoluble components can be observed on the obtained SERS spectra due to their interaction with the electromagnetic field of the AgNPs clusters. This scenario can be possible for smooth surfaces. However, due to the non-smooth and chaotic surfaces of 3D fibrous and porous substrates this scenario might not be applicable or at least can be difficult to estimate the real dynamics.

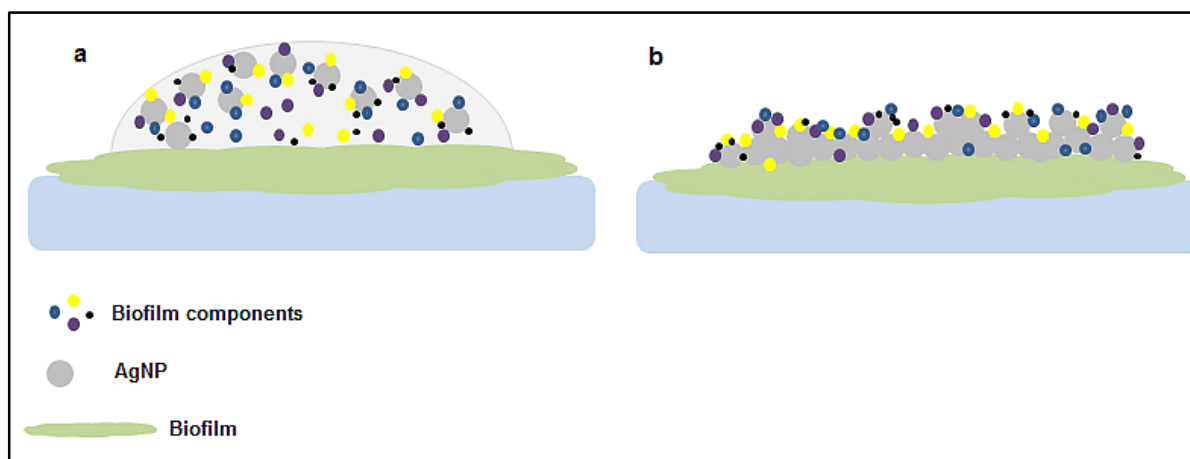


Figure 3.2. A possible scenario for interaction of AgNPs with biofilm components in silver colloidal suspension (a) and AgNPs aggregates on biofilm sample with components attached on their surface (b).

3.2. CHEMICALS

Tryptic Soy Agar (TSA), nutrient agar (NA), sabouraud 2 per cent glucose agar (SDA), nutrient broth (NB), glutaraldehyde (25 per cent solution in water) and tri-sodium citrate were purchased from Merck (Merck KGaA, Darmstadt, Germany). Tryptic soy broth (TSB), sabouraud dextrose broth (SDB), gelatin from porcine skin, D (+) glucose, poly (methyl methacrylate), acetone, and silver nitrate (AgNO_3) (99.5 per cent) was purchased from Sigma-Aldrich. FilmTracer SYPRO Ruby biofilm matrix stain was purchased from ThermoFisher Scientific.

3.3. MICROORGANISMS

The microorganisms *Pseudomonas aeruginosa* 15692, *Staphylococcus epidermidis* 35984D-5 and *Candida albicans* 10231D-5 were obtained from ATCC (England, UK).

3.4. SYNTHESIS OF SILVER NANOPARTICLES

The 50 nm AgNPs were synthesized by Lee and Meisel method [249]. A 90 mg of AgNO_3 was dissolved in a 500 mL double-distilled water (ddH_2O) and the AgNO_3 solution was heated under stirring until boiling. Then, a 10 mL (1 per cent) of tri-sodium citrate solution was added drop wise into the solution and the reaction stopped when the volume reduces to 250 mL. The concentration of the synthesized AgNPs colloidal suspension was named as 1X. The 1X suspension was centrifuged at 5500 rpm for 30 min and $\frac{3}{4}$ of the supernatant was removed to increase the final colloidal concentration 4-times, named as 4X, which was used for the SERS measurements.

3.5. PREPARATION OF 2D PMMA SUBSTRATES

The experimental design of preparing PMMA substrates is given in Figure 3.3. 250 mg PMMA was dissolved in 10 mL toluene with sonicating at 50 °C for 2 hours. PMMA substrates were prepared with drop casting approach using a mold. The PMMA coated

glass slides were incubated overnight at room temperature and then they were annealing at 90 °C for 2 hours in an oven.

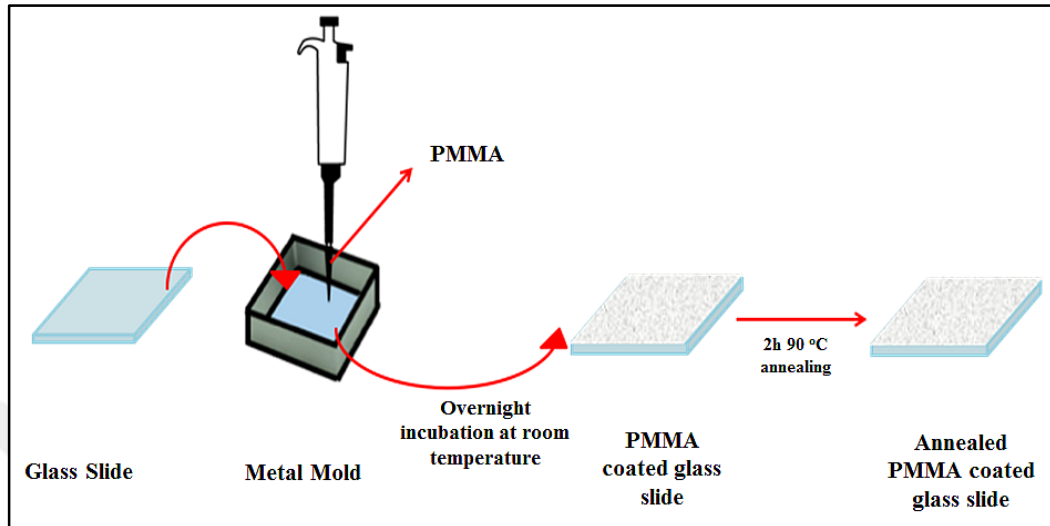


Figure 3.3. Experimental design of preparing a PMMA coated glass slide.

3.6. PREPARATION OF 3D PMMA SUBSTRATES

2 grams of PMMA were weighed and placed into 7 ml of acetone and incubated overnight at room temperature on a shaker. Then, the polymeric solution was placed in plastic syringe for electro-spinning. Figure 3.4 shows the electro-spinning preparation of 3D PMMA substrates. Polymeric material in the syringe is sent to the collection table with the aid of a pump at a rate of 0.5 ml / s and 18 kV voltage. The fibers were deposited on aluminum foil placed on the collector. The PMMA substrates were cut into 1 cm x 1 cm pieces for further use in the experiments.

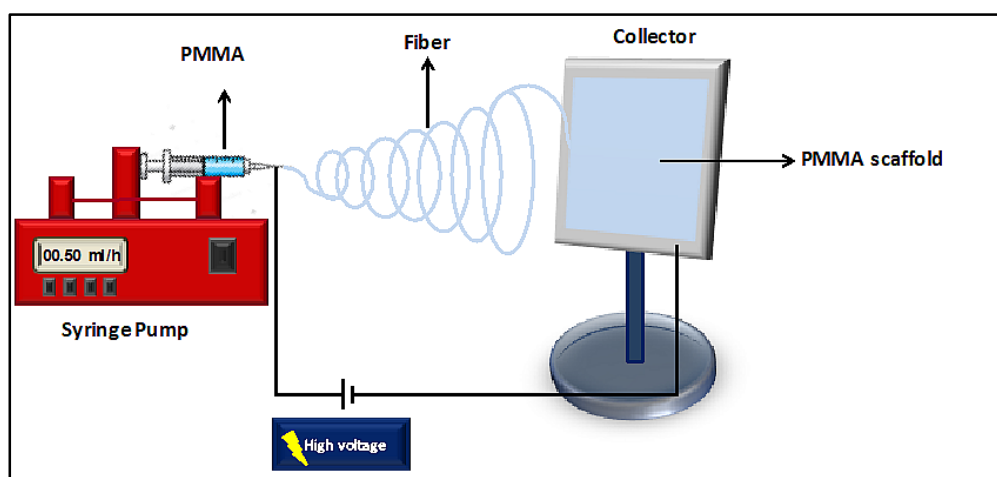


Figure 3.4. Experimental design of preparing 3D PMMA substrates.

3.7. PREPARATION OF 3D GLUCOSE-GELATIN SCAFFOLDS

Glucose containing gelatin porous structures were prepared by freeze dryer, which are planned to be used as an energy source by bacteria. Gelatin and glucose were dissolved in ddH₂O (5 per cent w/v, 2.2 per cent w/v) and stirred at 40 °C for two hours. Glutaraldehyde solution (5 per cent, g/ml) was added as a cross-linker to obtain rigid substrates in an aqueous media. The reaction was followed for half an hour after adding glutaraldehyde to allow the progress of the reaction. The glucose gelatin mixture was frozen at -80 °C overnight and freeze-dried for 24 hours [279].

3.8. PREPARATION OF MICROORGANISM SAMPLES

P. aeruginosa, *S. epidermidis* were sub-cultured at 37 °C for 18 hours in TSB, NB and *C. albicans* were sub-cultured at 37 °C for 48 hours in SDB. The 50 µl sub-cultured microorganisms (OD₆₀₀=1) were inoculated on the plates in order with TSA, NA and SDA by using beats to spread the microorganisms on the agar plates and on the 2D and 3D PMMA substrates and 3D glucose-gelatin scaffolds homogenously. The microorganisms were incubated on substrates between 4 and 120 h after inoculation to monitor biofilm formation.

Multi-species biofilm formation samples were prepared by inoculating the 20 μ l sub-cultured *P. aeruginosa*, *S. epidermidis* and *C. albicans* on the same NA plates homogenously with using beats. The multi-species microorganisms were incubated for 48 h after inoculation.

3.9. PREPARATION OF MICROORGANISMS TO OBTAIN THE BACKGROUND SERS SPECTRA

The microorganism samples of *P. aeruginosa*, *S. epidermidis* and *C. albicans* were cultivated on TSA, NA and SDA, respectively. The microorganism samples were collected from the agar plates with a loop and dispersed in 1 mL ddH₂O. The microorganism samples were washed three times with centrifuging at 7500 rpm for 5 min. A 5 μ l of each microorganism were mixed with 100 μ l of 4X AgNPs and dropped 2 μ l on a calcium fluoride (CaF₂) slide and incubated until get dried for SERS measurements.

3.10. SERS MEASUREMENTS

SERS spectra from biofilm were collected 20 \times long distance objective (N.A.=0.40) with 2.5 μ m spot sized and 5 s exposure time with 30 mW laser power from 830 nm excitation with 1200 line/mm grating using a Renishaw inVia Reflex Raman spectrometer equipped with a high speed encoded stage (Streamline™), a Leica DM2500 upright microscope. All the experiments repeated three times. In one experiment SERS spectra were obtained from 3 different spots. From each spot, total of 36 spectra were obtained, which brings the total spectra to 108 spectra from one experiment. Each experiment repeated three times. Totally each spectrum on figures are the average of 324 spectra on every time points of 3 microorganisms. Coefficient variants (CV) of the data set determined between 36 spectra of each spot and between the averages of spot-to-spot and sample-to-sample. CV values were determined with the formulation of dividing the standard deviation value by the mean value and multiplying this by 100 with using the spectral data.

3.11. DATA PREPROCESSING

Wire 4.1 software was used for preprocessing of the collected data. First, baseline subtraction and cosmic ray removal were applied to each spectrum. The acquired spectra were averaged after smoothed by Savitzky-Golay filtering and they were normalized to be equal to 1.

3.12. STATISTICAL ANALYSIS

Data analysis was performed with using SPSS 20.0. Principal Component Analysis (PCA) and Linear Discrimination Analysis (LDA) algorithms were used for statistical analysis to identify the unique spectral characteristics of biofilms of three model microorganisms on different substrates. First, the significant PCs were defined from the original spectral data. Then, the regression (REGR) factors were used for classification the model microorganisms with PC-LDA.

3.13. ULTRAVIOLET-VISIBLE SPECTROSCOPY ANALYSIS

Lambda 25, Perkin Elmer Ultraviolet-Visible (UV-Vis) spectrometer was used for the analysis of AgNPs colloidal suspension. The AgNPs concentrations were determined as 100 µg/mL before characterization with UV-Vis spectrometer.

3.14. TRANSMISSION ELECTRON MICROSCOPY ANALYSIS

JEOL 2100 transmission electron microscope (TEM) instrument equipped with an Oxford Instruments 6498 EDS system (Germany) was used for characterization of AgNPs. 200 kV operating voltage was used for the TEM analysis with LaB6 filament.

3.15. SCANNING ELECTRON MICROSCOPY ANALYSIS

The scanning electron microscopy (SEM) images were acquired by using a Carl Zeiss Evo 40 instrument at under high vacuum with a potential of 10 kV. For SEM analysis, the small agar samples cut and removed from the agar plates and the biofilm samples on 2D and 3D PMMA and 3D glucose-gelatin scaffolds were fixated with incubating the samples in glutaraldehyde solution (2.5 per cent in phosphate buffer saline) for 30 min. at 4 °C. The biofilm samples then incubated in 50 per cent, 70 per cent, 90 per cent and 100 per cent ethanol for 5 min at room temperature, respectively.

3.16. CONFOCAL LASER SCANNING MICROSCOPY ANALYSIS

The images were taken with 20× 0.8 N.A. objective, Zeiss LSM 780 Confocal Laser Scanning Microscope (CLSM) and FilmTracer SYPRO Ruby Biofilm Matrix Stain (ThermoFisher Scientific) were used. 150 µL of biofilm stain was added onto the biofilm sample and incubated for 30 min at room temperature in dark. Then, the samples were rinsed with filtered ddH₂O before imaging.

3.17. FOURIER TRANSFORM INFRARED SPECTROSCOPY

Fourier Transform Infrared Spectroscopy (FT-IR) characterization on both pristine and modified particles was performed using Thermo Scientific Nicolet iS50ATR equipment in Attenuated Total Reflectance (ATR) mode from 4000 to 400 cm⁻¹ at a resolution of 4 cm⁻¹ with a total of 32 scans.

4. RESULTS AND DISCUSSIONS

4.1. CHARACTERIZATION OF SILVER NANOPARTICLES

The synthesized AgNPs colloidal suspension were characterized with UV-Vis (Figure 4.1a) spectroscopy and TEM (Figure 4.1b). The maximum absorbance of the UV-Vis spectrum of AgNPs colloidal suspension was observed at 420 nm. In correlation with this observation, the average diameter of AgNPs were determined to be approximately 50 nm as seen in the TEM image.

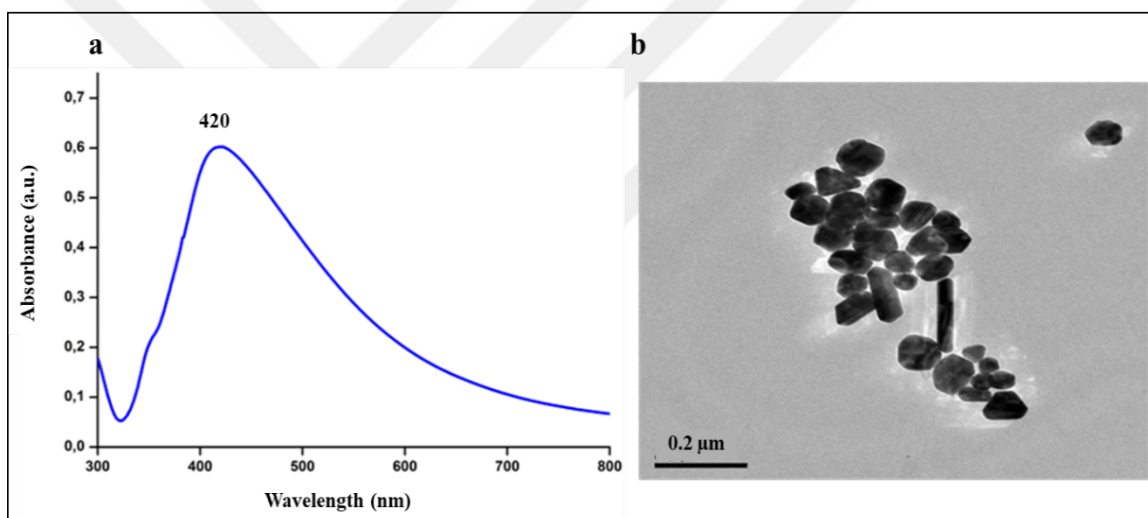


Figure 4.1. The UV-Vis spectrum and TEM image of AgNPs.

4.2. CHARACTERIZATION OF BIOFILM SUBSTRATES

4.2.1. Characterization of 2D PMMA Substrates

The PMMA coated glass surface was characterized by FT-IR. In Figure 4.2, comparative FT-IR spectra of pure PMMA and PMMA coated glass surface are given. All the characteristic peaks of PMMA were observed in the spectrum from PMMA coated glass surface. Digital and SEM images of the PMMA coated glass slides is shown in Figure 4.3 In Figure 4.3a-b it is seen that the entire surface was evenly covered with a polymeric

solution. The bubbles can be seen on the surface of the polymer coating in Figure 4.3c. The bubble formation is an expected situation that they formed during the evaporation of the polymer solvent. Also, thickness of the coating was determined as around 280 μm (Figure 4.3d).

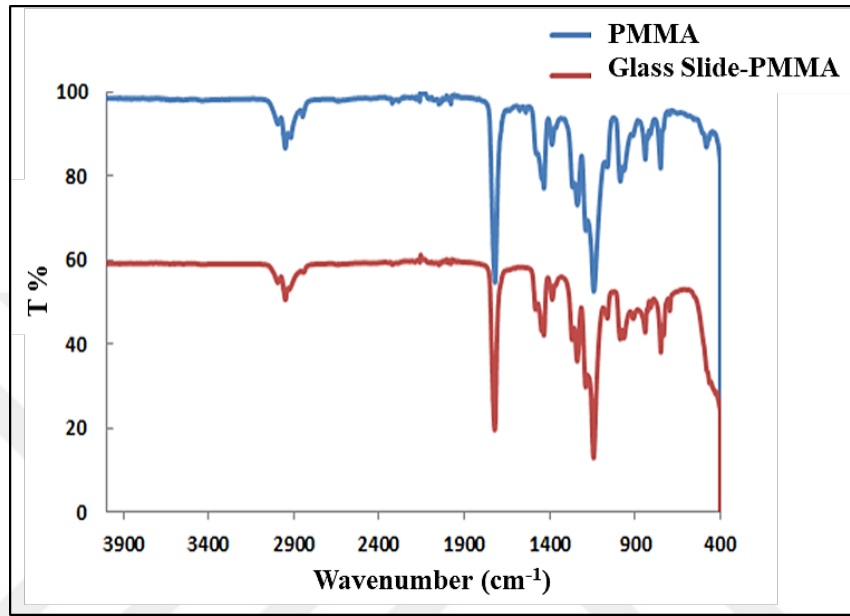


Figure 4.2. FT-IR spectra of PMMA and PMMA coated glass slide.

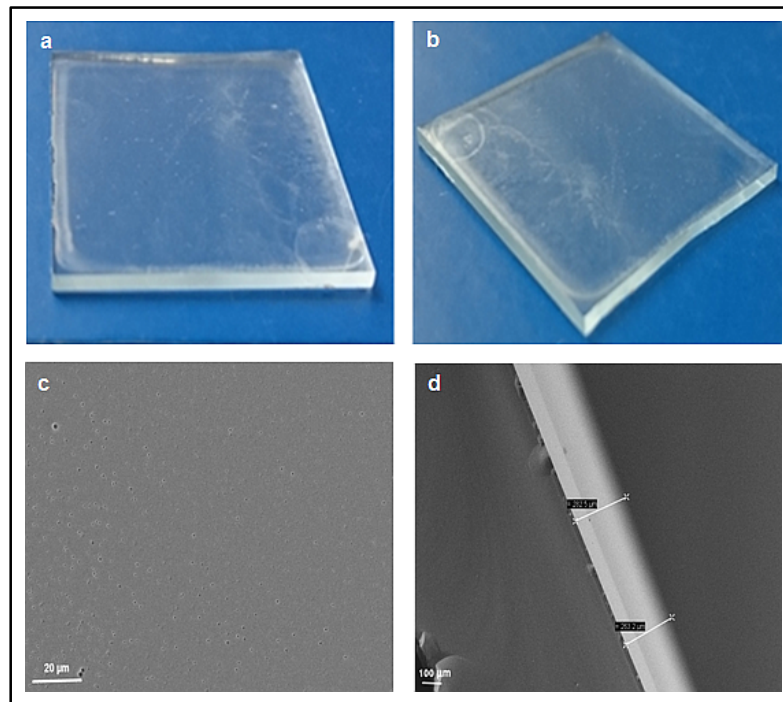


Figure 4.3. Digital images (a, b) and SEM images (c, d) of PMMA coated glass slides.

4.2.2. Characterization of 3D PMMA Substrates

The digital image of a 3D PMMA substrate, prepared with electrospinning, is given in Figure 4.4a. The average fiber diameter of polymeric substrate was determined to be approximately 2.9-5.3 μm as seen in SEM image in Figure 4.4b.

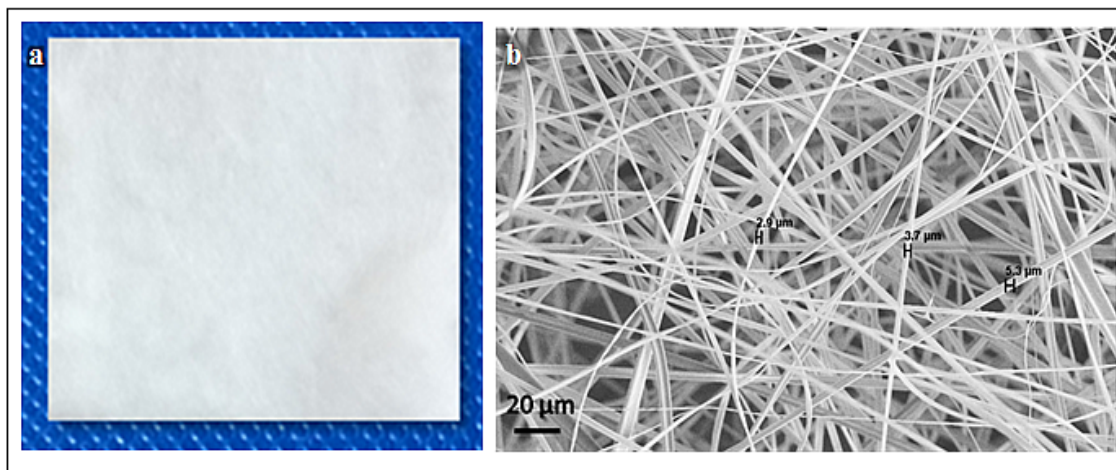


Figure 4.4. Digital image (a) and SEM image (b) of a 3D PMMA substrate. Scale bar is 20 μm .

4.2.3. Characterization of 3D Glucose-Gelatin Scaffolds

The 3D glucose-gelatin scaffolds were prepared by freeze-dryer to obtain a porous structure in order to provide adhesion of microorganisms. The digital image of the scaffold and also the SEM image in Figure 4.5 showed the regular porous structure.

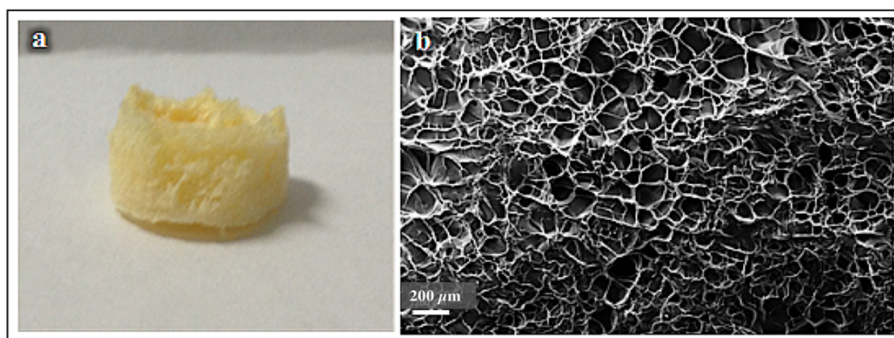


Figure 4.5. Digital image (a) and SEM image (b) of a 3D glucose-gelatin scaffold. Scale bar is 200 μm .

4.3. BACKGROUND SERS SPECTRA OF SILVER NANOPARTICLES AND MICROORGANISMS

The SERS spectrum of AgNPs was obtained to identify the possible interference from the background as seen in Figure 4.6. Because AgNPs were reduced with citrate, a C-C stretching peak of citrate on the surfaces of AgNPs was observed at 1050 cm^{-1} on the spectrum of dried AgNPs. The SERS spectra of *P. aeruginosa*, *S. epidermidis* and *C. albicans* were also obtained to observe the general spectral pattern of the planktonic cells given in Figure 4.7.

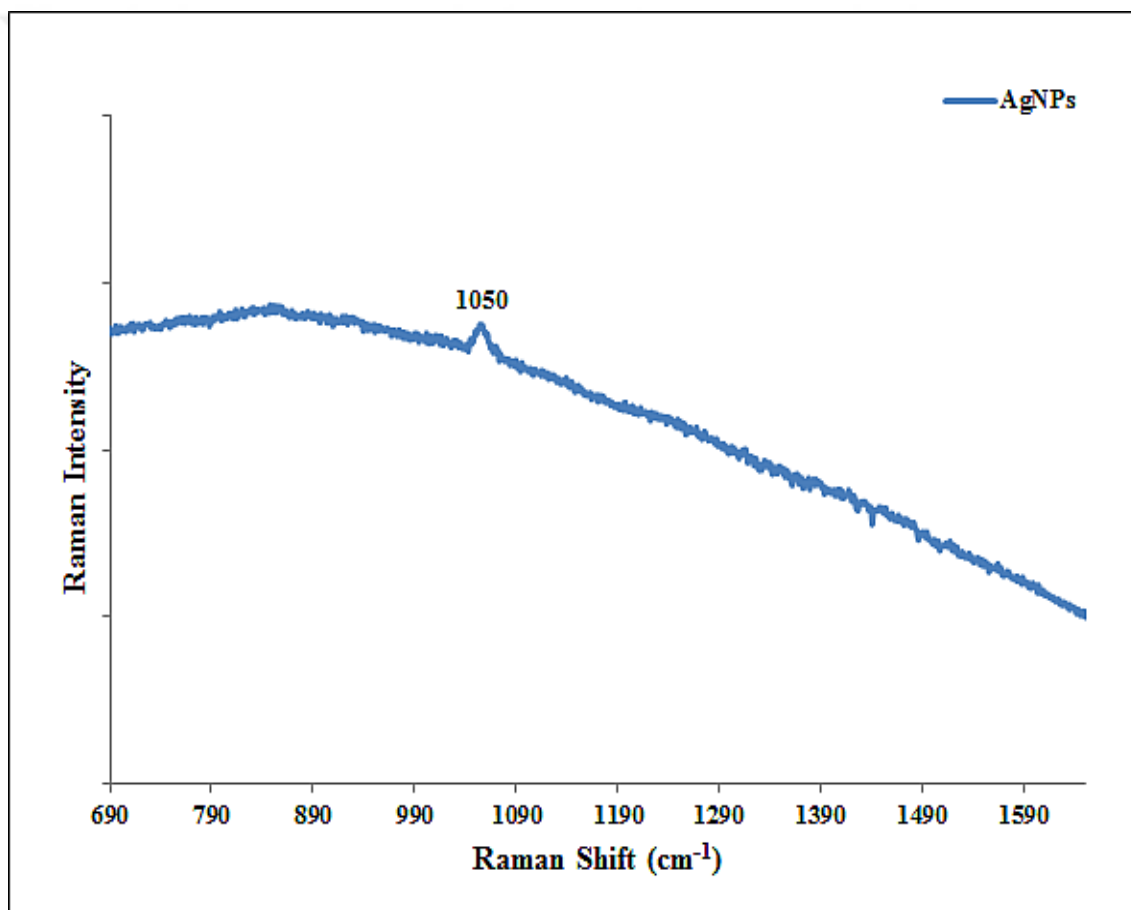


Figure 4.6. SERS spectra of AgNPs.

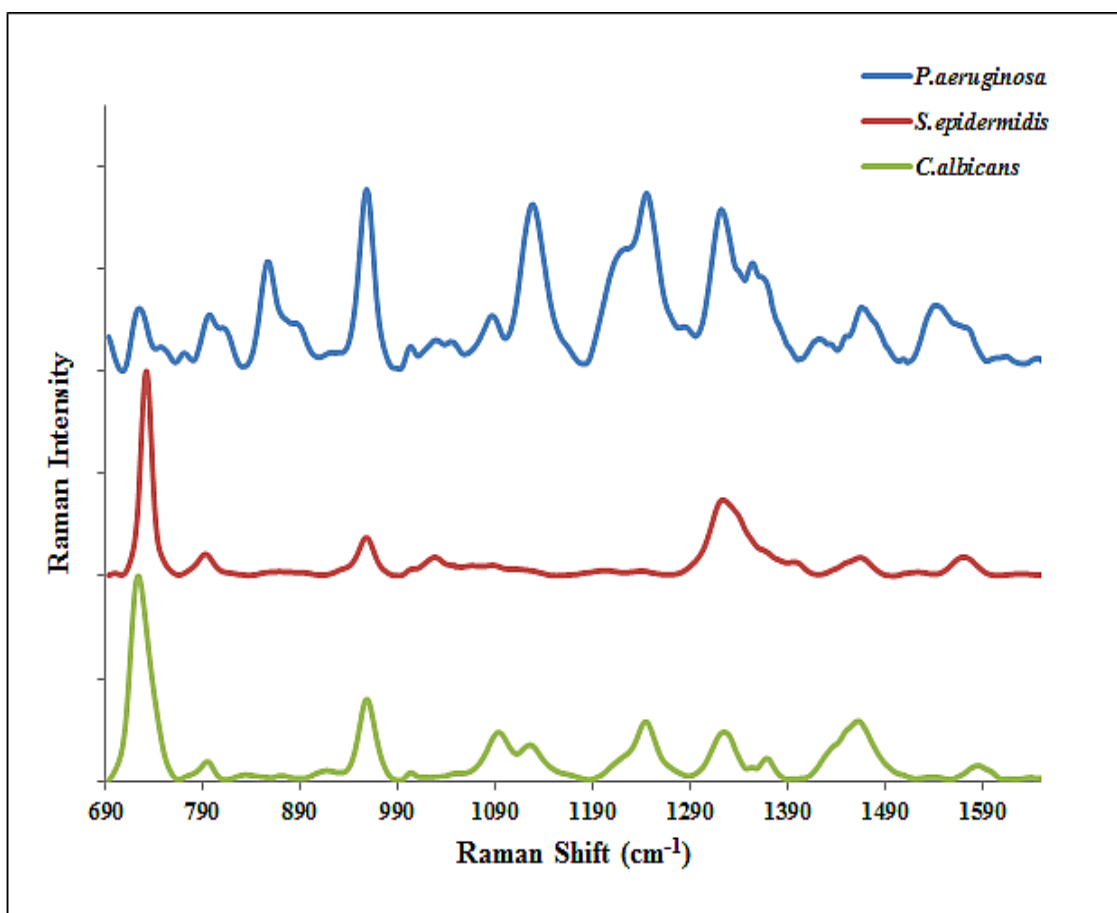


Figure 4.7. SERS spectra of *P. aeruginosa*, *S. epidermidis* and *C. albicans*.

4.4. BIOFILM FORMATION ON SUBSTRATES

4.4.1. Agar Plates

The SERS spectra from growth media (TSA, NA, SDA) were obtained in the same manner that the SERS measurements from biofilms were performed, where a 10 μl volume of colloidal AgNPs was placed onto the solid culture plate and waited until dryness, approximately 10 min., then SERS measurement was completed. The list of the tentative peak assignments was given in Table 4.1.

Table 4.1. Tentative peak assignments list for SERS spectra.

Peak (cm ⁻¹)	Assignment
730	*Purine bases [241, 242]
756-796	DNA/RNA fragments [228, 238, 251-254]
810-815, 837-853	Tyrosine [238, 255]
873-889	-C-C stretching and C-O-C 1,4-glycosidic link from carbohydrates [237, 238, 254, 256]
907, 909	C-COO ⁻ stretching from carbohydrates [257]
918-955	* * Possibly α -helices and/or carbohydrates [258]
1003	Phenylalanine [259]
1032	C-C stretching [260]
1045-1086	C-O and C-C stretching of carbohydrates [238]
1085-1181, 1355	Pyocyanin [250]
1103-1159	N-H Protein [185]
1211-1288	Amide III [185, 235, 240, 261]
1328-1413	COO ⁻ stretching of carbohydrate [187]
1445-1486	CH ₂ /CH ₃ deformation of lipids [233]
1485-1490	Adenine [262]
1505, 1527	N-H and C-H Bending, C=C Stretching [185]
1567	Amide II [185]
1600-1622	Amide I [263]

On the SERS spectra of growth media in Figure 4.8, the carbohydrate peaks of C-C stretching and C-O-C 1,4-glycosidic linkage were observed at 862 cm⁻¹ [237, 238, 256]. The peak at around 1003 cm⁻¹ attributed to phenylalanine and the peak 1032 cm⁻¹ belonging to C-C stretching as expected from the growth media [259, 260]. The peak attributed to N-H proteins observed at 1146 cm⁻¹. The peak at 1462 cm⁻¹ attributed to CH₂/CH₃ deformation of lipids [233]. Amide I band from proteins present in growth media were observed at 1608 cm⁻¹[263].

Figure 4.9 shows the SERS spectra of biofilm formation of *P. aeruginosa* at increasing incubation times from 4 to 120 h. The citrate reduced AgNPs were used as substrates by placing about 10 μ L of AgNP colloidal suspension on formed biofilm and waited approximately for 10 min for interaction of AgNPs with biological components. The metabolic activities of microorganisms were not affected from the interaction with AgNPs.

In a previous study of ours, we have shown that incubation with AgNPs does not change the growth profiles of microorganisms [241].

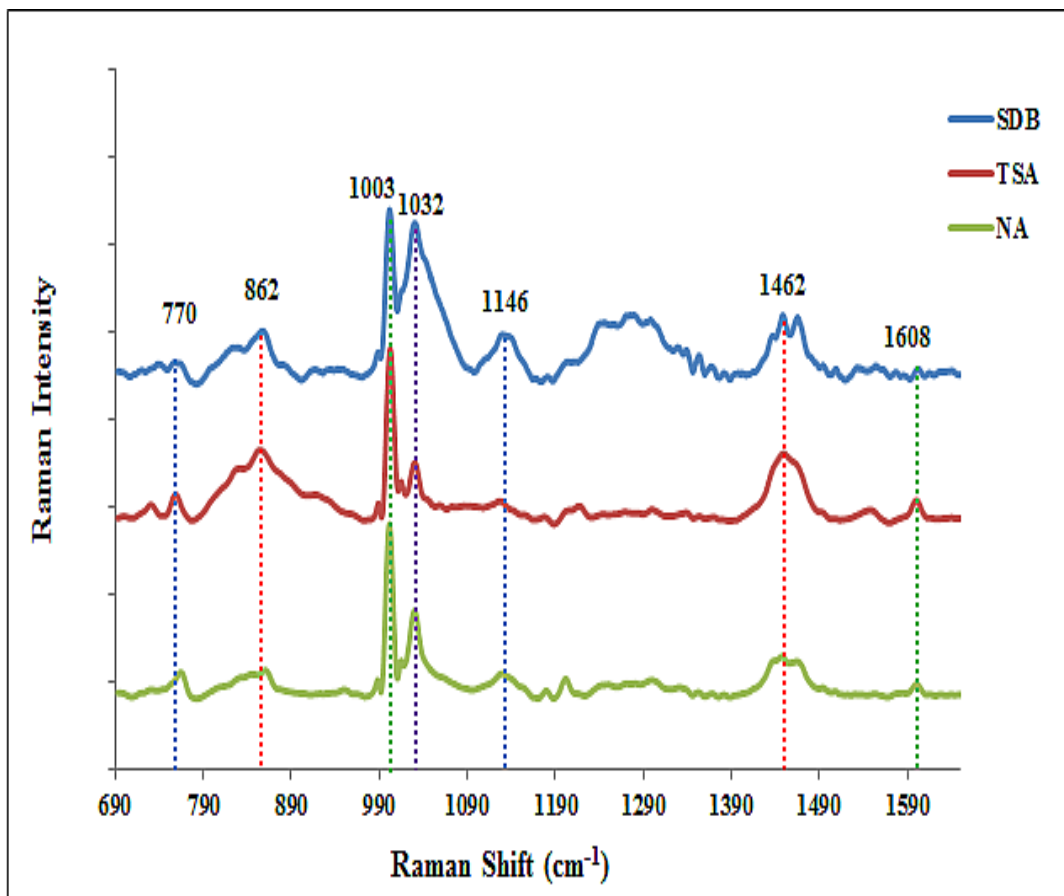


Figure 4.8. SERS spectra of growth media; TSA, NA and SDA.

The metabolic activity of microorganisms can be monitored from the spectral changes during accumulation of biofilm formation [185]. The intensity of the band at 730 cm^{-1} belonging purine bases at the outer layer of the bacteria and in the extracellular metabolome decreased after 48 h incubation within maturation phase of biofilm. Protein, carbohydrate and lipid synthesis increase in maturation phase of biofilm formation, which coats the microbial cells. The bands at 796 cm^{-1} and 1567 cm^{-1} are attributed to DNA/RNA fragments [228, 238, 251-254]. The intensity of these peaks started to decrease after 48 h with maturation of biofilm formation. Since the AgNP colloidal suspension is placed on the biofilm after a certain time interval, the AgNPs come into contact with whatever was secreted on the surface of a biofilm. A fluctuation in the intensity of a band indicates a change in the concentration profile of that specific biomolecular species in the biofilm matrix. The biofilm structure covers the bacterial cells and acts as a shell for the

living system and limits the interaction of the system with the external components as indicated previously. When the AgNP colloidal suspension is added on the next SERS measurement point, the secreted biomolecular species during previous time point is buried under newly formed biofilm matrix. This process continues until the completion of the biofilm, thus the added AgNPs come into contact with new biofilm matrix composition at every time point where the SERS measurements were performed. The band at 1485 cm^{-1} which is also attributed to adenine was observed after 8 h of incubation with an increasing intensity profile during incubation [262].

The band at 909 cm^{-1} could be attributed to C-COO^- stretching vibration of alginate, a polysaccharide, [257] started to decrease after 24 h incubation [264]. The expression of polysaccharides during accumulation of biofilm formation was demonstrated in a previous study [265]. The intensity of the band originating from alginate started to increase after 8 h. As it is known, alginate is the main EPS component expressed from *P. aeruginosa* to provide mechanical strength to 3D structure of the biofilm composition [266].

Proteins are the major component of EPS and are expressed during biofilm formation with increasing concentrations that was also observed in this study at increasing incubation times on the SERS spectra of *P. aeruginosa* [267]. Ring breathing band of tyrosine at 815 cm^{-1} , [238, 255] which is an amino acid in protein structure, was observed with a significant increase in intensity after 8 h of incubation. Amide I band of proteins was observed at near 1600 cm^{-1} with an intensity increase profile during the maturation of biofilm. The bands at 1235 cm^{-1} , 1256 cm^{-1} and 1288 cm^{-1} attributed to Amide III vibrations [185, 235, 240, 261], and their intensities started to increase significantly during the maturation phase. The intensity increase in Amide I and Amide III bands indicates the expression of proteins by *P. aeruginosa* as an ongoing process in all stages of biofilm formation. Following 8 h incubation, an increase was observed in the intensity of the bands at 1085 cm^{-1} and 1181 cm^{-1} , and also the band at 1355 cm^{-1} appeared after the 4 h incubation. These bands were suggested as characteristic peaks of pyocyanin in a recent study, which is known as a toxic blue-green pigment excreted by *P. aeruginosa*. Pyocyanin was also used as a biomarker in SERS studies for the identification of infections caused by *P. aeruginosa* [250].

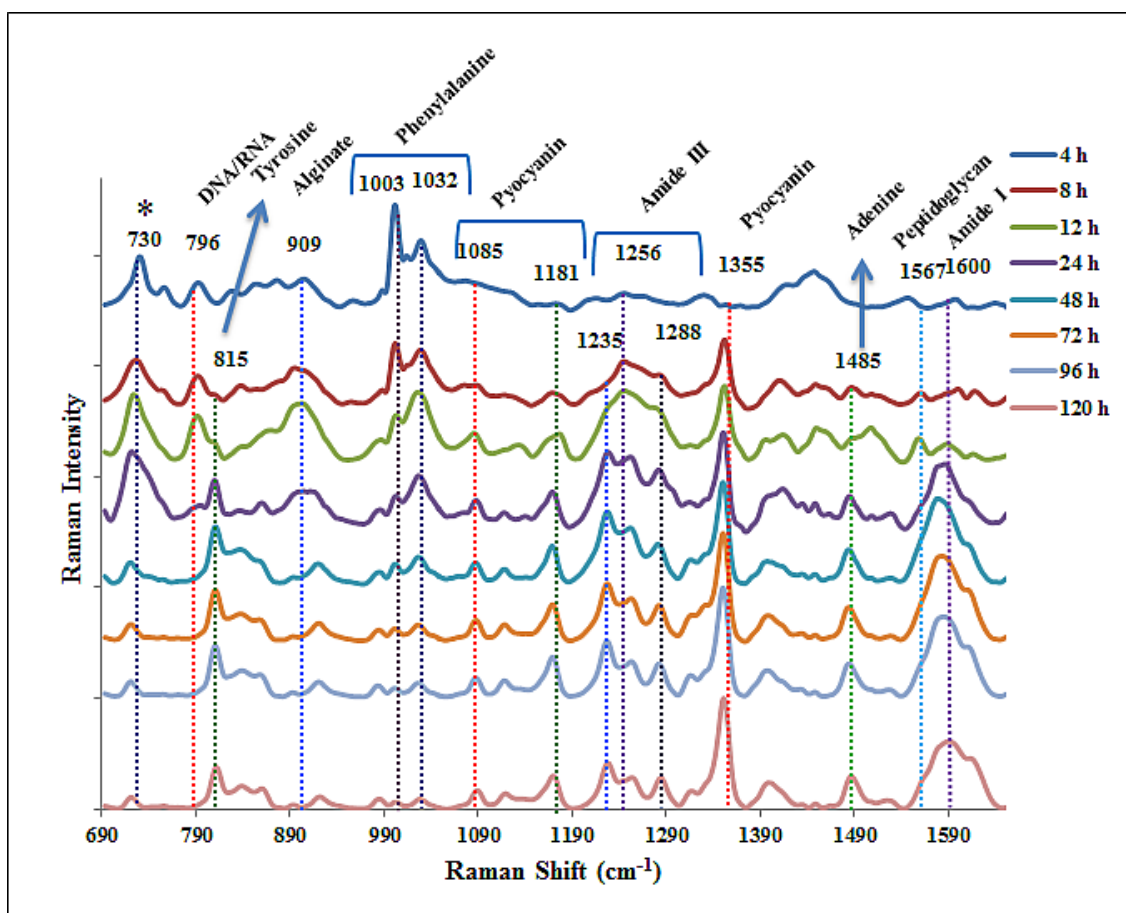


Figure 4.9. SERS spectra of *P. aeruginosa* biofilm formation at different cultivation times between 4 and 120 h.

Figure 4.10 shows the SERS spectra obtained from biofilm of *S. epidermidis* at increasing incubation times between 4 h and 120 h. The intensity of the band at 730 cm^{-1} decreased with the maturation of *S. epidermidis* biofilm, which can be explained again with decreasing interaction of AgNPs with the purine bases released from bacterial cells [241, 242]. A significant change was not observed on the band intensity of 756 cm^{-1} , which is attributed to DNA/RNA fragments. After 4 h of incubation, the intensity of the peak attributed to proteins at 1126 cm^{-1} increased. A slight increase was observed at the peaks 875 cm^{-1} and 1332 cm^{-1} attributed to carbohydrates. This slight increase can be explained with the general metabolism of *S. epidermidis* expressing polysaccharide PIA, which is the major component of the biofilm matrix allowing regulation of biofilm formation [76]. The bands at 849 cm^{-1} and 1213 cm^{-1} belonging to tyrosine and Amide III bands, respectively, started to increase during maturation of biofilm matrix. A significant intensity increase appeared for Amide I band of proteins at 1600 cm^{-1} after 48 h incubation with the

accumulation of biofilm. In a recent study, the importance of a specific protein, 18 kDa Small basic protein (Sbp), for biofilm formation of *S. epidermidis* was demonstrated. This scaffold protein is responsible for the accumulation of biofilm formation through promoting the synthesis of PIA and accumulative proteins [268]. This connection between the protein expression and regulation of biofilm formation is sufficient to explain the concentration increase on the protein bands with increasing incubation times. A significant change was not observed on the band intensities at 1445 and 1464 cm^{-1} attributed to lipids. From the spectral fluctuations, one can conclude that the metabolic activity of *S. epidermidis* was more stable than *P. aeruginosa* when their SERS spectra at increasing incubation times were compared.

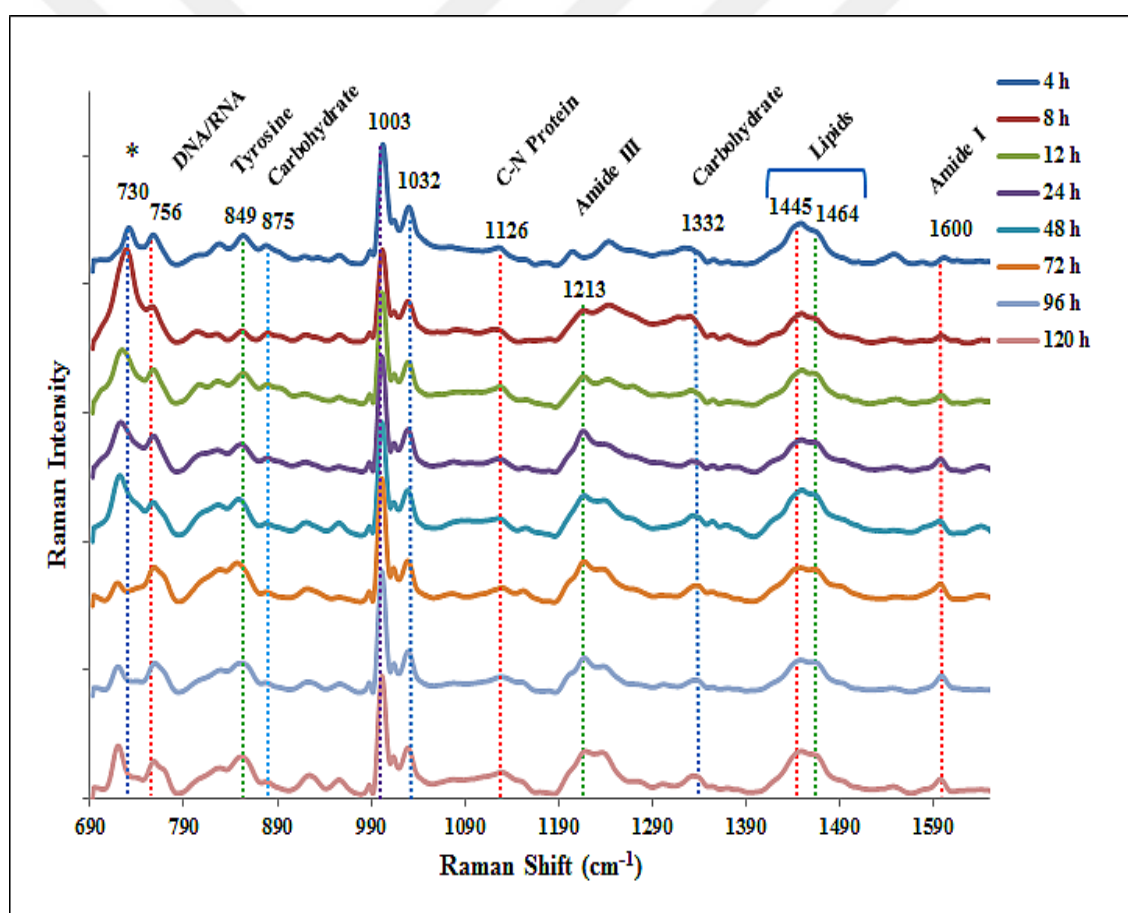


Figure 4.10. SERS spectra of *S. epidermidis* biofilm formation at different cultivation times between 4 and 120 h.

Figure 4.11 shows the SERS spectra of *C. albicans* biofilm formation at increasing incubation times between 4 and 120 h. The biofilm characteristic of *C. albicans* was demonstrated in the literature. *C. albicans* are metabolically very active in the first 8 h and

increase the cell number until maturation phase of biofilm formation. The enrichment of the matrix composition was observed with the accumulation of the biofilm process until 24 h and 48 h [269]. The band patterns of 837 cm^{-1} and 869 cm^{-1} attributed to tyrosine and carbohydrates, respectively, changed after the early phase of biofilm formation at 24 h and 48 h incubation times. The intensities of Amide III and Amide I bands at 1250 cm^{-1} , 1267 cm^{-1} and 1610 cm^{-1} also increased significantly at accumulative phase of biofilm formation (24-48h). The intensity of the band attributed to C-N stretching of proteins and the intensity of the bands at 1454 cm^{-1} and 1473 cm^{-1} , which are attributed to lipids, increased with the maturation of biofilm formation at 72 h incubation. After the 72 h incubation, the bands, which are attributed to proteins, could not be observed clearly due to decreasing penetration ability of AgNPs into the matured biofilm composition. In conclusion, the significant changes in the metabolic activities of *C. albicans* started to be observed after early phase of biofilm formation.

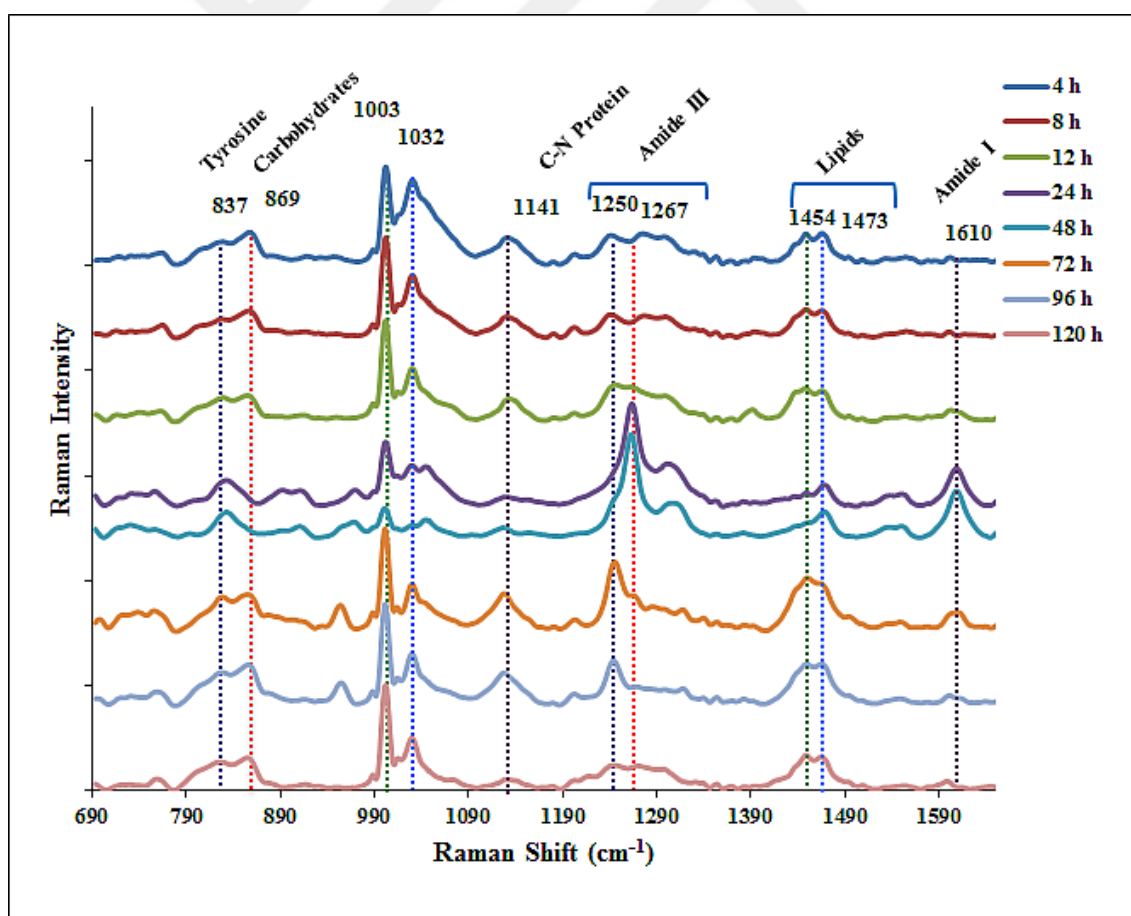


Figure 4.11. SERS spectra of *C. albicans* biofilm formation at different cultivation times between 4 and 120 h.

Figure 4.12 shows the SEM images of biofilms formed by *P. aeruginosa* on agar plates at incubation times between 4 and 120 h. As it is seen from the images, at 4 h incubation time bacteria cells could be observed individually, but with increased incubation time, a biofilm shell formed on the cells, which made it difficult to obtain SEM images from agar samples of *P. aeruginosa*. The SEM images showed the formation of biofilm, where the cells attached to the agar surface as well as each other irreversibly, and formed a layer on the agar surface.

Figure 4.13 shows the SEM images of *S. epidermidis* at incubation times between 4 and 120 h. The proliferation of microorganisms could be clearly seen from the SEM images with increasing incubation time. After 48 h incubation, the 3D shape of biofilm formation was observed, where the cells were imbricated.

Figure 4.14 shows the SEM images of agar samples of *C. albicans* at 4-120 h incubation times. The number of yeast cells increased during with increasing incubation time and again the 3D shape of biofilm formation after 48 h incubation was observed. At 96 h and 120 h incubation times, dead cells were also observed on the SEM images, which could occur due to nutrient depletion.

Biofilm samples of *P. aeruginosa*, *S. epidermidis* and *C. albicans* were evaluated with CLSM as seen in Figure 4.15-4.17. FilmTracer SYPRO Ruby biofilm matrix stain was used to stain proteins in the biofilm matrix. In CLSM images of *P. aeruginosa* (Figure 4.15), the individual cells could only be observed at incubation times 4 and 8 h. The microorganisms formed a smooth biofilm shell covering the whole surface. Although it was not possible to obtain clear images from biofilm samples, the thickness of the biofilm layer could be determined. It was found that the thickness of the biofilm increased in parallel with increasing incubation times; 7.96, 14.43, 28.00, 32.70, 44.24 μm at incubation times between 24-120 h, respectively. A significant cell aggregation and biofilm layer formation of *S. epidermidis* and *C. albicans* with increasing incubation times could be observed in Figures 4.16 and 4.17.

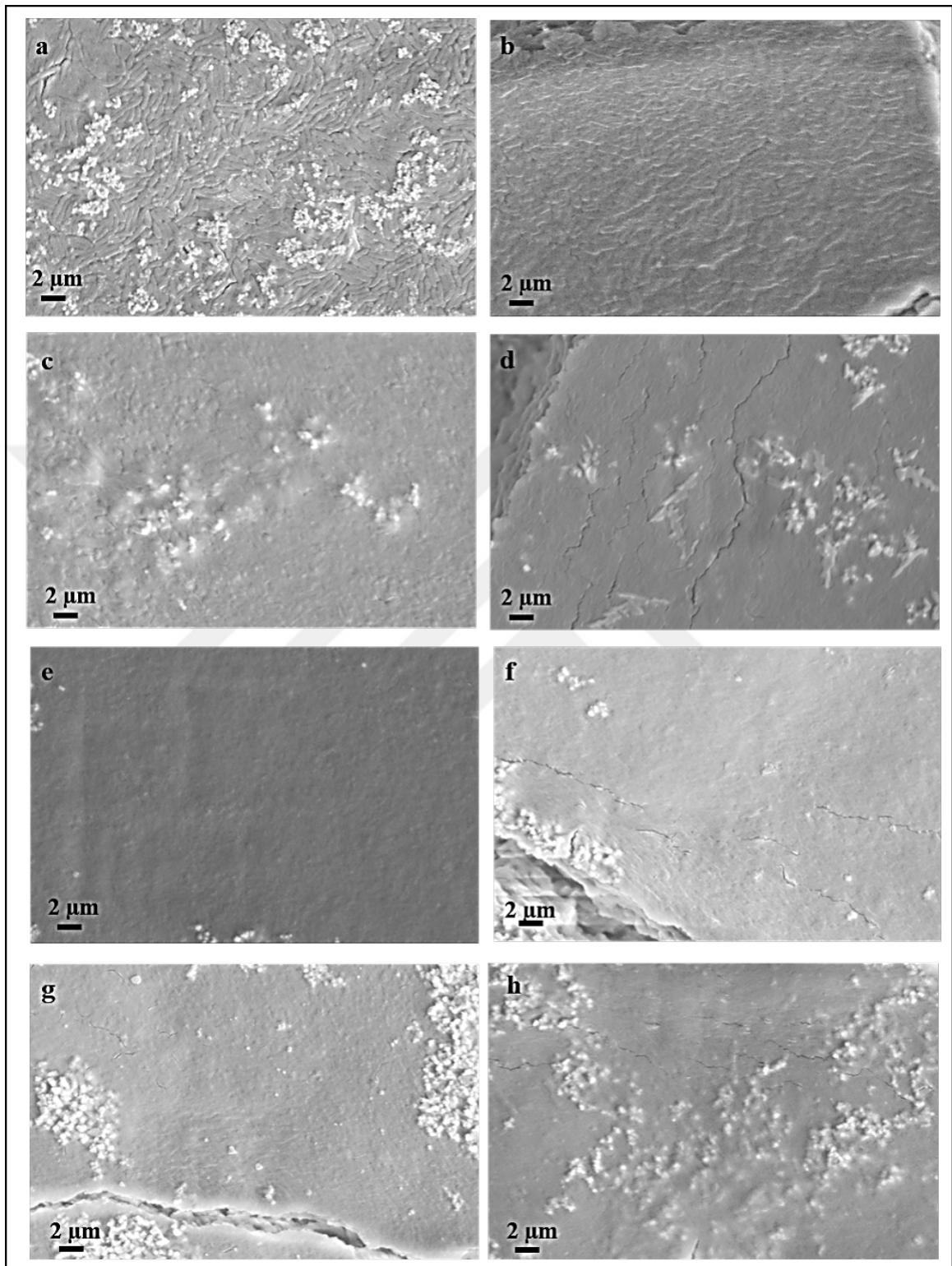


Figure 4.12. SEM images of *P. aeruginosa* biofilm formation at different cultivation times between (a-h) 4 and 120 h. Scale bars are 2 μm.

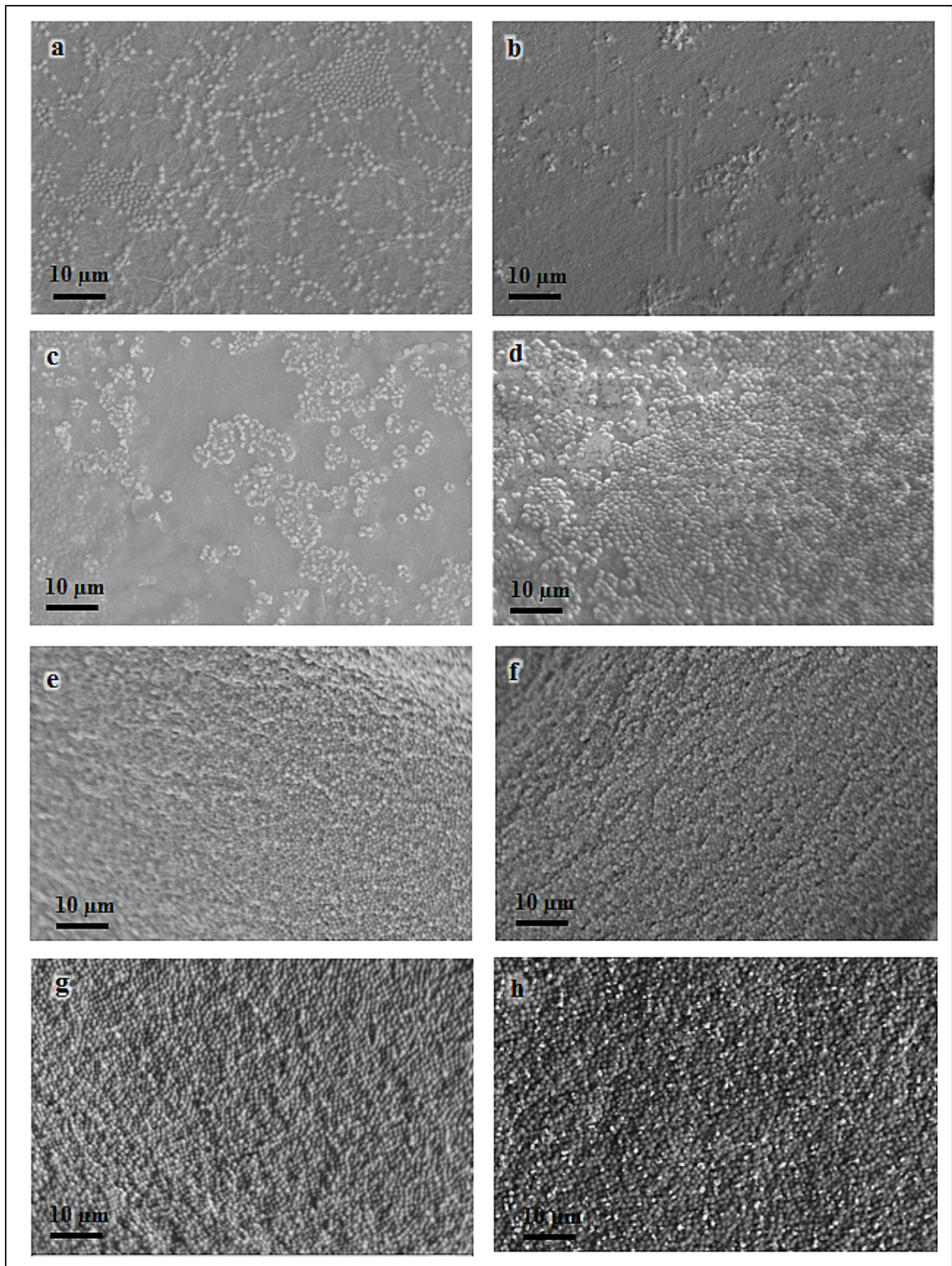


Figure 4.13. SEM images of *S. epidermidis* biofilm formation at different cultivation times between (a-h) 4 and 120 h. Scale bars are 10 μm.

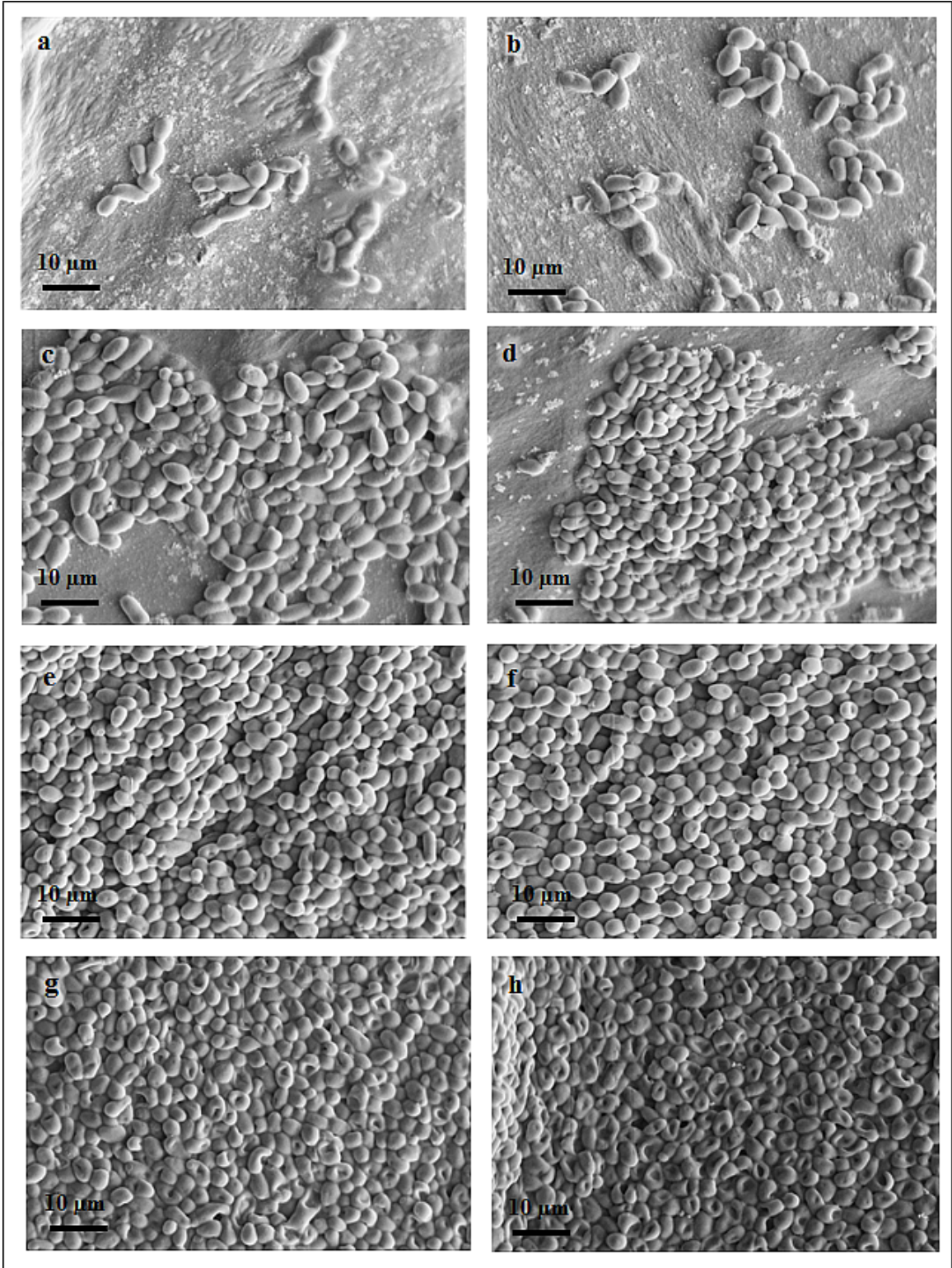


Figure 4.14. SEM images of *C. albicans* biofilm formation at different cultivation times between (a-h) 4 and 120 h. Scale bars are 10 µm.

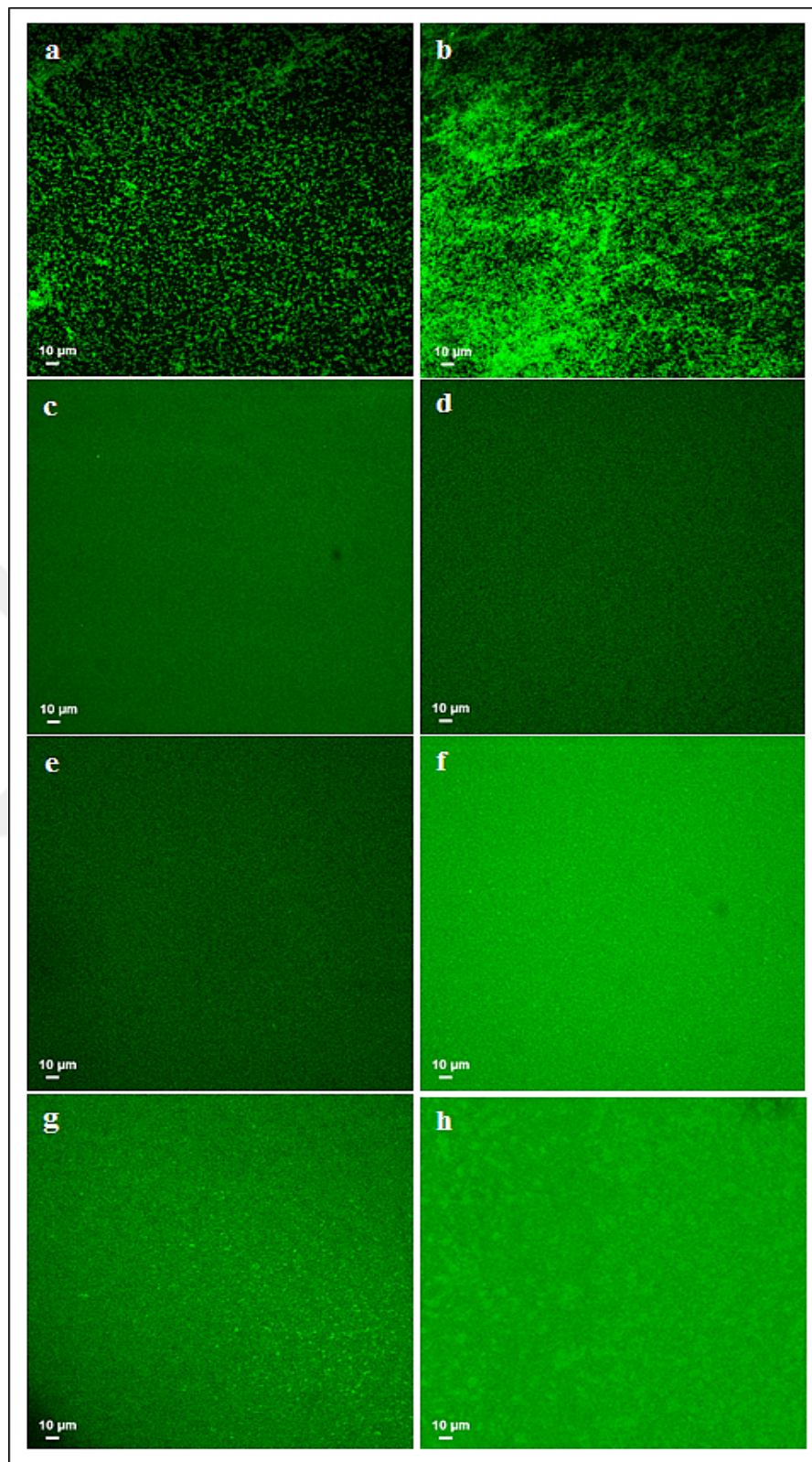


Figure 4.15. CLSM images of *P. aeruginosa* biofilm formation at different cultivation times between (a-h) 4 and 120 h. Scale bars are 10 μm.

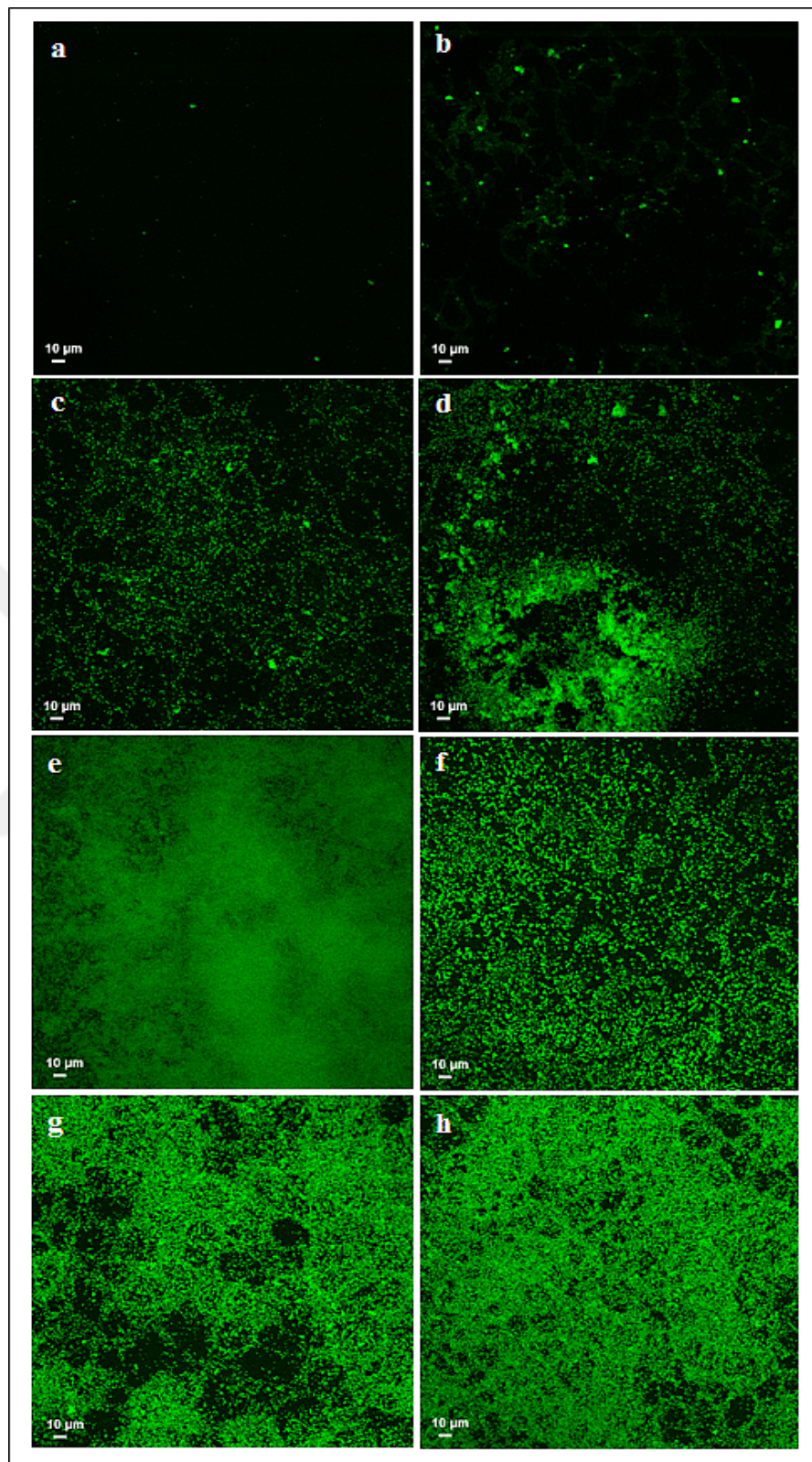


Figure 4.16. CLSM images of *S. epidermidis* biofilm formation at different cultivation times between (a-h) 4 and 120 h. Scale bars are 10 μm.

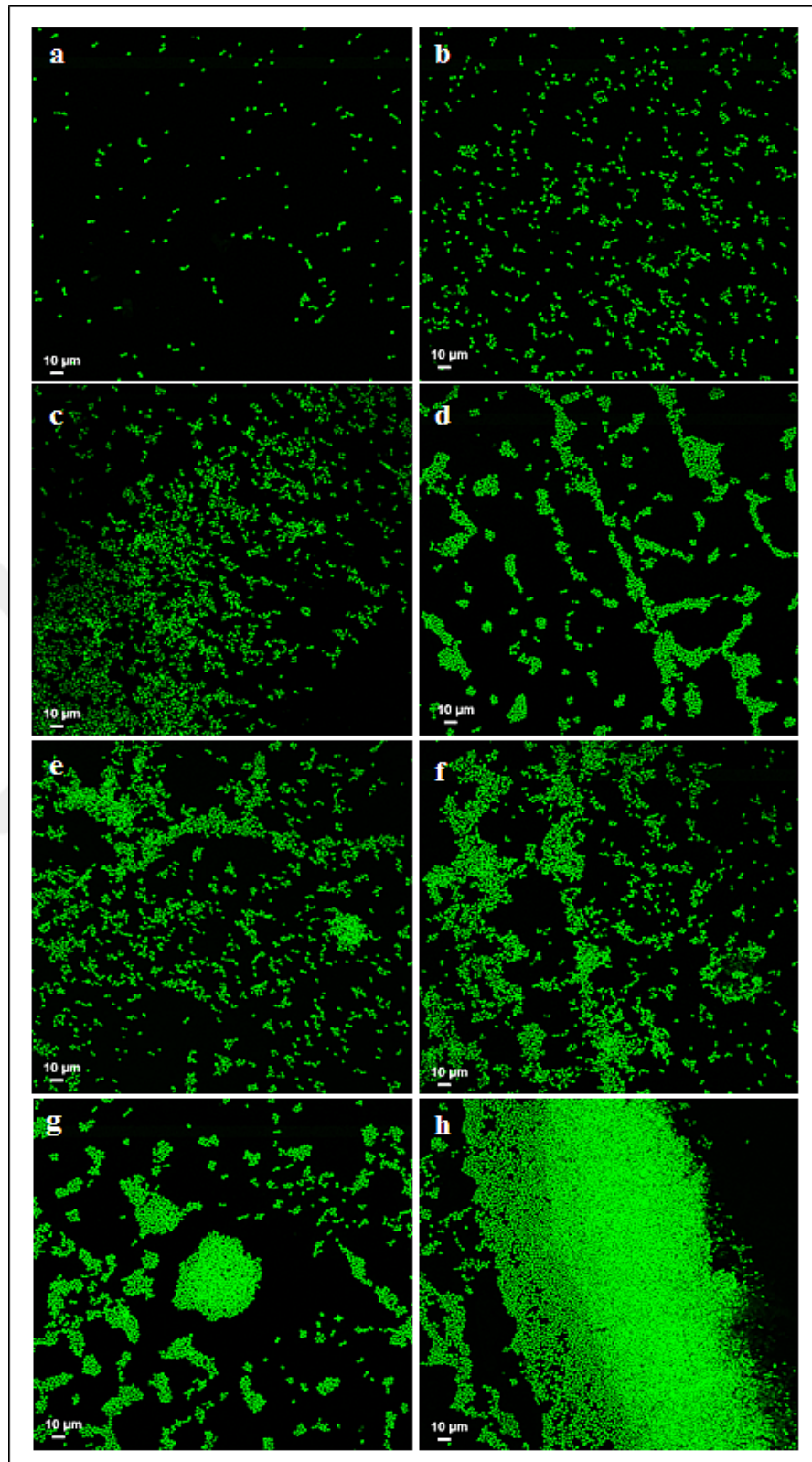


Figure 4.17. CLSM images of *C. albicans* biofilm formation at different cultivation times between (a-h) 4 and 120 h. Scale bars are 10 µm.

4.4.2. 2D PMMA Substrates

The SERS spectrum of 2D PMMA substrate was obtained to clarify the possible interferences from the background as seen in Figure 4.18. A droplet of AgNPs colloidal suspension was added on the polymeric substrate and SERS measurements were performed after the droplet got dried. A sharp peak was observed at 1062 cm^{-1} from the PMMA substrate as a background.

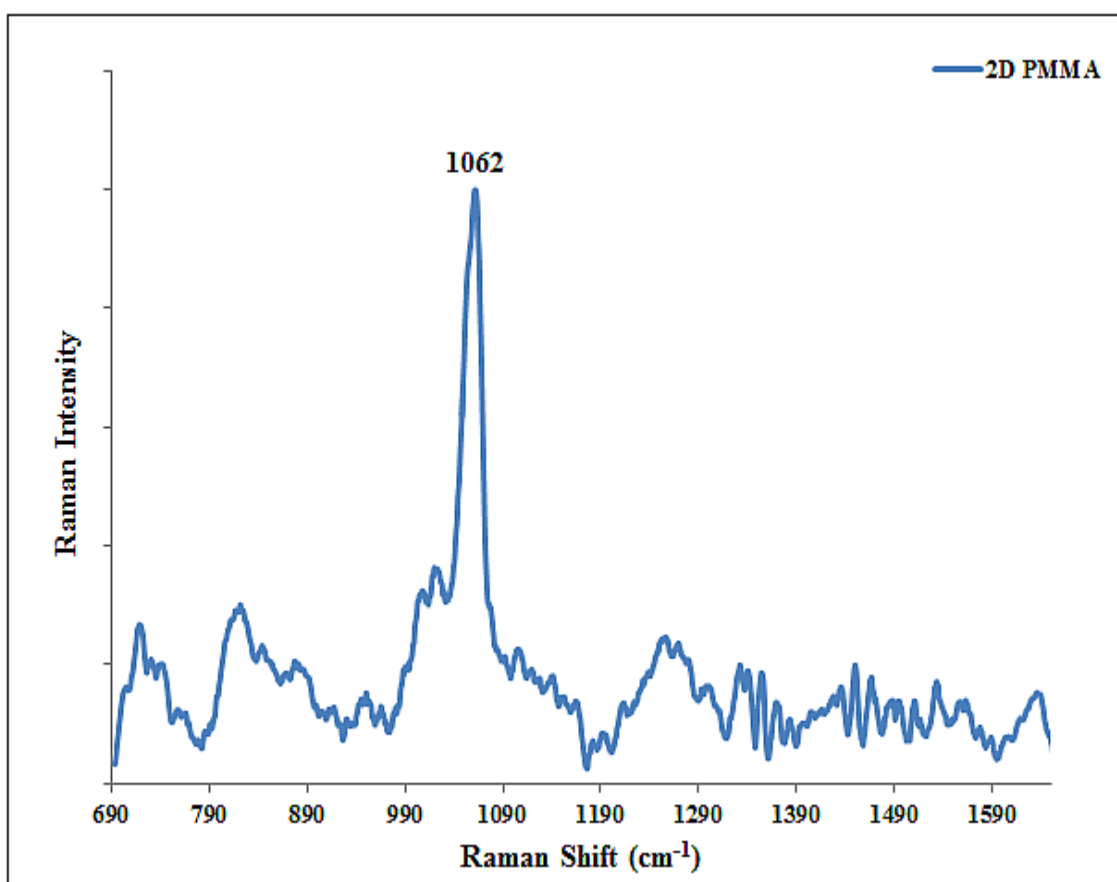


Figure 4.18. SERS spectra of a 2D PMMA substrate.

The metabolic activity changes of *P. aeruginosa* on a 2D PMMA substrate during biofilm formation is given in Figure 4.19. The peaks at 1355 , 1405 , 1489 , 1562 , 1600 and 1618 cm^{-1} attributed to pyocyanin, COO^- stretching of carbohydrates, adenine, Amide II and Amide I and these peaks appeared suddenly after 8 h incubation and their intensities increased rapidly during incubation. 72 h incubation time was especially very important for *P. aeruginosa* on a 2D PMMA substrate because a very sharp change was observed on the spectral pattern. The intensity change in determined peaks demonstrated the increased

expression of protein, carbohydrate and pyocyanin with the maturation of biofilm. It is possible to designate the 72 h as a time point of maturation of biofilm due to the intensity decrease at the peak 730 cm^{-1} belonging to purine bases. However, an intensity increase was observed at the peak belonging to adenine ring stretching mode as a result of eDNA synthesis as a biofilm component. The sticky polymeric shell coated the cells at 72 h incubation time and prevented their interaction with AgNPs.

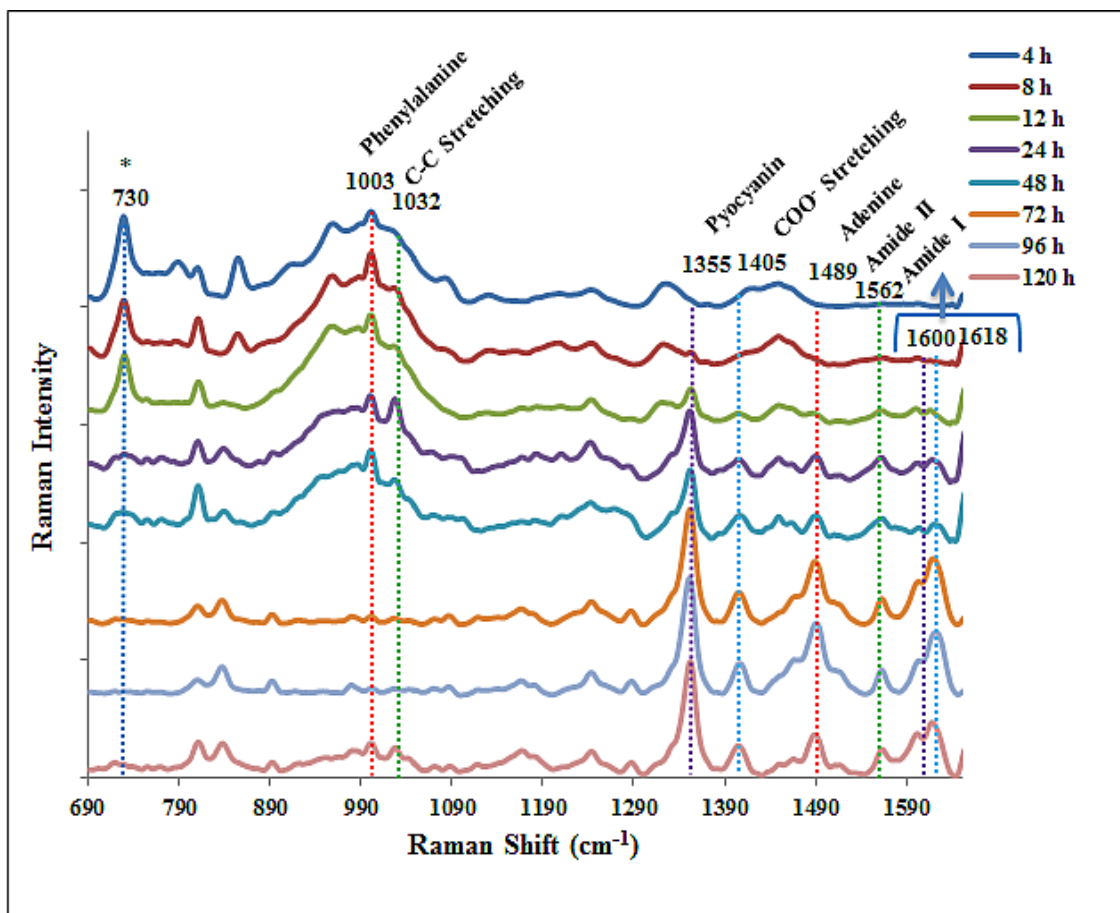


Figure 4.19. SERS spectra of *P. aeruginosa* biofilm formation at different cultivation times between 4 and 120 h.

The supportive studies in the literature shows that eDNA has a very important role in biofilm formation, which acts as an antibiotic barrier and provides the mechanical strength of the structure along with polysaccharides and proteins [51, 52]. One can conclude that surface properties can change the metabolic activity of *P. aeruginosa* during biofilm formation. Although 24 h was determined as a time point for biofilm regulation on agar plates, the accumulation of the process reduced on 2D PMMA substrates.

The spectra obtained during the biofilm formation of *S. epidermidis* are given in Figure 4.20 at cultivation times between 4-120 h. The metabolic activity of *S. epidermidis* was very slow on hydrophobic PMMA surface, in which it is known that *S. epidermidis* is widely forms biofilm on human skin and mucosa membranes beside hydrophobic medical implants [153]. Polymeric carbohydrates and proteins have primary roles for intercellular adhesion and providing resistance to neutrophils and antibiotics on a host surface [75-77, 80, 81]. The determined peaks on *S. epidermidis* SERS spectra were consistent with the literature reports. The peaks belonging to phenylalanine, C-C, C-O, C-C and C-N stretching and Amide I of proteins and COO⁻ stretching of carbohydrates showed a slight increase in the intensities with the formation of biofilm. A distinct change was observed in spectral pattern at incubation time 96 h. Although an indefinite fluctuation throughout incubation was observed in the intensity of the peak at 730 cm⁻¹, attributed to purine bases, due to the heterogenic structure of the biofilm, a distinct intensity increase was observed at 96 h incubation with enrichment of the biofilm component with carbohydrates and proteins.

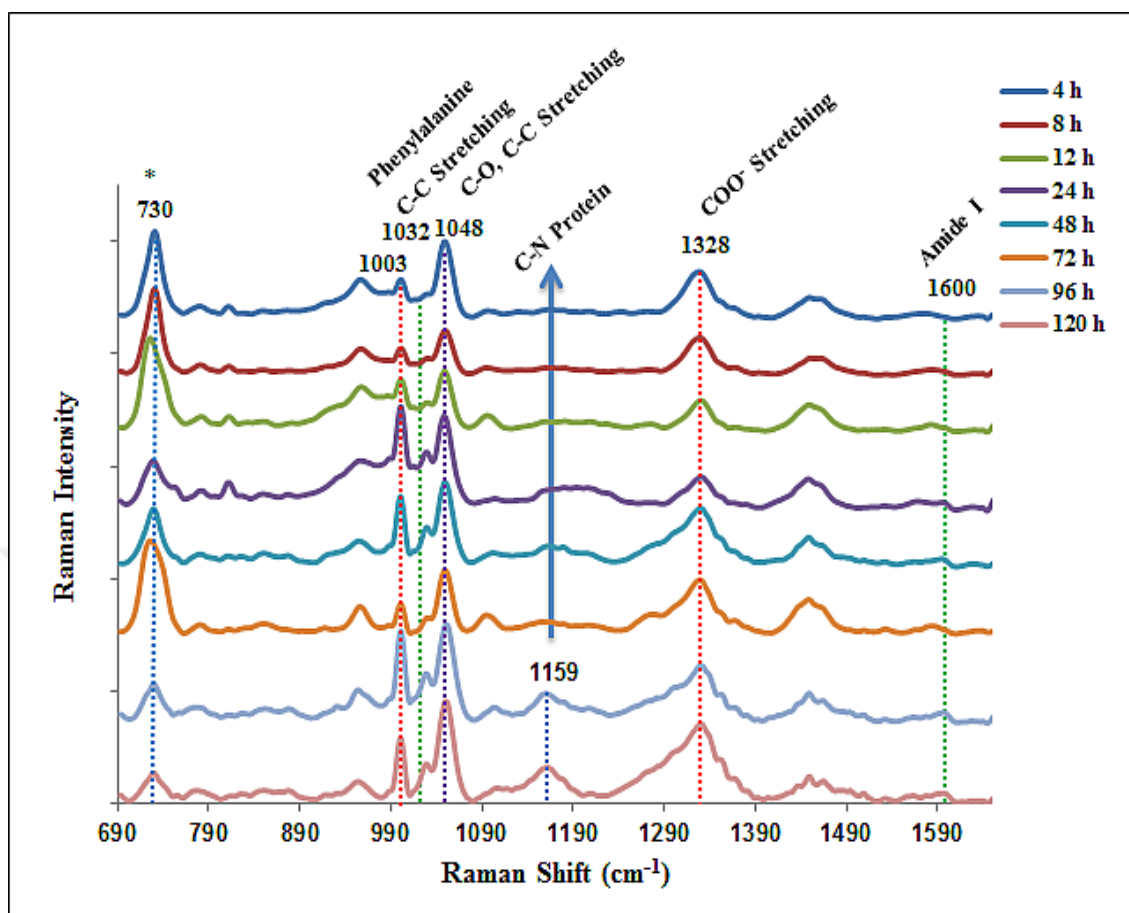


Figure 4.20. SERS spectra of *S. epidermidis* biofilm formation at different cultivation times between 4 and 120 h.

Figure 4.21 shows the SERS spectra of biofilm formation of *C. albicans* on 2D PMMA substrates. The intensity of the carbohydrate peaks at 955, 1032, 1045 and 1322 cm^{-1} increased with accumulation of biofilm during the incubation and showed an impressive fluctuation after 48 h. It has recently been assigned that arabinose, mannose, glucose, and xylose are the main polysaccharides synthesis by *C. albicans* constituted a significant part of a mature biofilm [91]. An increase in protein and lipid content in *C. albicans* biofilm was also determined with the increased intensities of the peaks at 1242 and 1450 cm^{-1} . Different from *P. aeruginosa* and *S. epidermidis*, it was observed that purine bases were expressed in increasing amounts over time at 730 cm^{-1} .

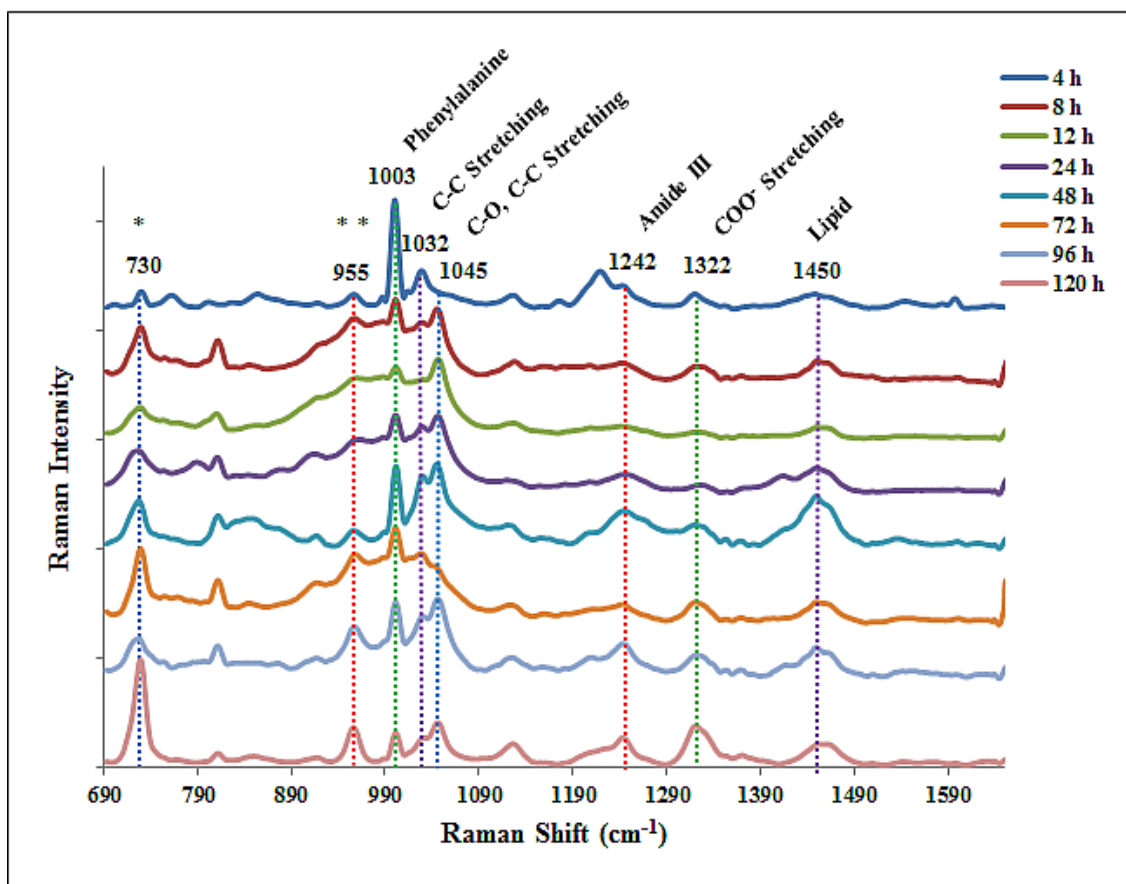


Figure 4.21. SERS spectra of *C. albicans* biofilm formation at different cultivation times between 4 and 120 h.

SEM images of biofilm formation of *P. aeruginosa*, *S. epidermidis* and *C. albicans* are given in Figure 4.22, 4.23 and 4.24. Colony growth and assembly on the polymeric surface could be observed from the images. The aggregation of the cells and formation 3D architecture was also seen at increased incubation times. Pseudohyphae morphology of *C. albicans* and daughter and mother cells could be also observed clearly at incubation times 4 and 8 h before the cells imbricated.

Biofilm samples were characterized with CLSM as seen in Figure 4.25, 4.26 and 4.27. Formation of extracellular matrix and cell aggregates could be seen significantly after incubation 72 h for *P. aeruginosa*, 96 h for *S. epidermidis* and 48 h for *C. albicans* consistent with SERS measurements.

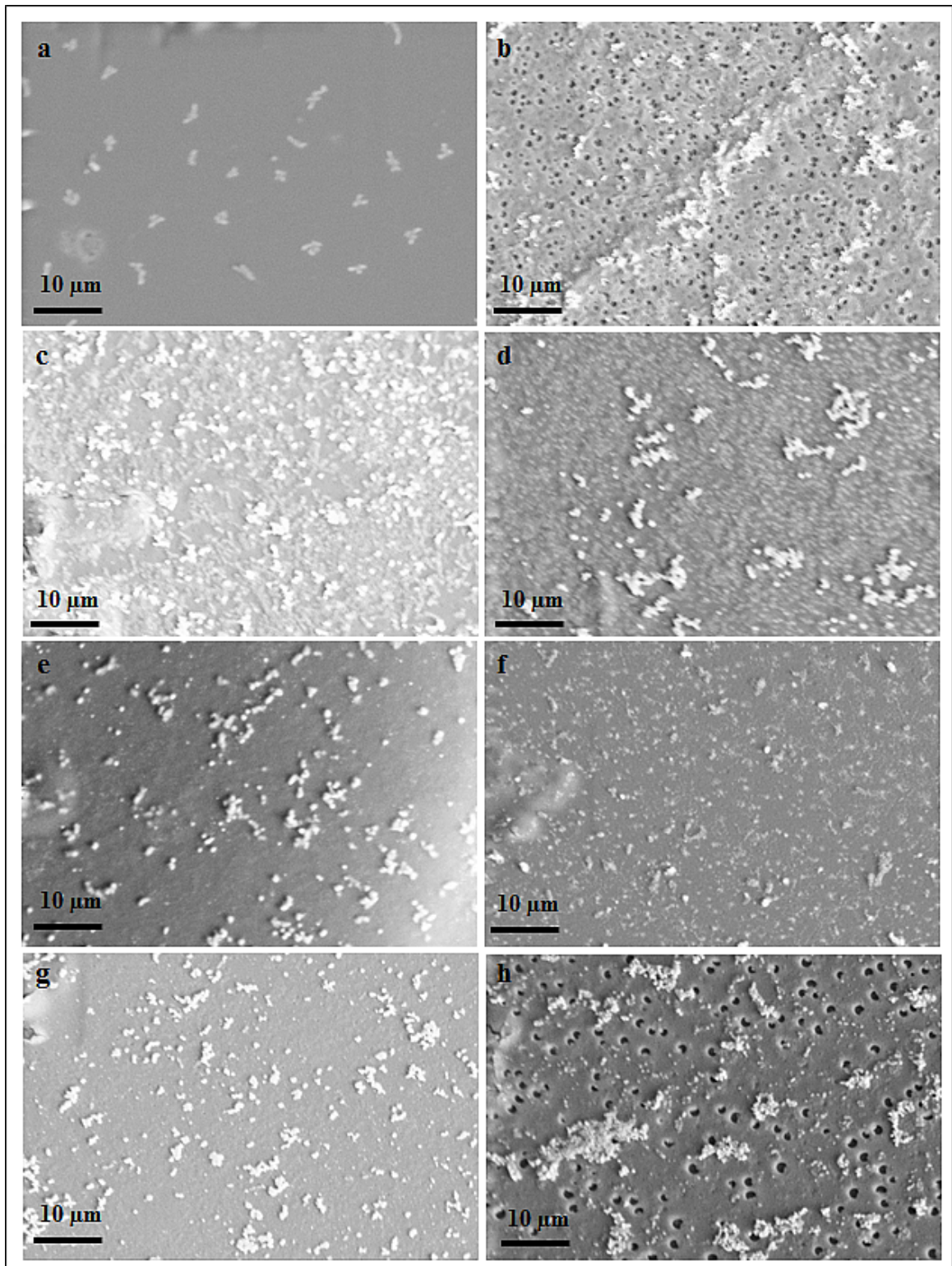


Figure 4.22. SEM images of *P. aeruginosa* biofilm formation at different cultivation times between (a-h) 4 and 120 h. Scale bars are 10 μm.

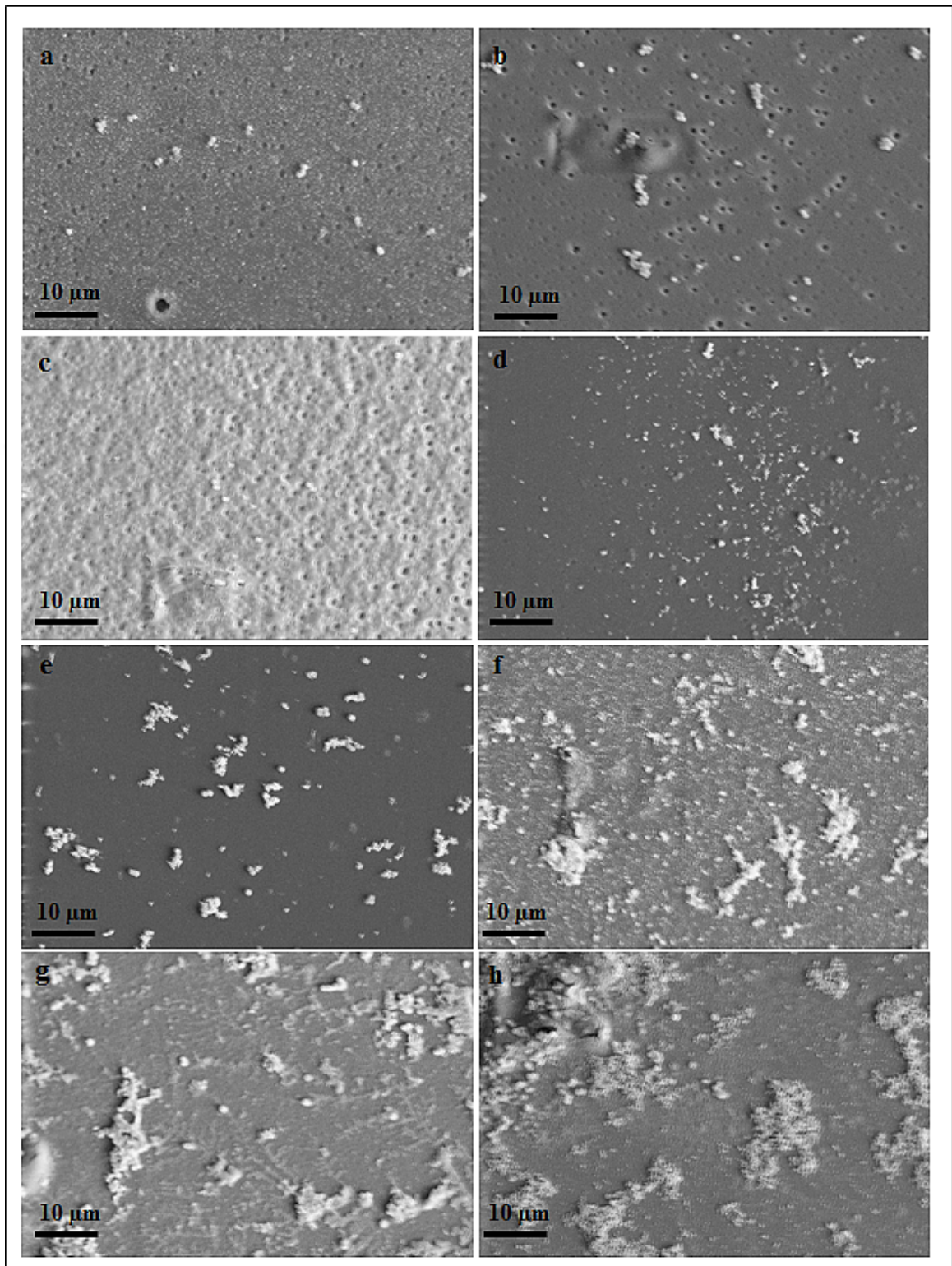


Figure 4.23. SEM images of *S. epidermidis* biofilm formation at different cultivation times between (a-h) 4 and 120 h. Scale bars are 10 µm.

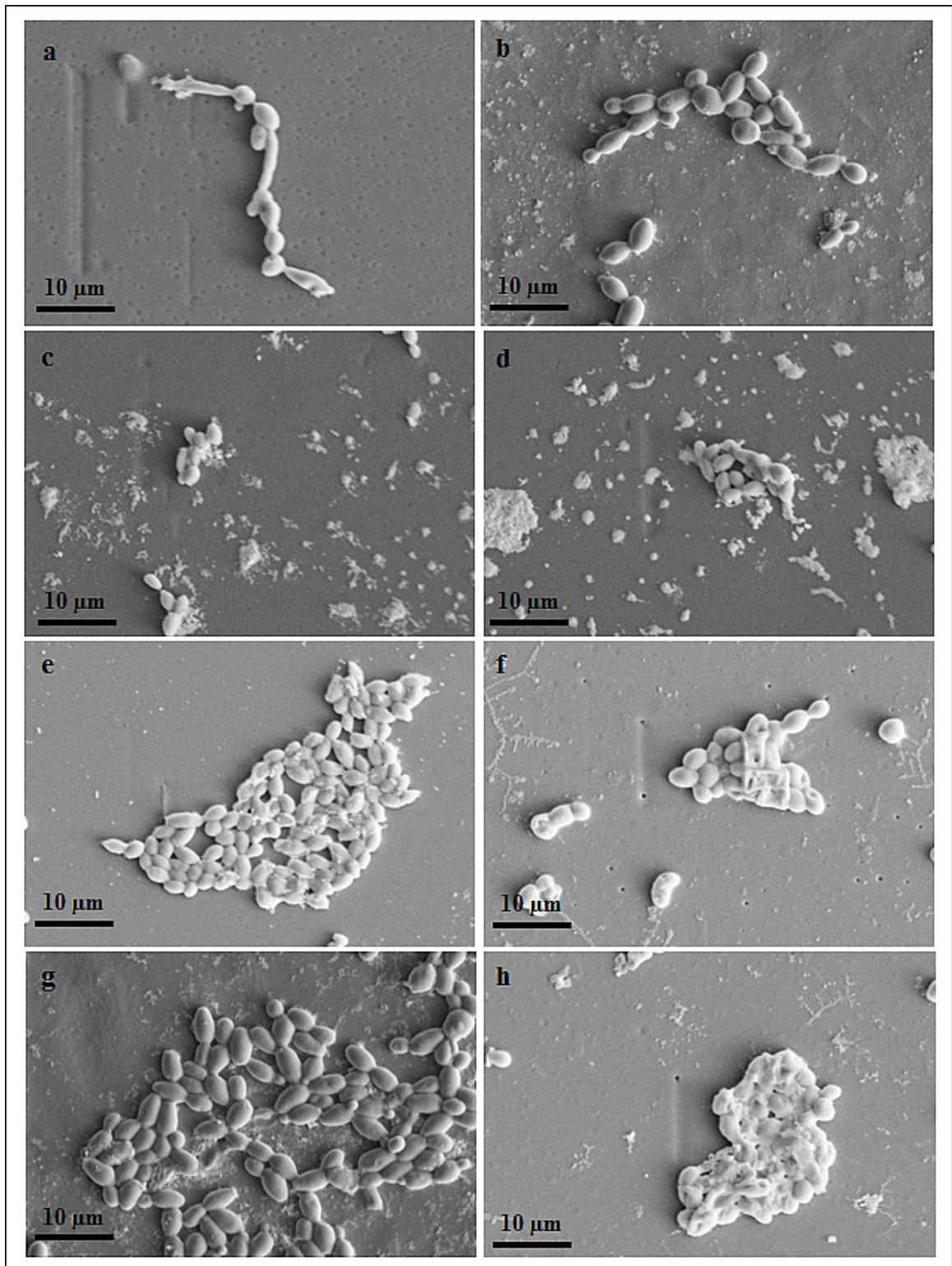


Figure 4.24. SEM images of *C. albicans* biofilm formation at different cultivation times between (a-h) 4 and 120 h. Scale bars are 10 μm.

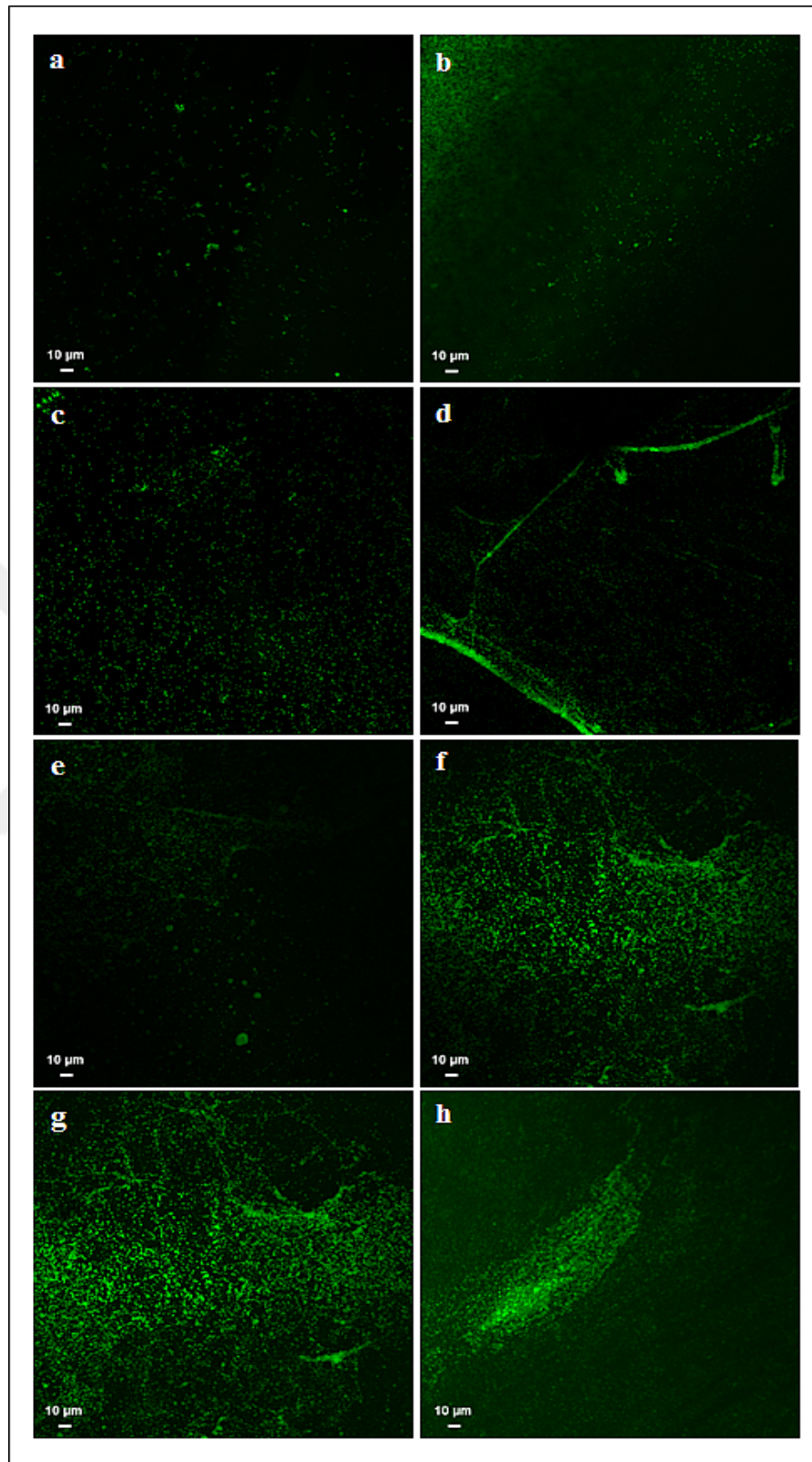


Figure 4.25. CLSM images of *P. aeruginosa* biofilm formation at different cultivation times between (a-h) 4 and 120 h. Scale bars are 10 μm.

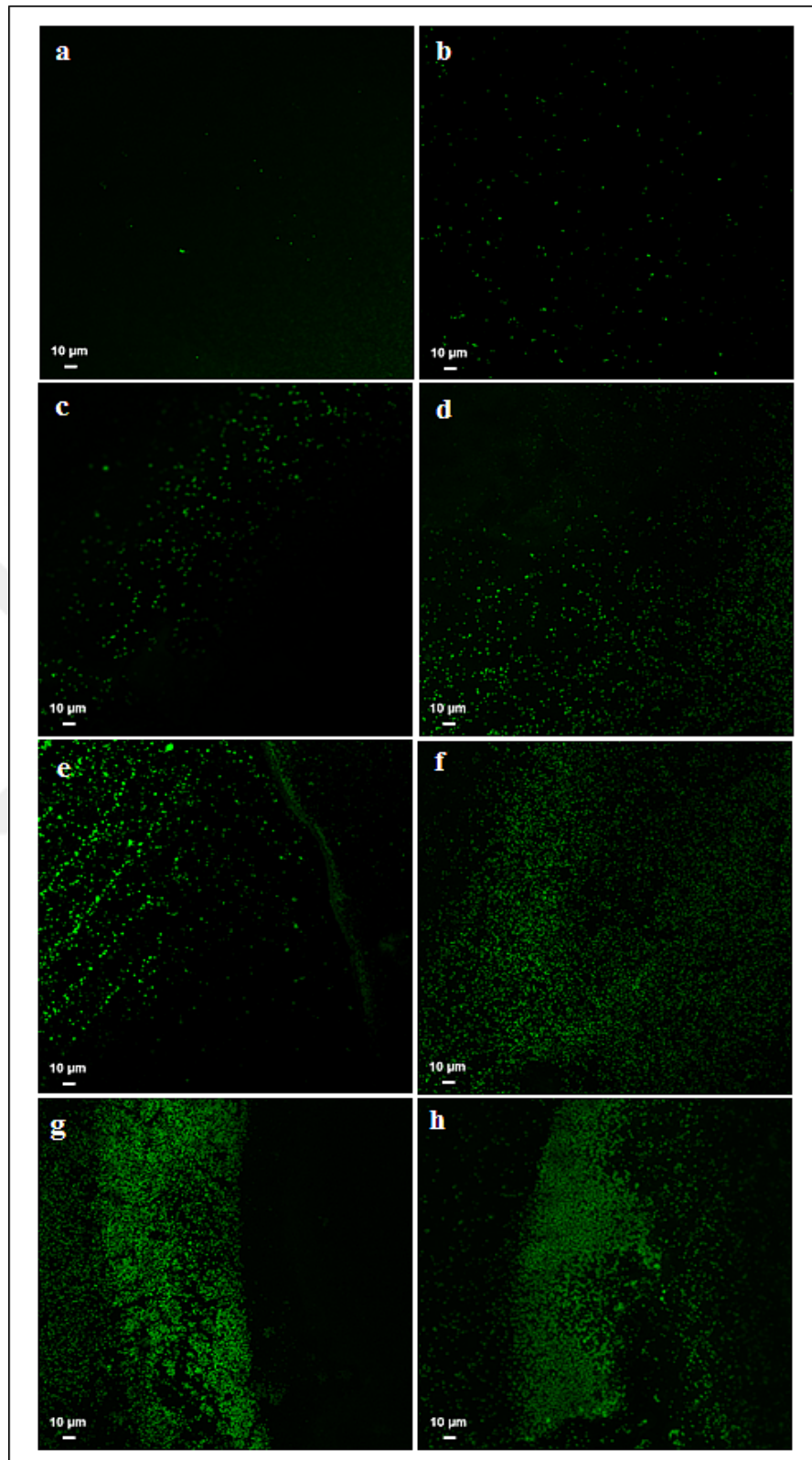


Figure 4.26. CLSM images of *S. epidermidis* biofilm formation at different cultivation times between (a-h) 4 and 120 h. Scale bars are 10 μm.

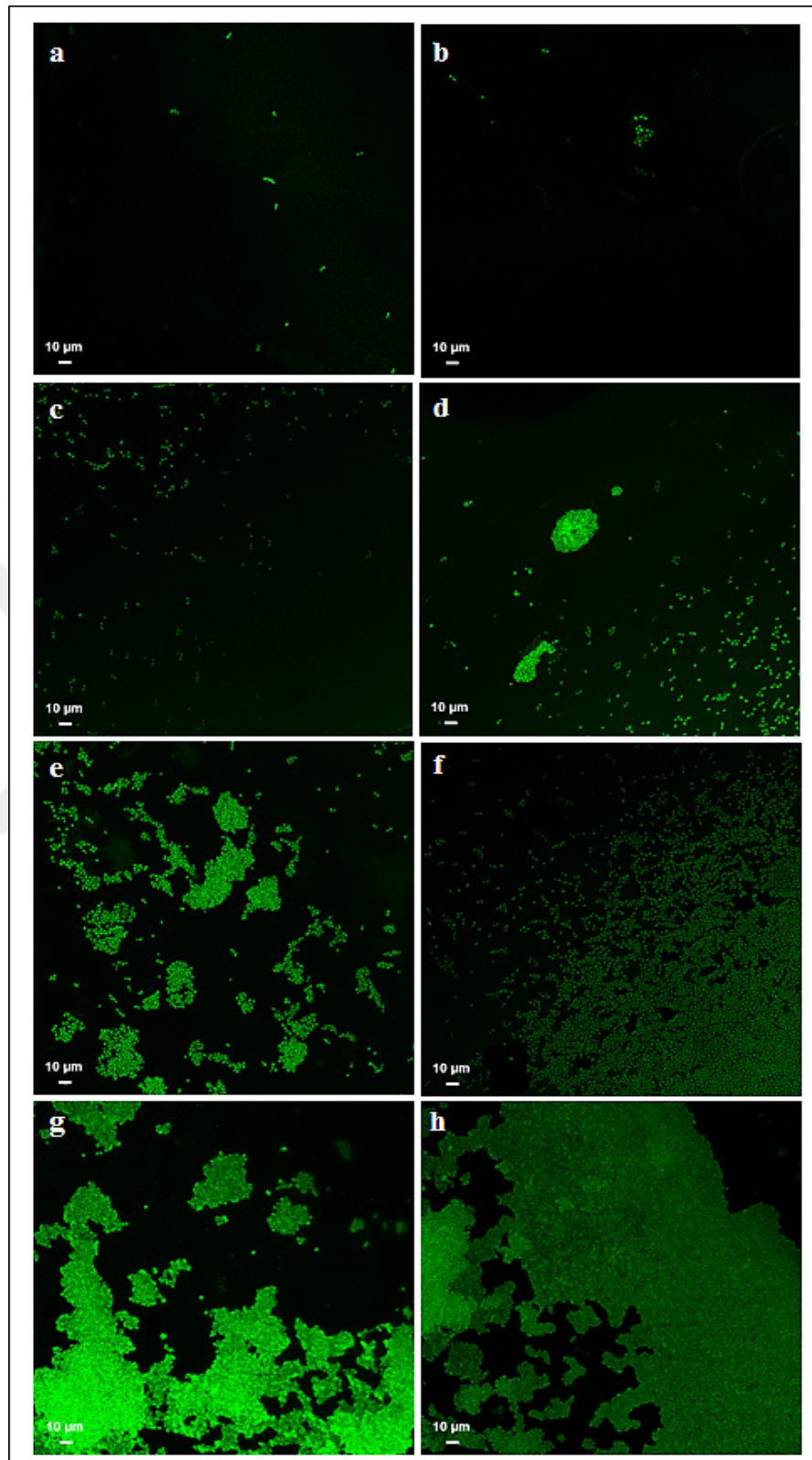


Figure 4.27. CLSM images of *C. albicans* biofilm formation at different cultivation times between (a-h) 4 and 120 h. Scale bars are 10 μm.

4.4.3. 3D PMMA Substrates

SERS spectra of 3D PMMA substrates incubated in TSB, NB and SDB is given in Figure 4.28. The fibrous structure of the PMMA substrate has the ability to absorb the liquid media in biofilm experiments. Therefore, to obtain the real background spectra the polymeric surfaces were incubated in liquid medium. The excess amount of liquid medium was removed after incubation and 10 μl of AgNPs suspension was dropped onto the PMMA substrate and waited until it dried. The SERS measurements were performed and the peak observed at 730 cm^{-1} attributed to glycosidic ring of polysaccharides included in liquid media [186]. The peaks at 955 cm^{-1} and 1324 cm^{-1} attributed to COO^- stretching and C-N stretching of proteins were observed at 1128 cm^{-1} [185]. Phenylalanine, C-C stretching, Amide III and CH_2/CH_3 deformation of lipids peaks were also observed at $1003, 1032, 1245$ and 1464 cm^{-1} belonging to the liquid media [233, 259, 260].

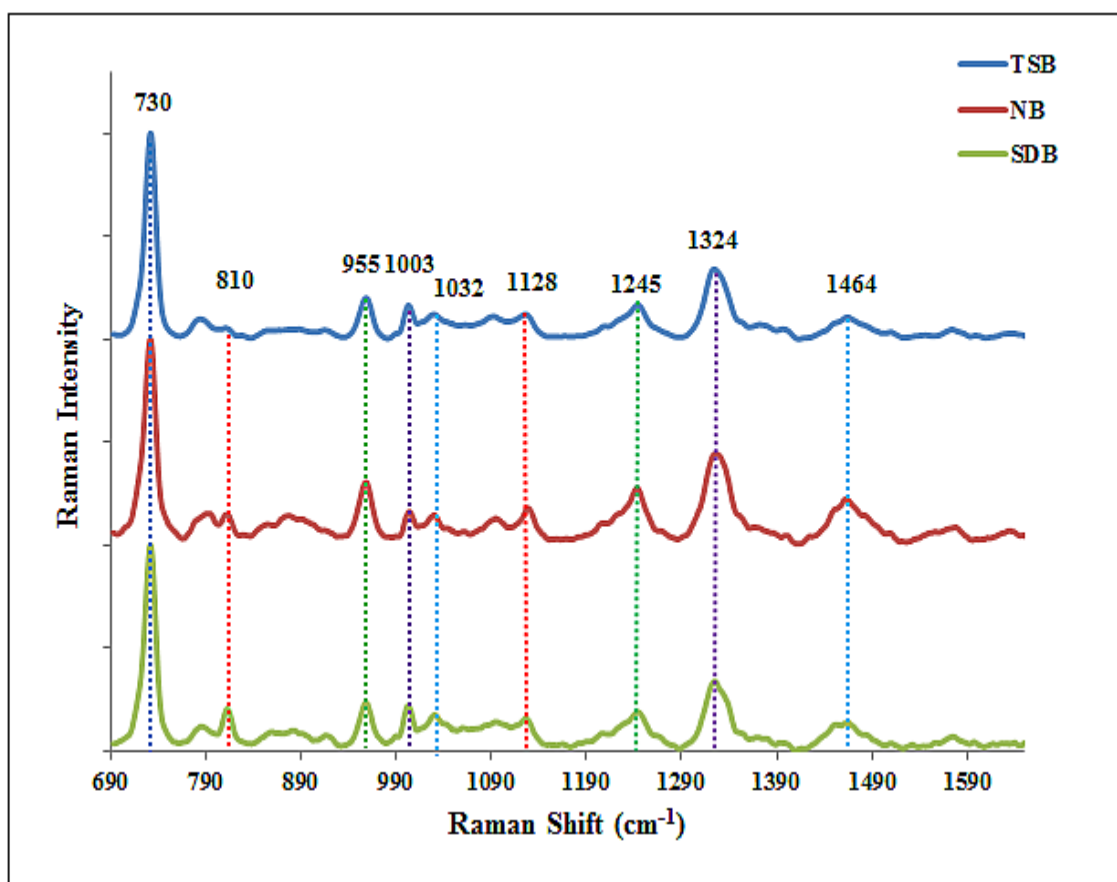


Figure 4.28. SERS spectra of 3D PMMA substrates incubated with TSB, NB and SDB.

The main metabolic change of *P. aeruginosa* was observed after 72 h during biofilm formation on 3D PMMA substrates as seen from the SERS spectra in Figure 4.29. A slight increase was observed in the intensity of the peaks belonging to pyocyanin observed at 1087, 1120, 1173 and 1355 cm^{-1} at 72 h incubation. It should be noted that there was not always a linear change in the spectral pattern. The observed fluctuations on peak intensities between the incubation times were the result of the non-smooth fibrous surface of the polymeric substrate. However, an instantaneous change was observed on the peaks of Amide III and Amide I of proteins, COO^- stretching of carbohydrate and adenine peaks after 72 h.

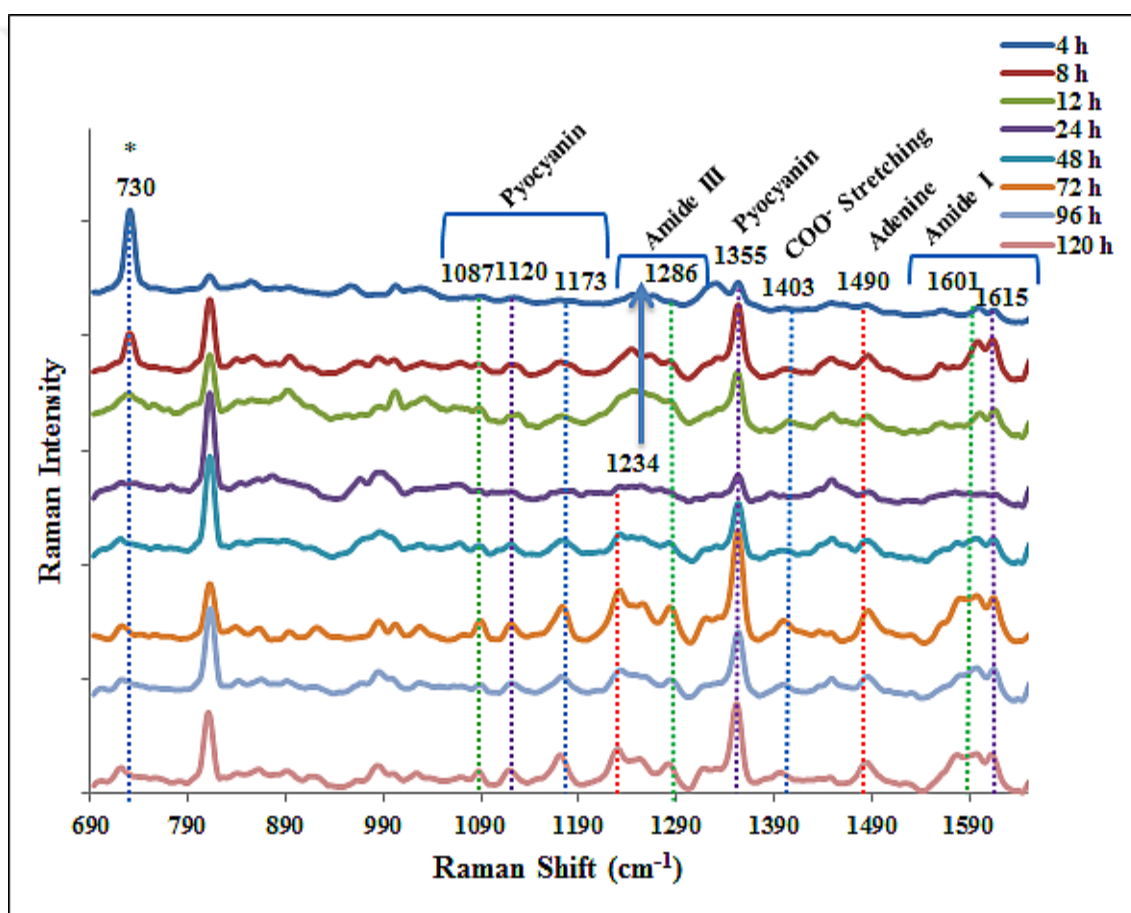


Figure 4.29. SERS spectra of *P. aeruginosa* biofilm formation at different cultivation times between 4 and 120 h.

SERS spectra of *S. epidermidis* at cultivation times between 4-120 h is given in Figure 4.30. A significant change was not observed in the amount of protein and carbohydrate synthesis during the incubation period. A slight increase was noticed in the intensity of the peaks at 1086, 1217 and 1569 cm^{-1} belonging to C-O, C-C stretching, Amide III and

Amide II, respectively. The first significant adhesion on the surface was observed at 24 h indicated the expression of the carbohydrate and protein. Fibrillary proteins have a major role on initial adhesion of microorganisms and early maturation of biofilm [84]. Also, note that the biofilm component PIA enhanced the intercellular adhesion, which can explain the correlated increase of carbohydrate and proteins at the same cultivation time [76]. We can conclude that *S. epidermidis* entered the early maturation phase of the biofilm during this incubation period at 120 h.

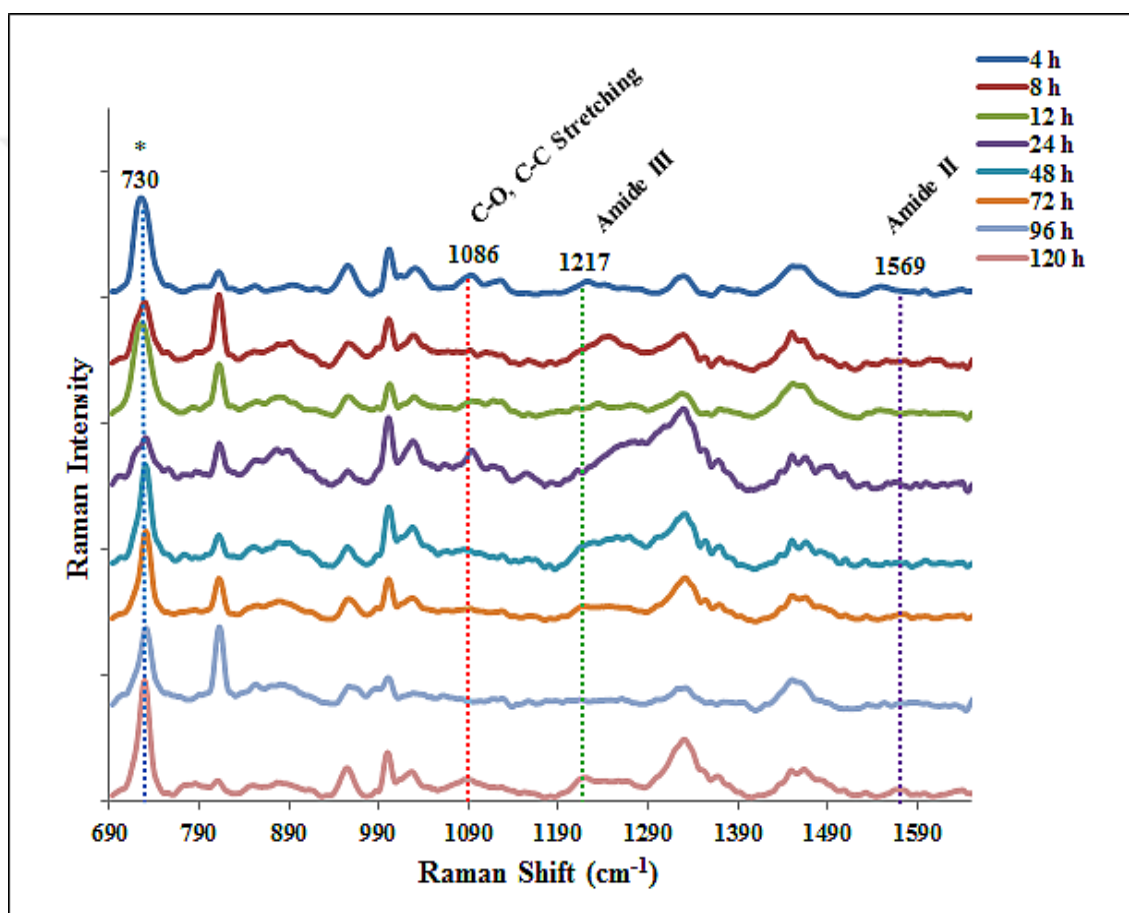


Figure 4.30. SERS spectra of *S. epidermidis* biofilm formation at different cultivation times between 4 and 120 h.

The main metabolic activity of biofilm formation of *C. albicans* on 3D PMMA substrates can be evaluated from the SERS spectra given in Figure 4.31. Biofilm matrix enrichment was observed especially at 48 and 72 h incubation times. Carbohydrate, protein and eDNA synthesis increased dramatically as seen from the peaks at 791, 873, 907, 1260, 1413, 1527 and 1610 cm^{-1} . The hydrophobic polymeric substrate increased the adaption and biofilm formation period of the yeast cells because main metabolic activity of *C. albicans* were

observed at 24 and 48 h on agar plates. Also, the fibrous structure of the surface can affect the obtained results. The yeast cells tended to be buried in the depths of polymeric fibers, which slowed down the interaction of the metabolites with AgNPs.

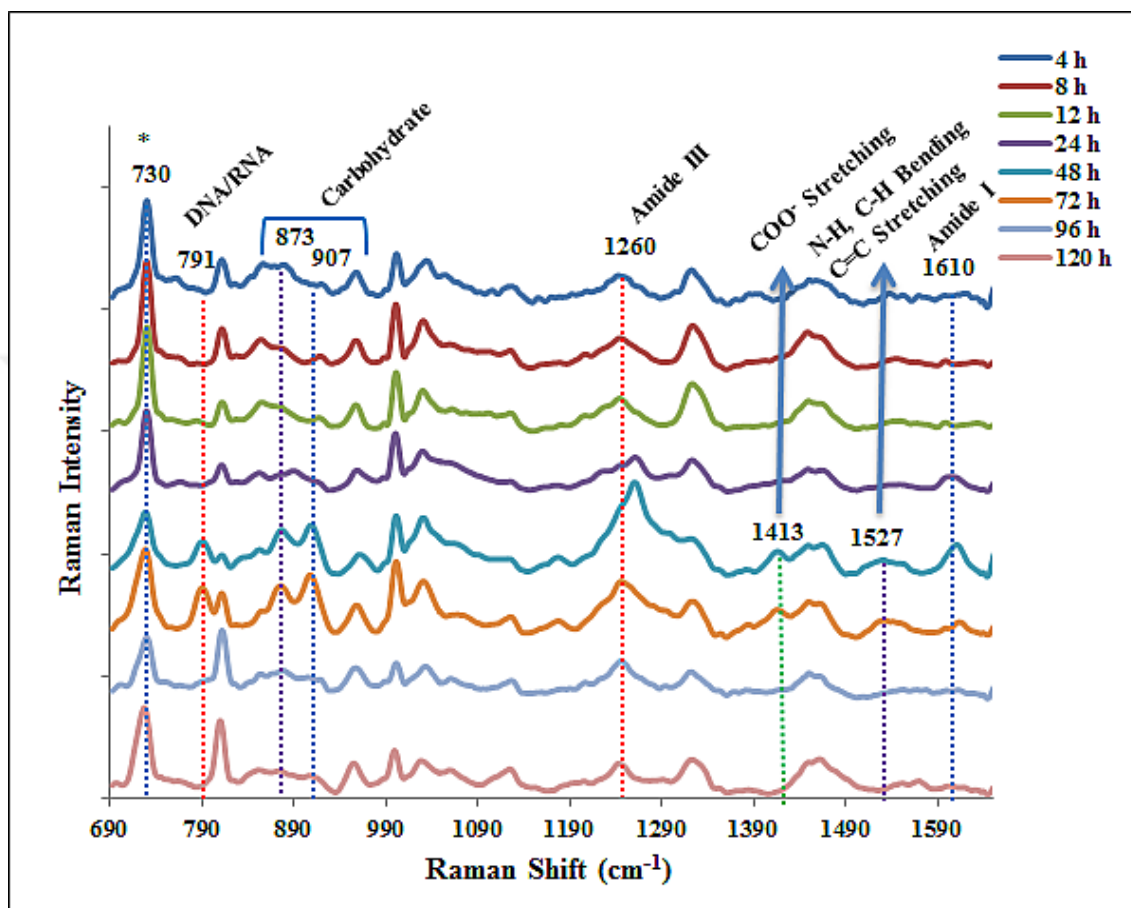


Figure 4.31. SERS spectra of *C. albicans* biofilm formation at different cultivation times between 4 and 120 h.

SEM images of biofilm samples of *P. aeruginosa*, *S. epidermidis*, and *C. albicans* can be seen in Figure 4.32, 4.33 and 4.34. It was clearly seen that the microorganisms not only proliferated on the surface, but also they embedded between the fibers. The accumulation of the biofilm formation was also demonstrated with the images taken in the later incubation times. Protein matrix enrichment in all microorganisms was imaged with the CLSM as seen in Figure 4.35, 4.36 and 4.37, which supported the data obtained from SERS measurements.

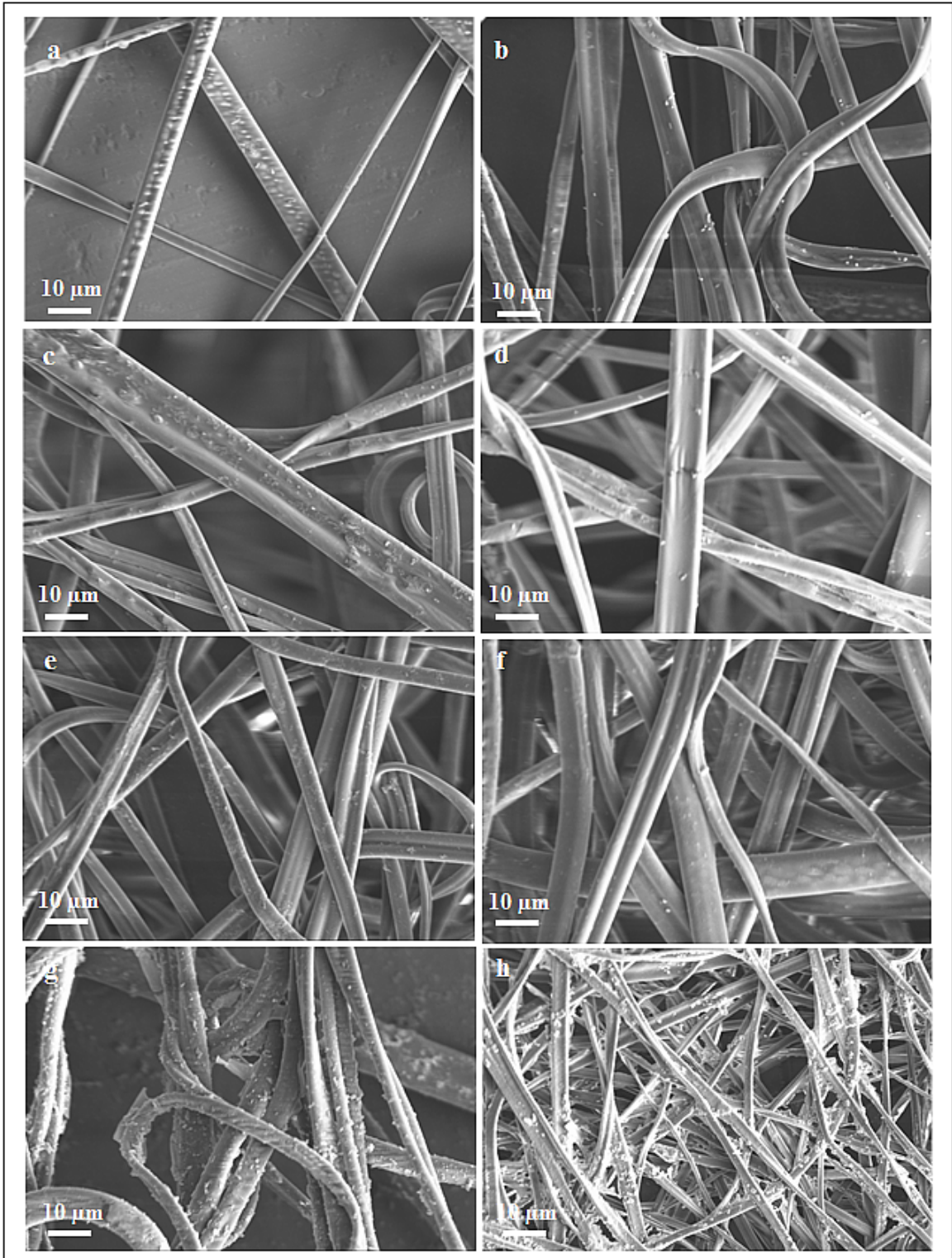


Figure 4.32. SEM images of *P. aeruginosa* biofilm formation at different cultivation times between (a-h) 4 and 120 h. Scale bars are 10 μm.

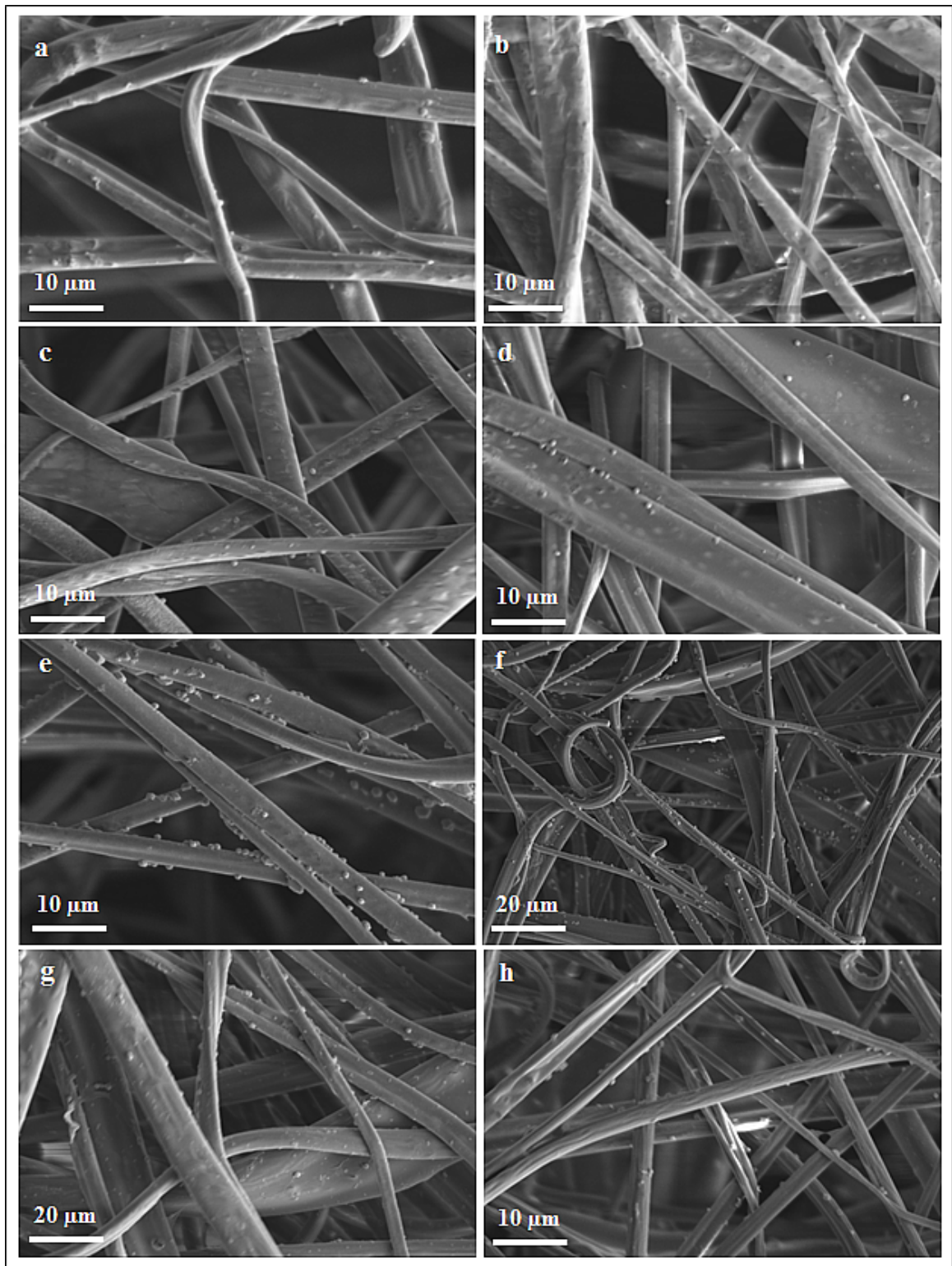


Figure 4.33. SEM images of *S. epidermidis* biofilm formation at different cultivation times between (a-h) 4 and 120 h. Scale bars are 10 μm (a-e, h) and 20 μm (f, g).

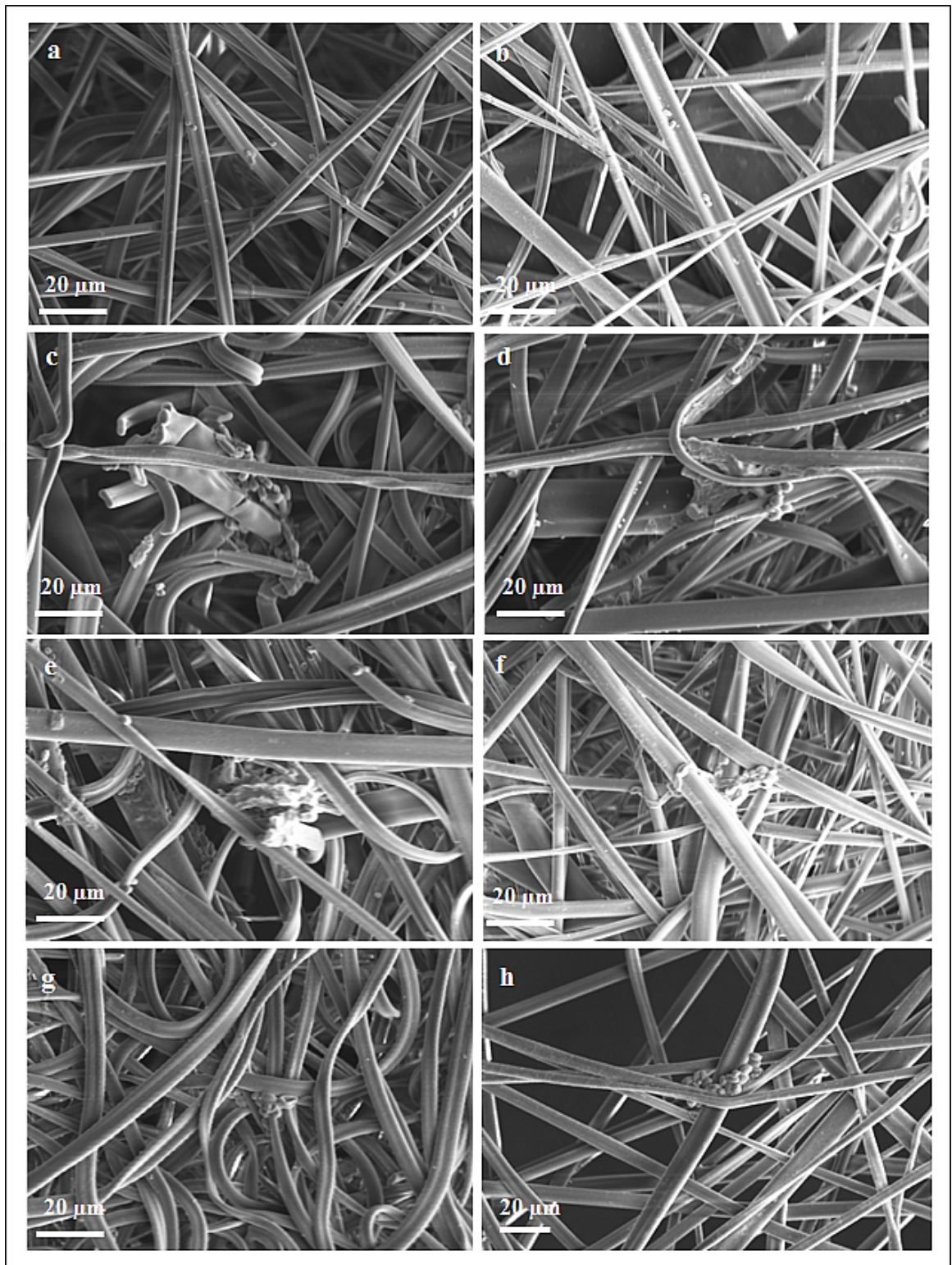


Figure 4.34. SEM images of *C. albicans* biofilm formation at different cultivation times between (a-h) 4 and 120 h. Scale bars are 20 μm.

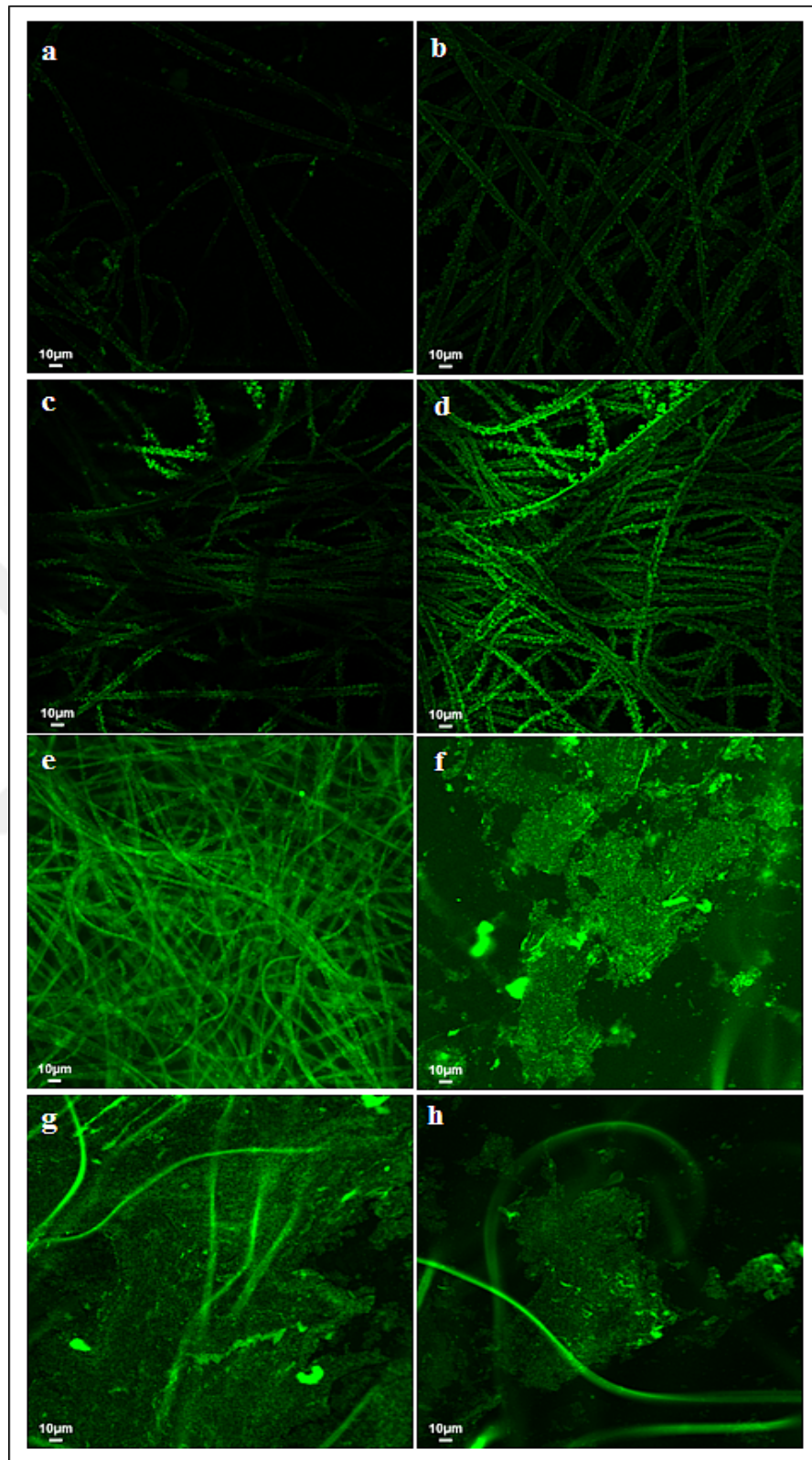


Figure 4.35. CLSM images of *P. aeruginosa* biofilm formation at different cultivation times between (a-h) 4 and 120 h. Scale bars are 10 μm.

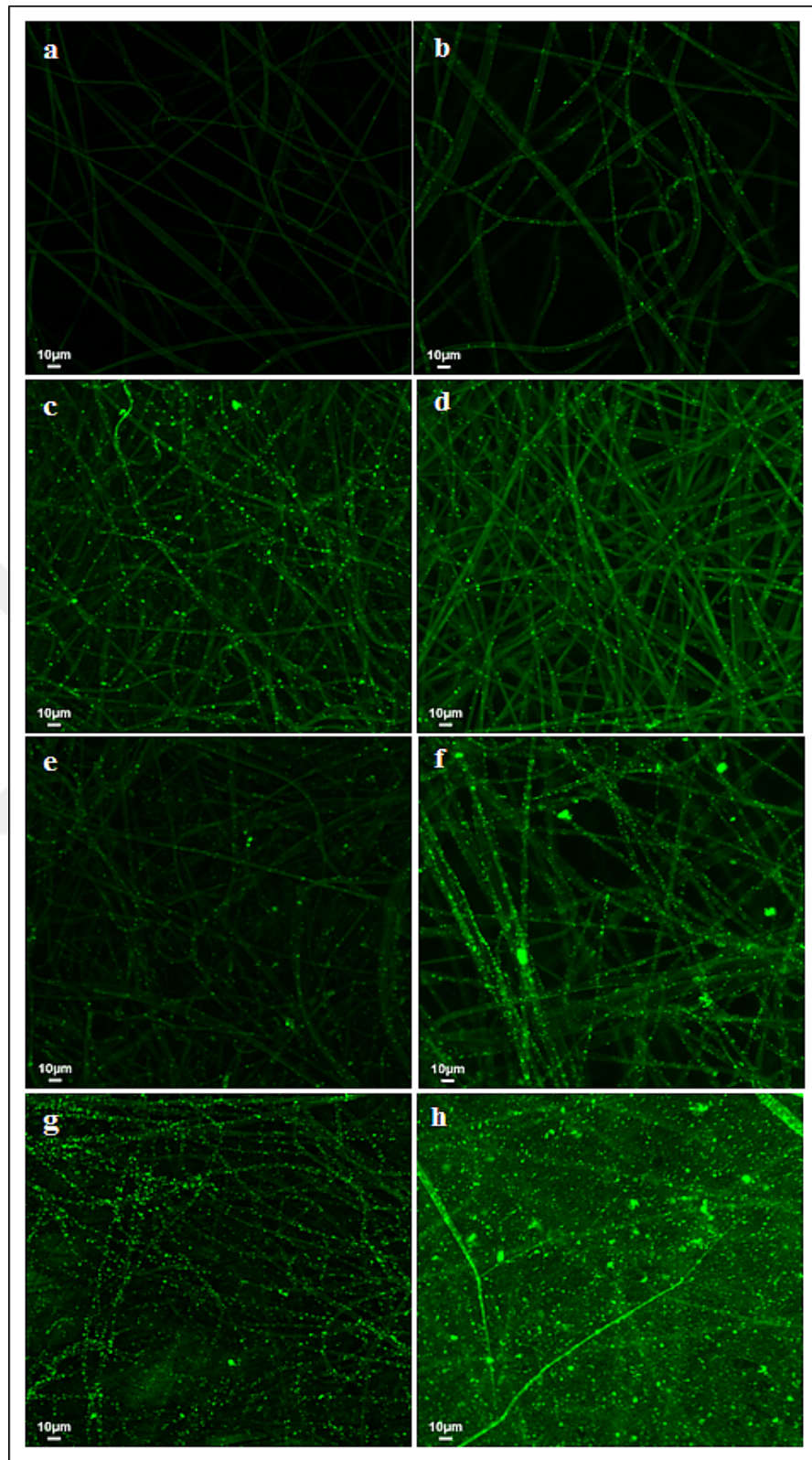


Figure 4.36. CLSM images of *S. epidermidis* biofilm formation at different cultivation times between (a-h) 4 and 120 h. Scale bars are 10 µm.

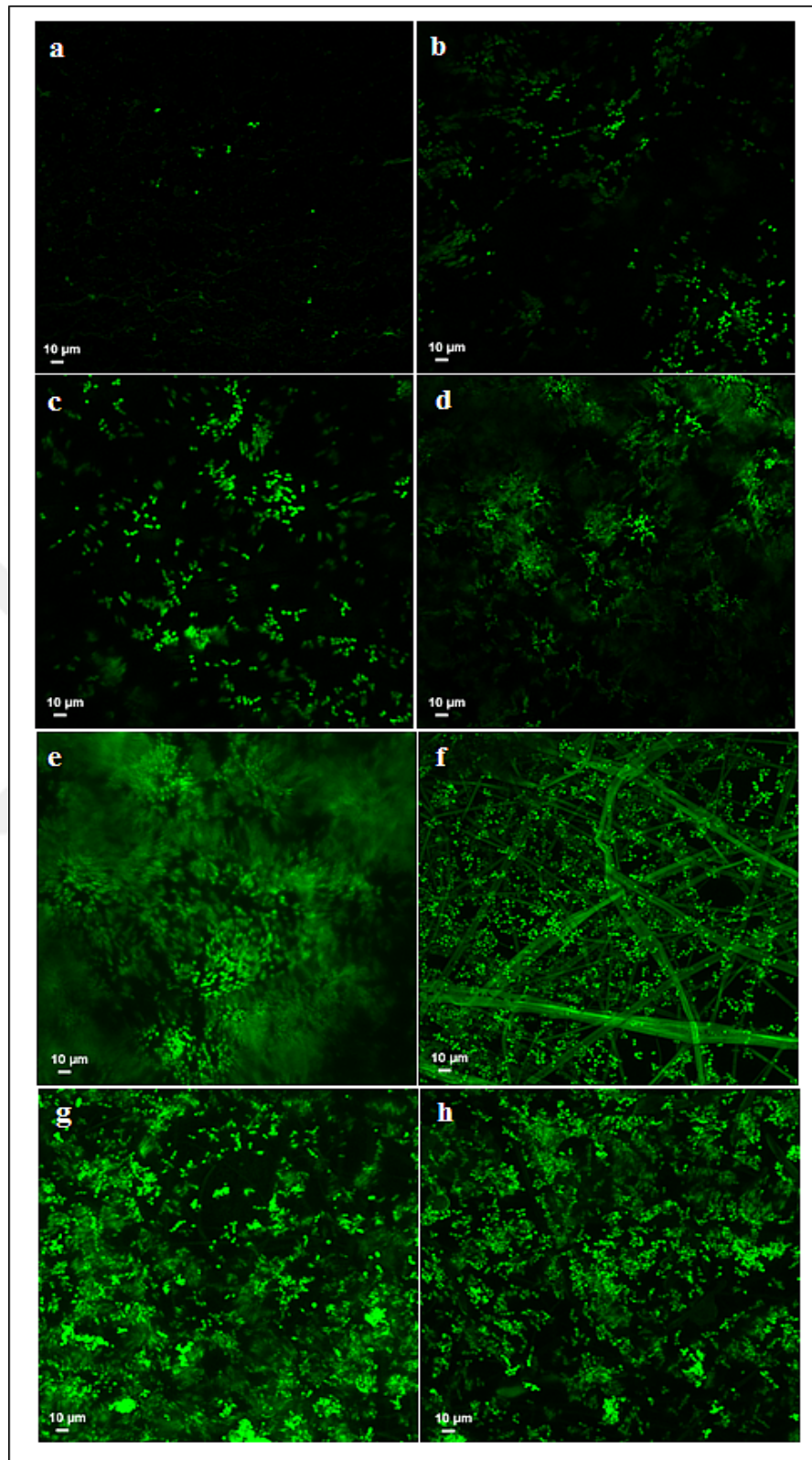


Figure 4.37. CLSM images of *C. albicans* biofilm formation at different cultivation times between (a-h) 4 and 120 h. Scale bars are 10 μm.

4.4.4. 3D Glucose-Gelatin Scaffolds

3D glucose-gelatin scaffolds, such as 3D PMMA substrates used in this thesis work, can also absorb the liquid media with their spongy structure. Therefore, the scaffold was incubated with SDB, NB and TSB. The experimental conditions are the same as given in the part of biofilm formation on 3D PMMA substrates. The determined peaks were both attributed to scaffold components glucose and gelatin, and also the ingredients in the nutrients in Figure 4.38.

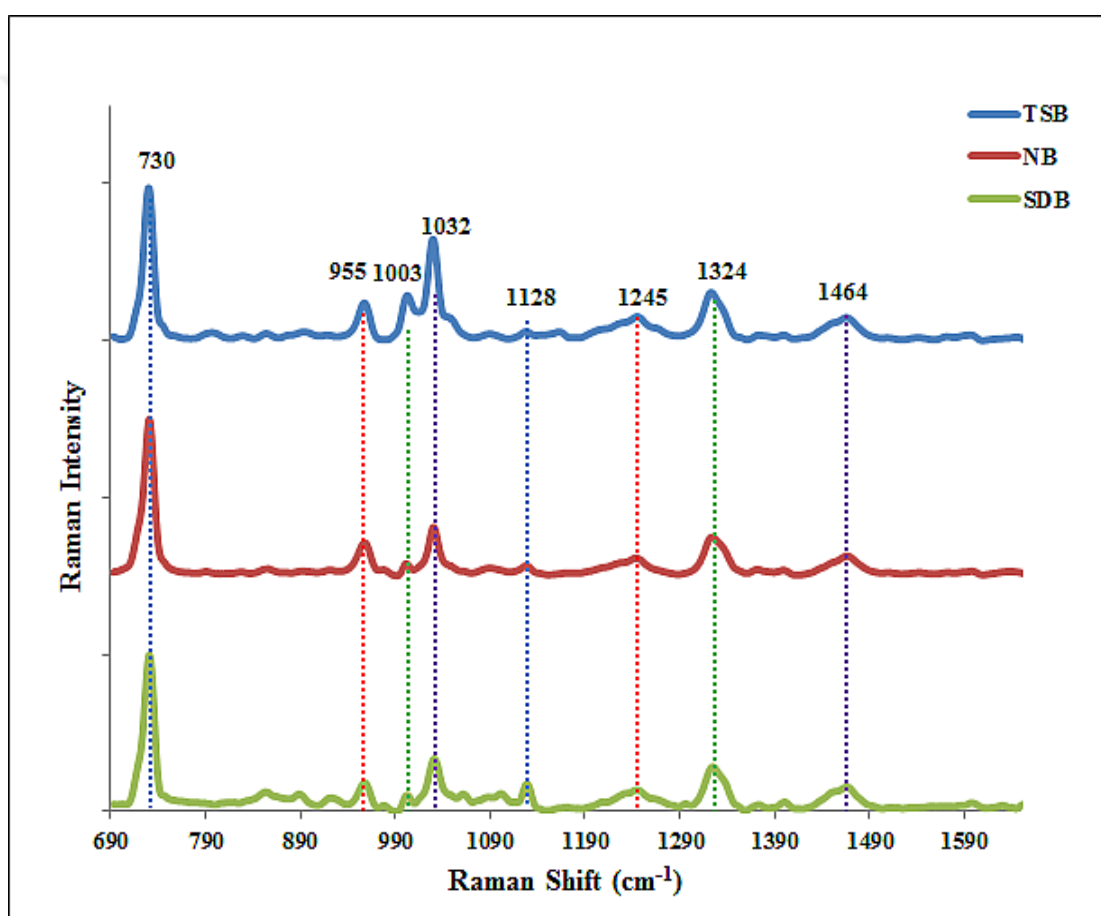


Figure 4.38. SERS spectra of glucose-gelatin scaffolds incubated with SDB, NB and TSB.

The peak observed at 730 cm^{-1} can be both attributed to nucleic acids included in gelatin and glycosidic ring polysaccharides in liquid media. The peaks at 955 cm^{-1} and 1324 cm^{-1} can both belong to COO^- stretching of glucose and also C-N stretching observed at 1128 cm^{-1} . The other determined peaks are both attributed to nutrients. Phenylalanine, C-C stretching, Amide III and CH_2/CH_3 deformation of lipids were observed at 1003, 1032, 1245 and 1464 cm^{-1} , respectively [233, 259, 260].

The main purpose of using glucose and gelatin to prepare a scaffold for a biofilm substrate was the hypothesis that the microorganisms could use these scaffold ingredients as an energy source and also the spongy structure could enhance the adhesion and proliferation of microorganisms. Therefore, the objective of using this substrate was to identify the metabolic activity changes during the biofilm formation, depending on the nutrient source and surface properties.

SERS spectra of *P. aeruginosa* biofilm formation is given in Figure 4.39. The bacteria were incubated on glucose-gelatin scaffold for 4-120 hours. *P. aeruginosa* expresses gelatinase enzyme [270], thus hydrolyzed the scaffold after 12 h incubation. The SERS spectra of biofilm samples were performed from the sticky biofilm sample of *P. aeruginosa* after 12 h. The biofilm samples after 12 h incubation were mixed with 4×AgNPs one-to-one, followed by dropping 2 μ l of suspension on CaF₂ substrate. The droplet was incubated until dry. At 8 and 12 h incubation, protein expression increased significantly, in correlation with the gelatinase enzyme expression, which was observed with an intensity increase at Amide III peaks at 1211, 1245, 1269 cm^{-1} and at Amide I peaks at 1602 and 1622 cm^{-1} . Pyocyanin synthesis was also observed clearly at the peaks 1162 and 1355 cm^{-1} after 8 h incubation. A COO- stretching of a carbohydrate peak appeared after 8 h incubation at 1369 cm^{-1} with the adhesion, adaptation and proliferation of the bacteria on the scaffold surface in the early phase of biofilm formation. The first spectrum after the whole scaffold was hydrolyzed was obtained at 24 h incubation time. The critical incubation time for biofilm formation can be defined as 48 h due to the changes of spectral pattern significantly at this time point. An increase in protein synthesis was determined at 48 h with the peaks of tyrosine, Amide III, Amide II and Amide I observed at 814, 1211, 1245, 1269, 1283, 1559, 1602 and 1622 cm^{-1} . The intensities of the peaks attributed to lipids at 1461 and 1486 cm^{-1} and pyocyanin at 1355 cm^{-1} also increased after 48 h incubation with the maturation of the biofilm. Referring to the literature, the increase in the lipid synthesis was expected in a mature *P. aeruginosa* biofilm, rhamnolipid synthesis was reported, which enhances the formation of the sticky mushroom shape [58, 59].

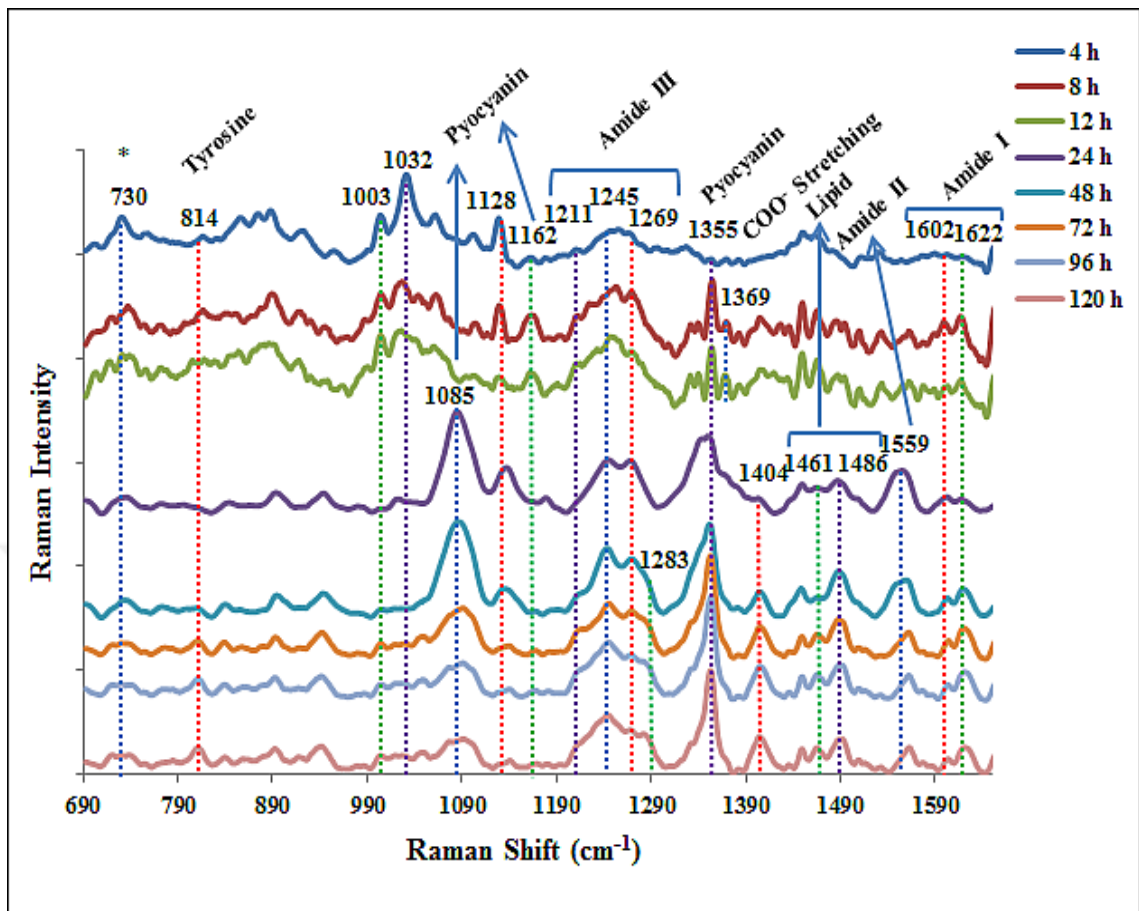


Figure 4.39. SERS spectra of *P. aeruginosa* biofilm formation at different cultivation times between 4 and 120 h.

Figure 4.40 shows the SERS spectra of *S. epidermidis* biofilm formation on 3D glucose-gelatin scaffold at incubation times between 4-120 h. The adaptation process of *S. epidermidis* on a host surface is slower than *P. aeruginosa*. In addition, *S. epidermidis* cannot express gelatinase enzyme to hydrolyze gelatin base scaffold, which explains the slow rate of metabolic process. Carbohydrates and matrix proteins are responsible for initial attachment and regulation of biofilm formation in biofilm mechanism of the bacteria [75-77]. The peaks at 1061 and 1103 cm^{-1} attributed to C-O, C-C stretching and C-N stretching of proteins, and the peaks at 853, 889 and 922 cm^{-1} belonging to tyrosine and carbohydrates, respectively. According to the spectral changes, the carbohydrate synthesis of *S. epidermidis* started after 24 h incubation and increased significantly at 96 h incubation. In addition, protein synthesis started after 96 h incubation as the carbohydrate mechanism. The Amide II and Amide I peaks at 1572 and 1605 cm^{-1} appeared in this incubation period.

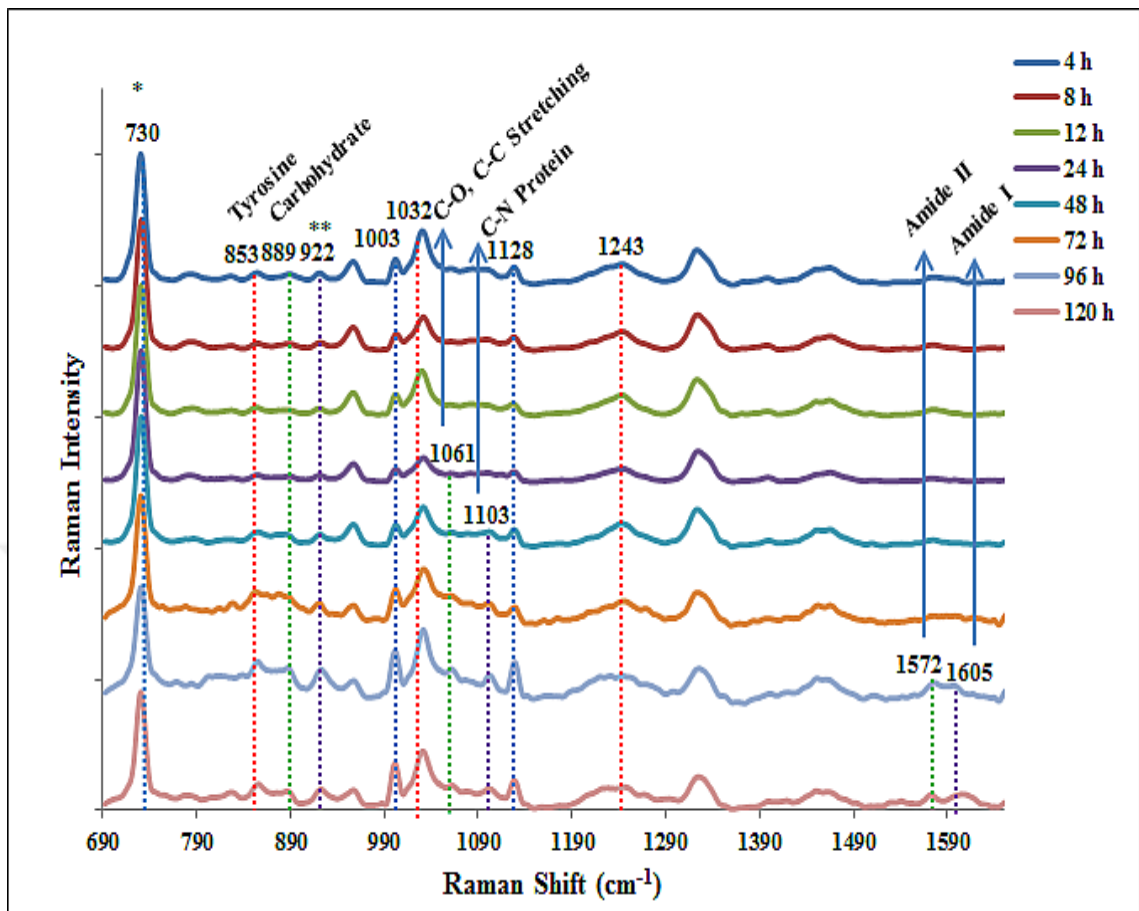


Figure 4.40. SERS spectra of *S. epidermidis* biofilm formation at different cultivation times between 4 and 120 h.

The metabolic activity process of *C. albicans* can be evaluated based on the spectral changes on the SERS spectra in Figure 4.41. Compared to the other two microorganisms used in this thesis work, a highly significant spectral change was observed at 48 h incubation. The whole pattern was effected by the metabolic change with the proliferation on glucose-gelatin scaffold. The sharp decrease in the intensity of DNA fragments at 730 cm^{-1} was observed with the appearance of carbohydrate, protein and lipid peaks. Expressed polymeric substances block the interaction of DNA fragments with the AgNPs added on the surface. The formation of polymeric shell with the maturation phase could be demonstrated with the peaks at 852, 884, 918 and 1505 cm^{-1} belonging to carbohydrates, the peaks at 1450 and 1462 cm^{-1} attributed to lipids and most importantly the Amide I peak observed at 1610 cm^{-1} . In addition, although *C. albicans* has ability to express gelatinase enzyme, it is not as effective as *P. aeruginosa* to hydrolyze the substrate that the scaffold preserved its architecture during 120 h incubation.

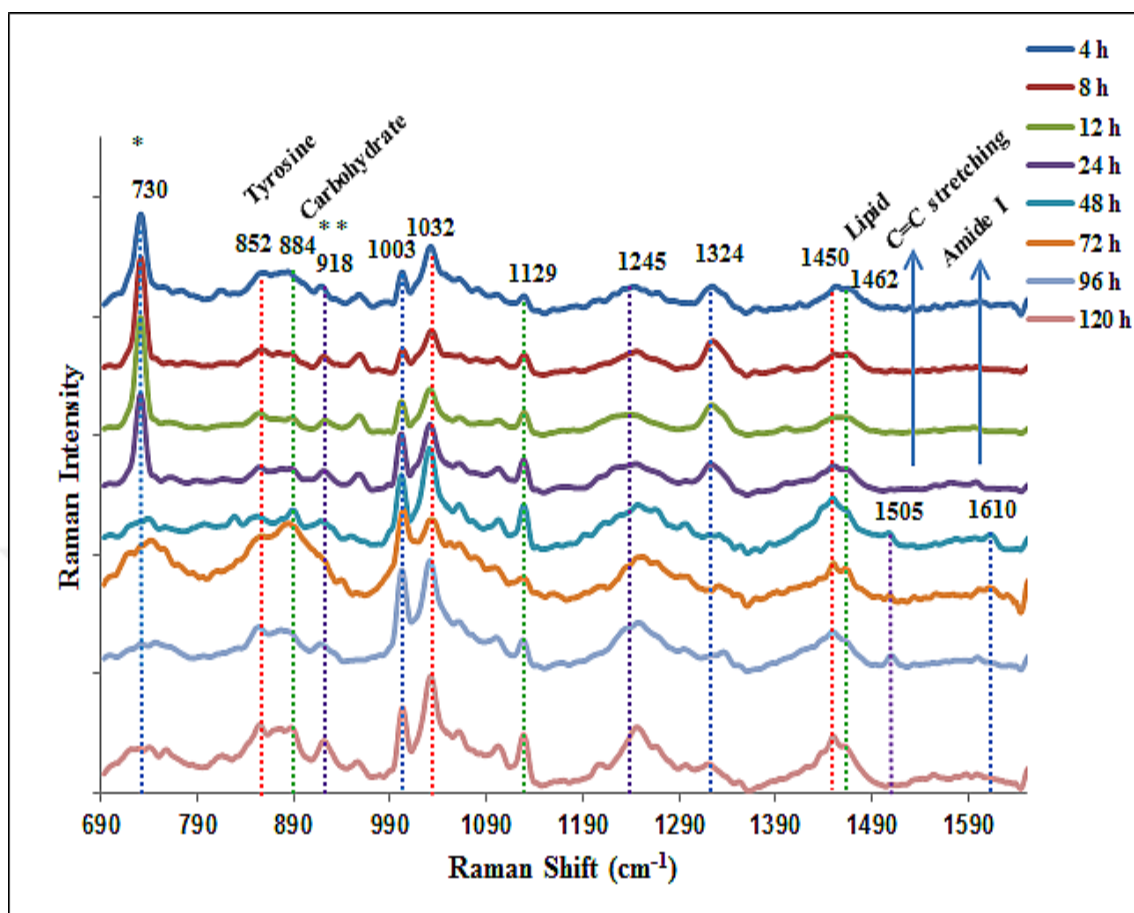


Figure 4.41. SERS spectra of *C. albicans* biofilm formation at different cultivation times between 4 and 120 h.

The SEM images of biofilm formation of *P. aeruginosa*, *S. epidermidis* and *C. albicans* are given in Figure 4.42, 4.43 and 4.44. The scaffold structure could be observed between 4-12 h incubation for *P. aeruginosa* before being hydrolyzed. The proliferation of the bacteria was not only observed on the surface of the scaffold but also inside the structure as seen in the SEM images. After 12 h incubation, the scaffold was totally hydrolyzed and the sticky smooth biofilm including bacteria colonies could be observed significantly. Biofilm regulation of *S. epidermidis* could be clarified clearly with increasing incubation time as seen in Figure 4.43. At incubation times 96 and 120 h, the bacterial assembly coated with a transparent polymeric shell could be observed on all over the surface, which were consistent with the SERS measurements. Biofilm formation of *C. albicans* is given in Figure 4.44. The yeast cells formed mushroom shape with the increasing incubation time, and they were buried in the scaffold surface.

Biofilm samples of *P. aeruginosa*, *S. epidermidis* and *C. albicans* were also characterized with CLSM as seen in Figure 4.45, 4.46 and 4.47. Formation of microorganism aggregates and a significant increase in protein expression, which coated the cells were monitored at increasing incubation time.



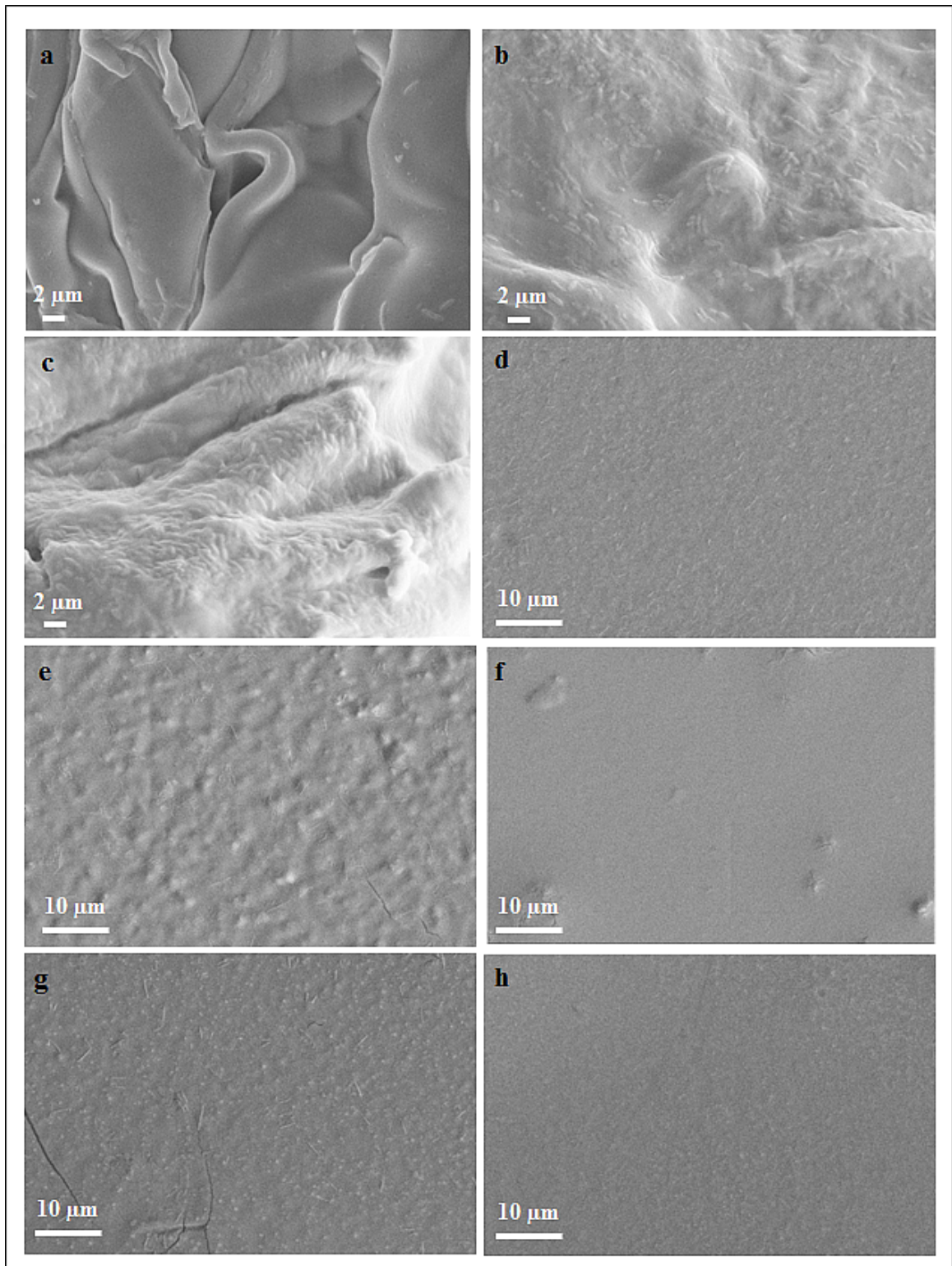


Figure 4.42. SEM images of *P. aeruginosa* biofilm formation at different cultivation times between (a-h) 4 and 120 h. Scale bars are 2 μm (a-c) and 10 μm (d-h).

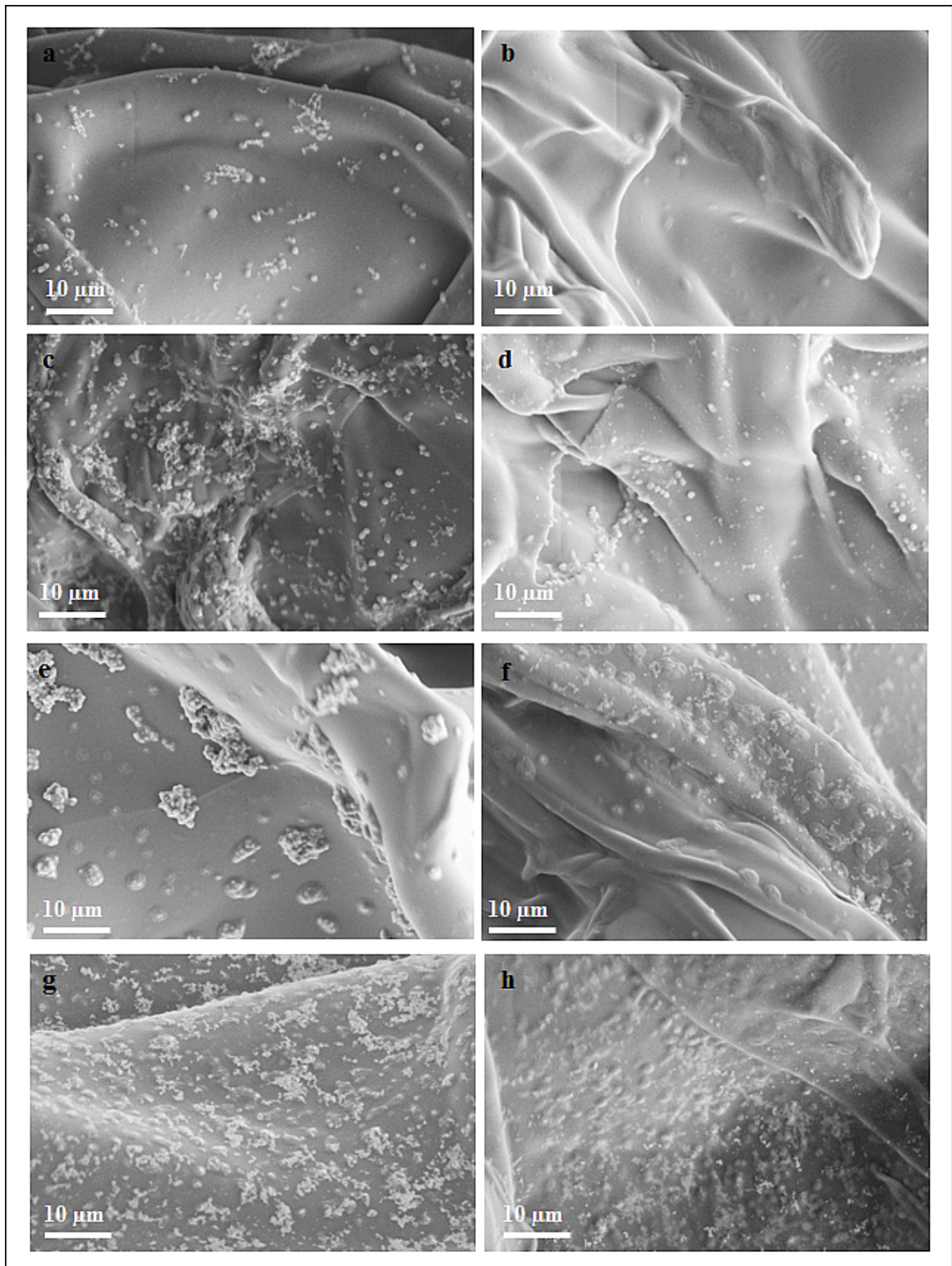


Figure 4.43. SEM images of *S. epidermidis* biofilm formation at different cultivation times between (a-h) 4 and 120 h. Scale bars are 10 μm.

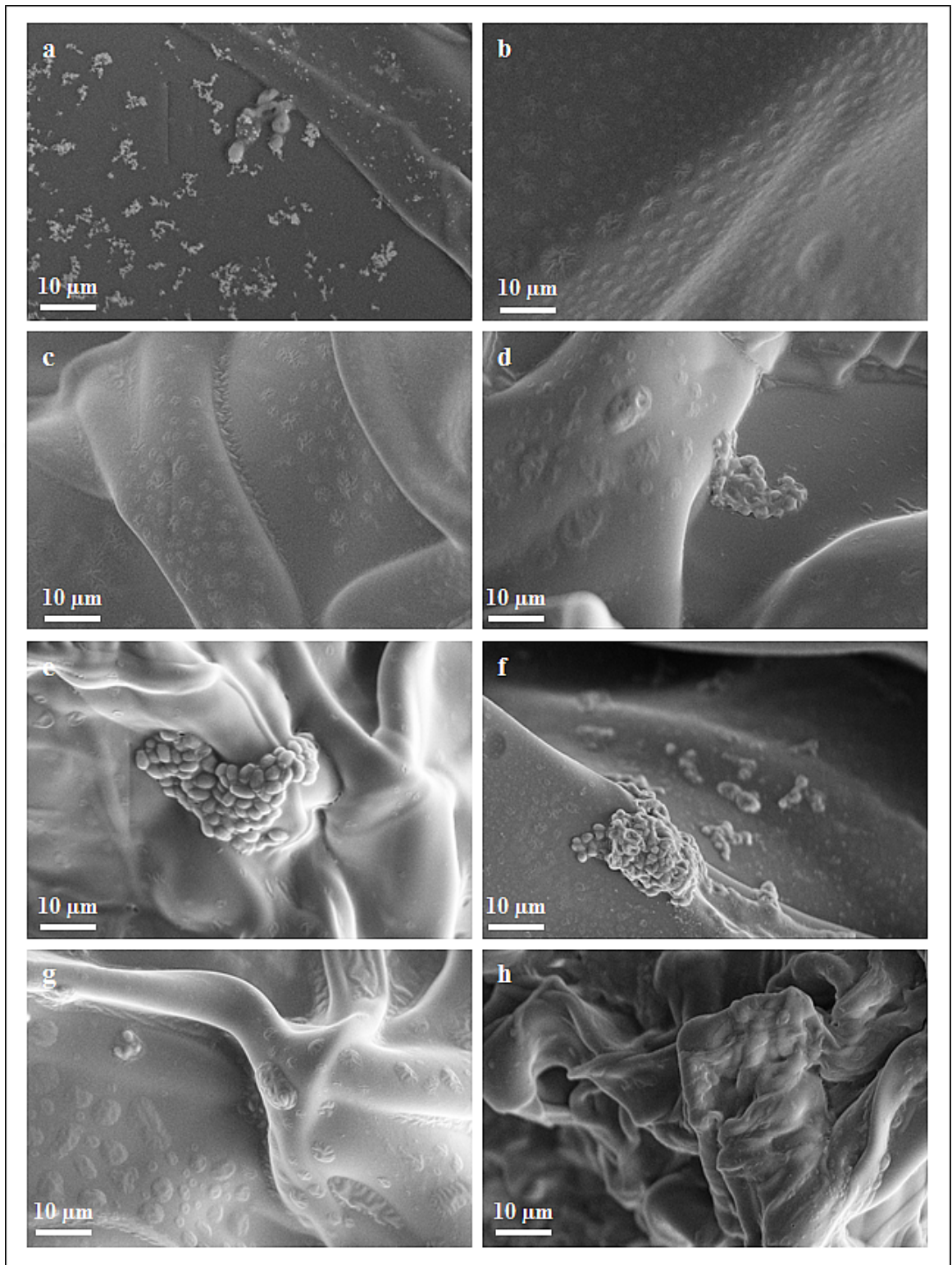


Figure 4.44. SEM images of *C. albicans* biofilm formation at different cultivation times between (a-h) 4 and 120 h. Scale bars are 10 μm .

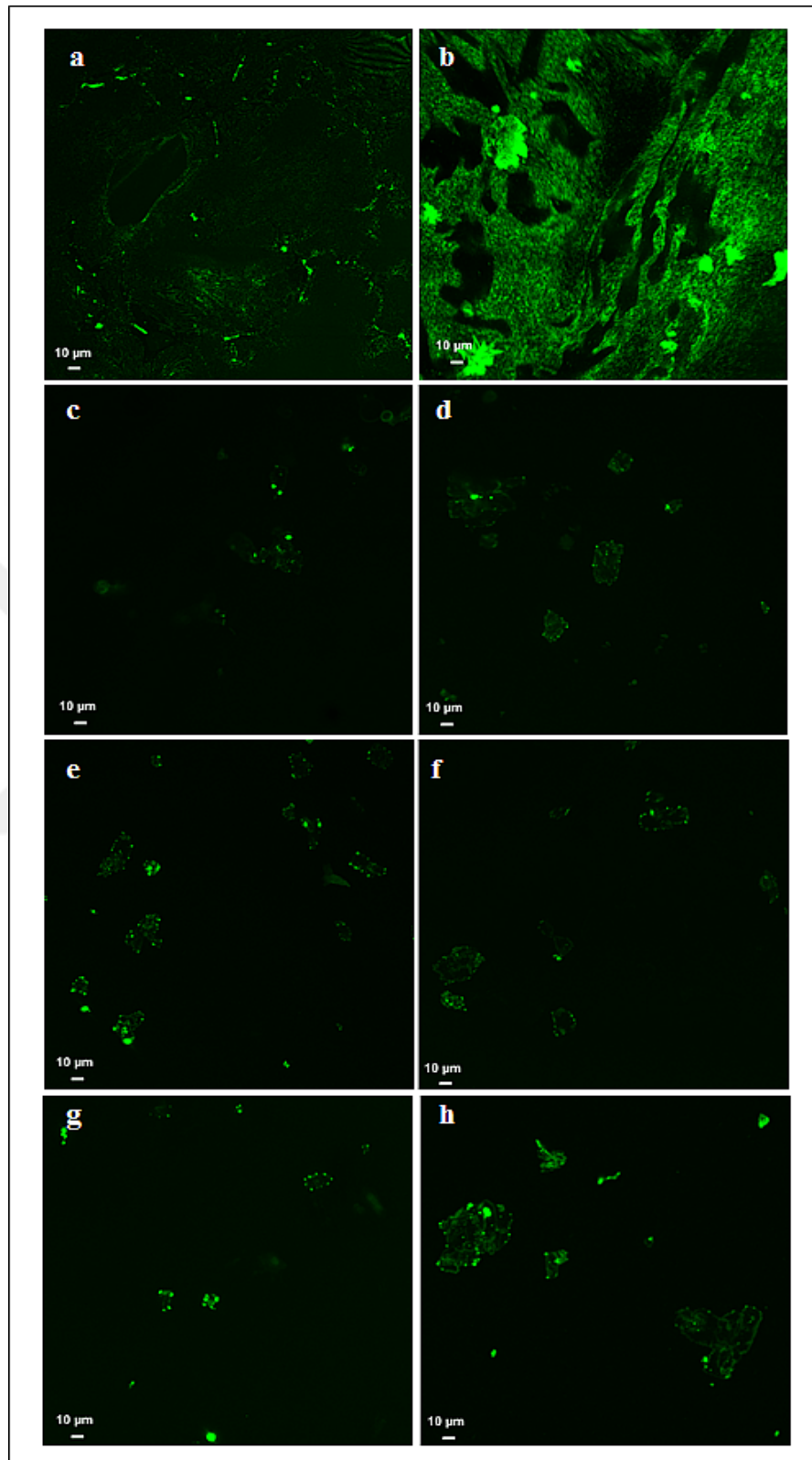


Figure 4.45. CLSM images of *P. aeruginosa* biofilm formation at different cultivation times between (a-h) 4 and 120 h. Scale bars are 10 μm.

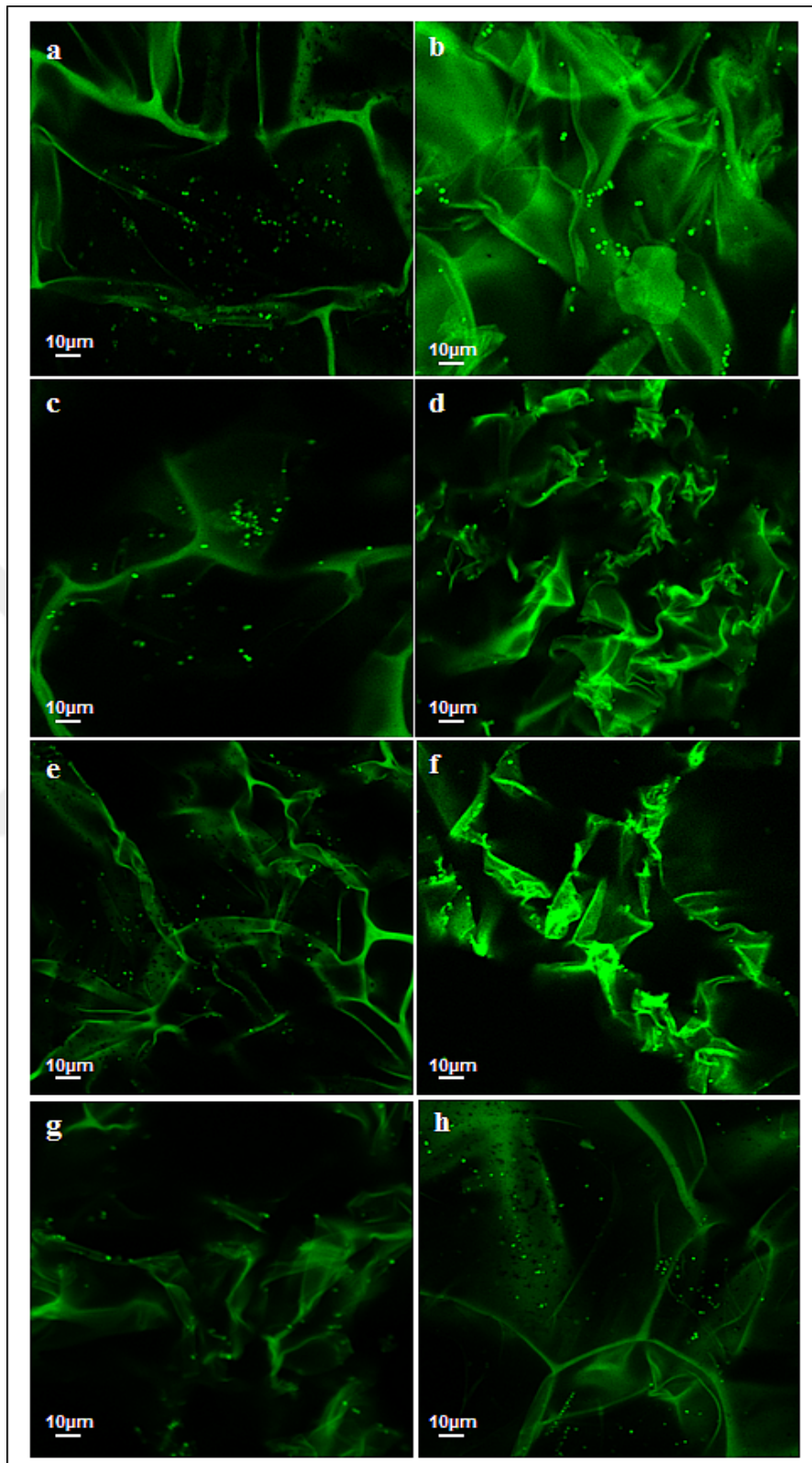


Figure 4.46. CLSM images of *S. epidermidis* biofilm formation at different cultivation times between (a-h) 4 and 120 h. Scale bars are 10 μm.

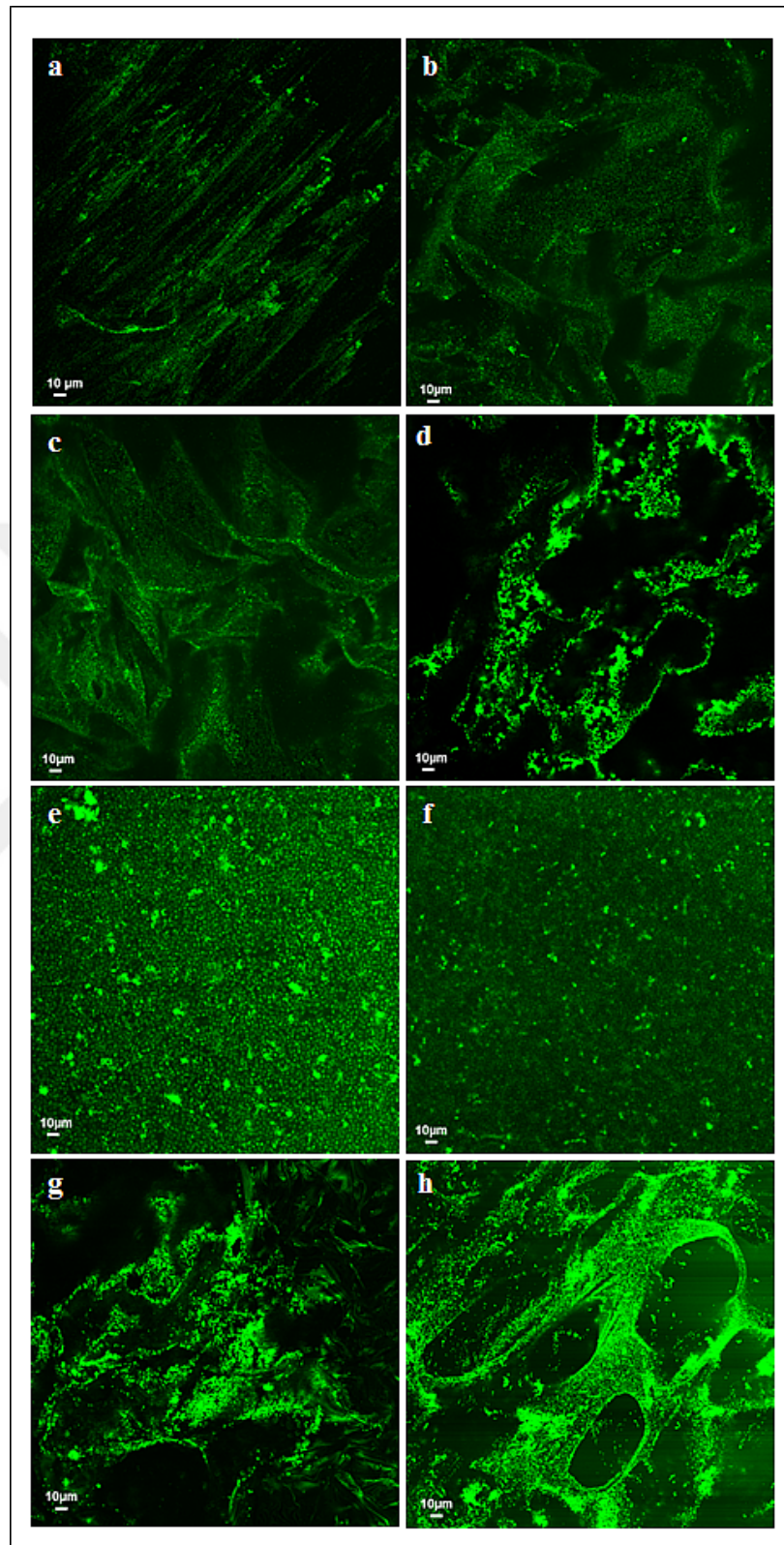


Figure 4.47. CLSM images of *C. albicans* biofilm formation at different cultivation times between (a-h) 4 and 120 h. Scale bars are 10 μm.

4.5. MULTI-SPECIES BIOFILM FORMATION

Biofilms can be formed both by a single-species or a multi-species of bacteria and yeast [271]. The biofilm can consist of several different species of microorganisms in both medical devices and water pipes in industry, which increases the importance of evaluating the metabolic activities of microorganisms at molecular level in a multi-species biofilm sample. However, there are limited multi-species biofilm studies in the literature [272-277]. In the scope of this thesis work, the single-species metabolic activities of *P. aeruginosa*, *S. epidermidis* and *C. albicans* were also compared with their mixture form, followed by the possible discrimination of the dominant species in the biofilm matrix with SERS. To do this, both species were inoculated in a nutrient agar plate at the same time and were incubated for 48 h. After the incubation time ended, 10 μ l AgNPs were dropped on the agar plate and waited until the droplet got dried to move on to obtain the SERS spectra. The SERS spectrum of the multi-species biofilm is given in Figure 4.48 with comparison of the single-species of microorganisms on agar plates incubated for 48 h. It was clearly observed from the spectra that *P. aeruginosa* was the dominant species in the mixture and inhibited proliferation of *S. epidermidis* and *C. albicans* significantly. The spectral pattern of *P. aeruginosa* and multi-species biofilm was exactly the same that all the peaks overlapped. Therefore, from the obtained SERS spectra, it could be said that the winner of this competition was *P. aeruginosa*. Also, the SEM and CLSM images supported the SERS data that the only species observed in the images was *P. aeruginosa* (Figure 4.49). The inhibition of *C. albicans* by *P. aeruginosa* was first demonstrated by Kerr et. al in 1994 [275]. Also, the antifungal effect of *P. aeruginosa* was noticed in several studies [276, 277]. In a study published by Bandara et. al, a significant inhibition of *C. albicans* was reported and interestingly it was also demonstrated that *C. albicans* had an effect to slow down the proliferation of *P. aeruginosa* [273]. Indeed, the inhibition effect of the other microorganisms on biofilm formation of *P. aeruginosa* could be clearly seen in the obtained results, when the SEM images obtained from agar plates at 48 h incubation time from the single-species *P. aeruginosa* and multi-species biofilm were compared (Figure 4.12e and 4.49a). The thickness of the biofilm decreased dramatically and in multi-species biofilm sample *P. aeruginosa* cells could be imaged individually, whereas in a single-species biofilm we could only observed the slime biofilm shell at 48 h incubation. The thickness of the *P. aeruginosa* biofilm on an agar plate at 48 h determined 14.43 μ m

(Figure 4.15e) but the thickness of a multi-species biofilm found 1.92 μm (Figure 4.49b). In another study, Adam et. al showed that in a multi-species biofilm of *C. albicans* and *S. epidermidis*, the polymeric matrix produced by *S. epidermidis* prevent the antifungal drugs activity on *C. albicans* and on the other hand *C. albicans* supported *S. epidermidis* through fighting against vancomycin, where they showed a mutualist life form [272]. However, a multi-species biofilm is an environment where microorganisms shows a struggle of survival. They compete to be the winner and the most aggressive species secrete virulence factors to kill the other species as *P. aeruginosa* always do [273, 274]. In addition, signaling molecules are the main players in this competition. N-acyl homoserine lactone autoinducers provide the intra-cellular communications [278].

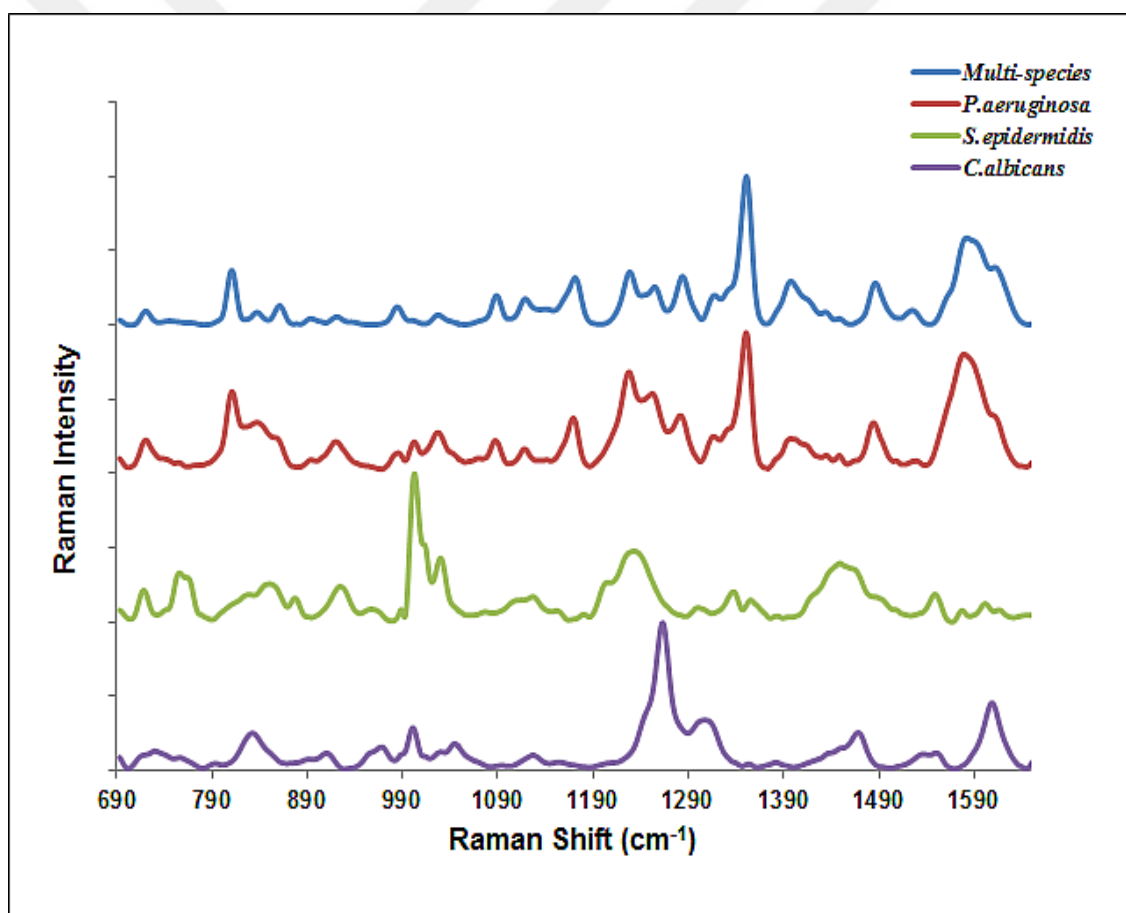


Figure 4.48. SERS spectra of multi-species, *P. aeruginosa*, *S. epidermidis* and *C. albicans* biofilm on agar plates at 48 h incubation time.

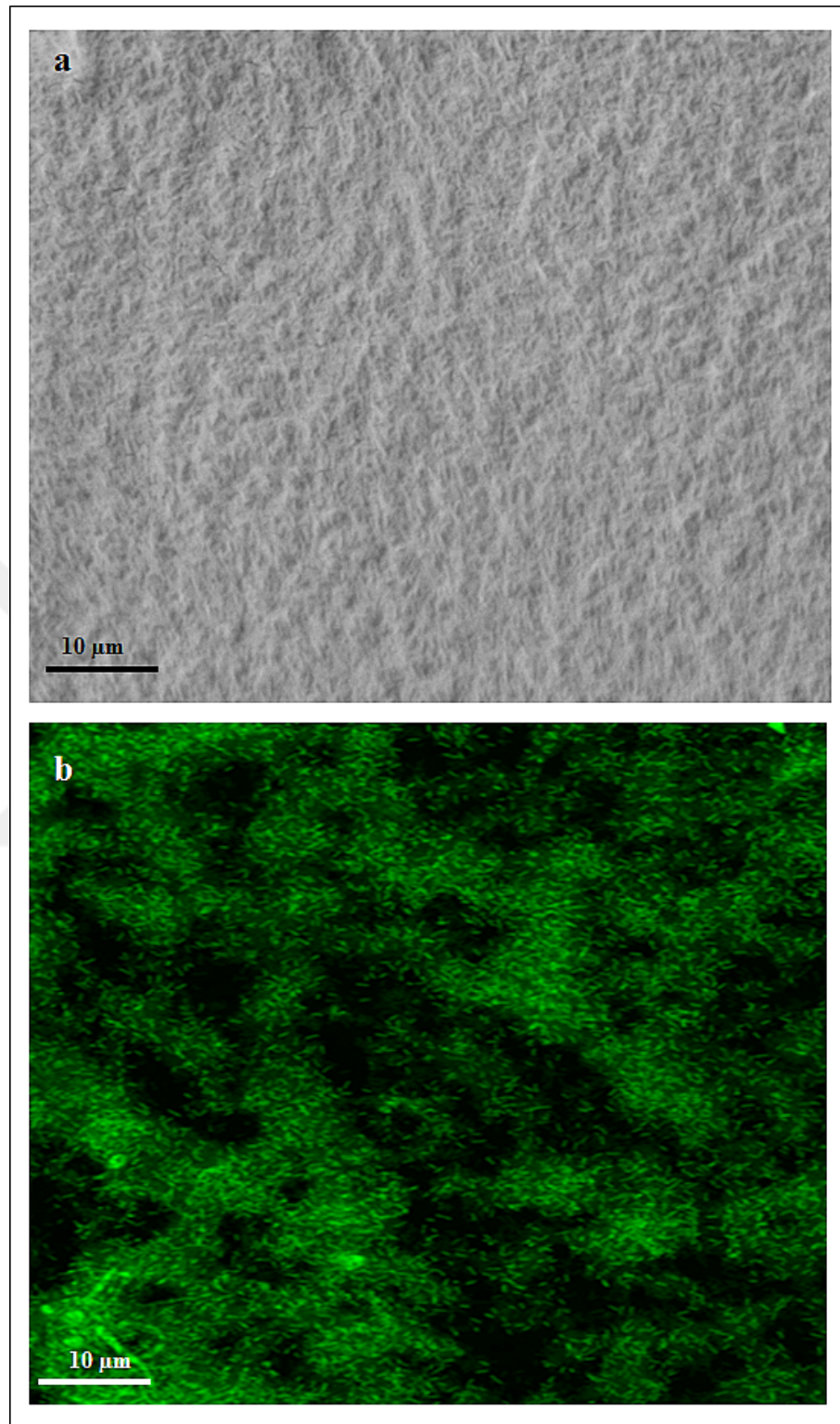


Figure 4.49. SEM and CLSM images of the multi-species biofilm. Scale bars are 10 μm .

4.6. DISCRIMINATION OF MICROORGANISMS IN A BIOFILM STRUCTURE

PCA is a multivariate analysis method used to identify the principal components (PCs) responsible for the discrimination of the datasets based on the variations between the spectral data of the different species. Further in this thesis work, the discrimination between the biofilms formed by the studied microorganisms was demonstrated based on their main metabolic activity changes during their biofilm formation process with SERS. Figure 4.50, 4.51, 4.52 and 4.53 show PCA plots and PCs of the SERS spectra obtained from biofilms of *P. aeruginosa*, *S. epidermidis* and *C. albicans* on agar plates, 2D and 3D PMMA substrates and 3D glucose-gelatin scaffolds at different incubation times between 4 h and 120 h, respectively. The PCA plots in Figure 4.50-4.53 showed that the microorganisms could be differentiated significantly especially in maturation phases of biofilm formation because their unique metabolic activities could be observed clearly with the accumulation of molecular process.

The loadings of the PCs show the spectral variabilities at molecular level as seen in Figure 4.50-4.53. The negative and positive loadings showed the differentiation of three model microorganisms in PCA plots. The PCs of biofilm formation of the model microorganisms on agar plates used the 52.35, 21.52 and 10.35 per cent of the data as seen in Figure 4.50. PC 1, PC 2 and PC 3 had the peaks belonging to nucleic acids (730, 794, 1485, 1517 cm^{-1}), amino acids (809, 858 and 1003 cm^{-1}), carbohydrates (909, 919, 956, 1129, 1169, 1396 cm^{-1}), proteins (1127, 1241, 1250, 1253, 1283, 1288, 1582, 1610 cm^{-1}), lipids (1451 cm^{-1}) and pyocyanin (1088 and 1355 cm^{-1}).

The PCs of biofilm formation of the microorganisms on 2D PMMA substrates represented the variations of 51.42, 23.14 and 9.17 per cent from the present data as shown in Figure 4.51. The bands of nucleic acids (730, 794 and 1489 cm^{-1}), amino acids (837 and 1003 cm^{-1}), carbohydrates (1046, 1103, 1327, 1329 and 1405 cm^{-1}), proteins (1561 and 1622 cm^{-1}) and pyocyanin (1160 and 1355 cm^{-1}) were observed on the loadings of PC 1, PC 2 and PC 3.

The PC loadings of biofilm formation on 3D PMMA substrates represented the 37.17, 28.83 and 11.05 per cent of the dataset is given in Figure 4.52. The identified bands were the nucleic acids (730, 791, 1485 and 1526 cm^{-1}), carbohydrates (907, 1398 and 1412 cm^{-1}

¹), proteins (1230, 1253, 1259, 1282, 1595 and 1613 cm^{-1}) and pyocyanin (1172 and 1355 cm^{-1}).

The PCs of the biofilm formation on 3D glucose-gelatin scaffolds used the 63.57, 26.38 and 3.93 per cent of the dataset showed in Figure 4.53. The bands of nucleic acids (730 and 1489 cm^{-1}), amino acids (810 and 839 cm^{-1}), carbohydrates (891, 942, 1139, 1166 and 1405 cm^{-1}), proteins (1253, 1270, 1561 and 1618 cm^{-1}) and pyocyanin (1086, 1162 and 1355 cm^{-1}) were identified.

It can be concluded that, nucleic acids, amino acids, carbohydrates, proteins and lipids are the main discriminant components for the *P. aeruginosa*, *S. epidermidis* and *C. albicans*. The main important output of the PCA results was that pyocyanin can be used as a discrimination component for *P. aeruginosa*, which can provide a sufficient separation of the bacteria from the other species in a heterogenic biofilm structure.

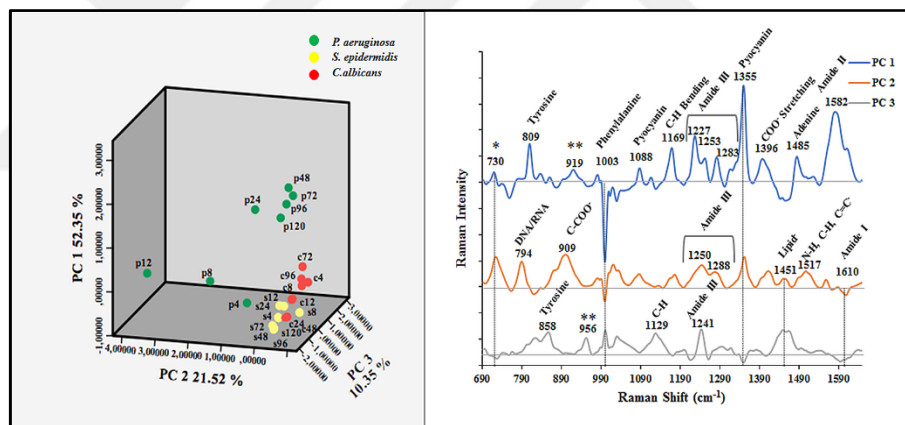


Figure 4.50. PCA plot and PCs of biofilm formation on agar plates.

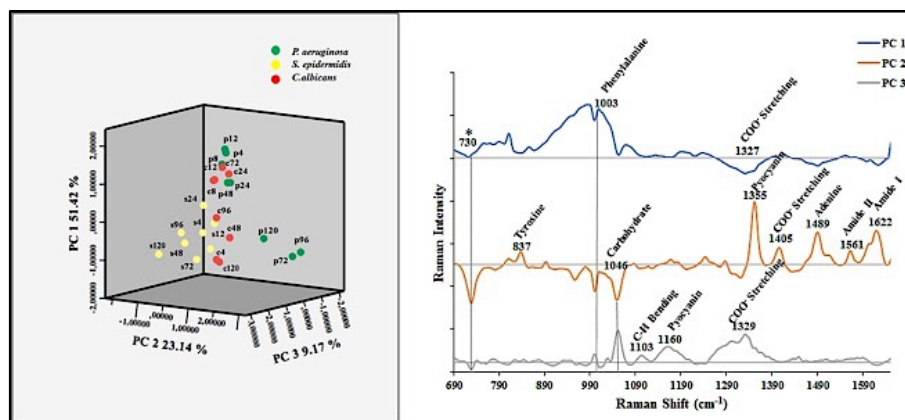


Figure 4.51. PCA plot and PCs of biofilm formation on 2D PMMA substrates.

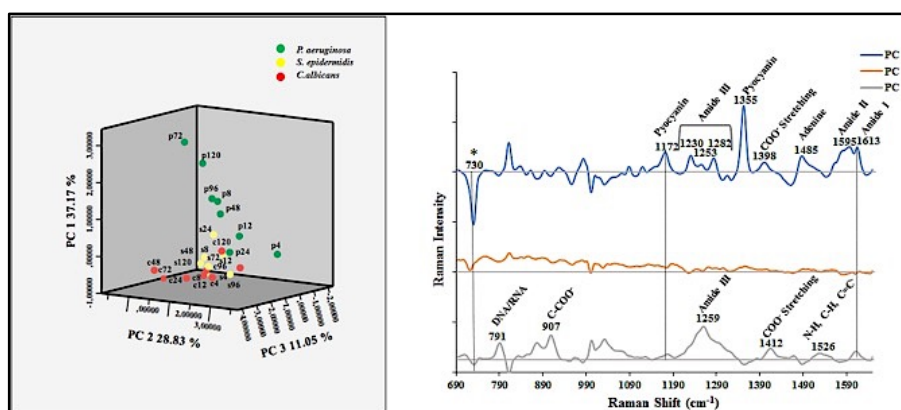


Figure 4.52. PCA plot and PCs of biofilm formation on 3D PMMA substrates.

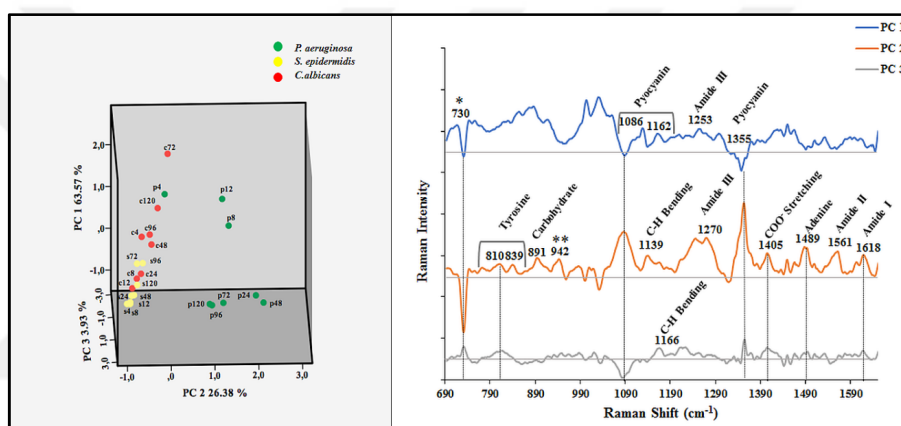


Figure 4.53. PCA plot and PCs of biofilm formation on 3D glucose-gelatin scaffolds.

To discriminate the biofilms of three model microorganisms on different substrates, significant PCs were used for the LDA model. Two-dimensional scatter plots of the two linear discriminant functions (function 1 (F1) and function 2 (F2)) based on the PC-LDA model are given in Figure 4.54 a-d shows the classification of *P. aeruginosa*, *S. epidermidis* and *C. albicans* in three different groups. The 100 per cent of the original grouped cases correctly classified on agar plates, 2D and 3D PMMA substrates, while 79.2 per cent original grouped cases classified on 3D glucose-gelatin scaffolds. The biofilm samples of *C. albicans* at the time points between 4-48 h were found around the group centroid of *S. epidermidis*, which decreased the sensitivity of the classification on glucose-gelatin scaffolds.

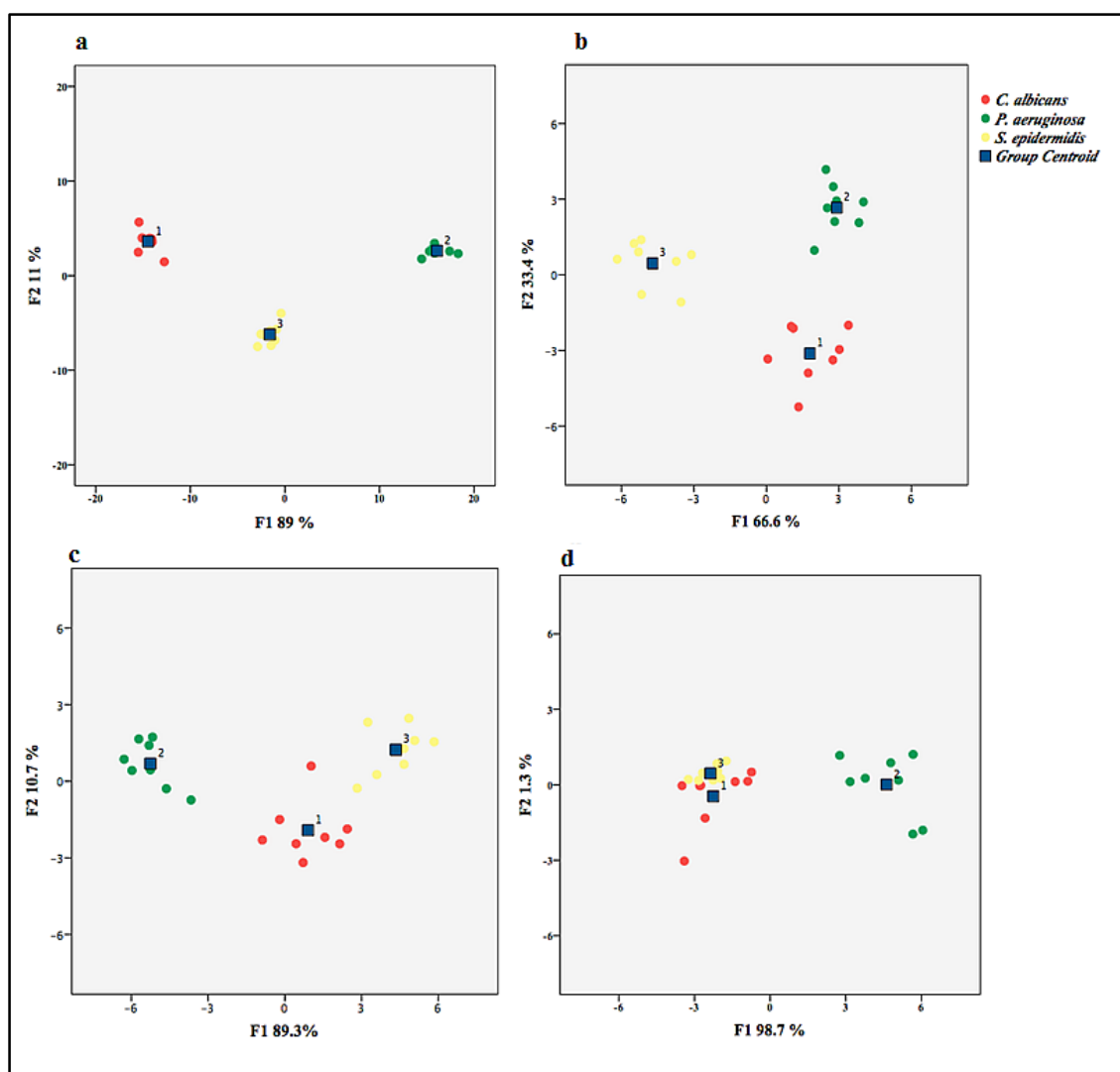


Figure 4.54. PC-LDA plots of *C. albicans*, *P. aeruginosa* and *S. epidermidis* (a) on agar plates, (b) 2D PMMA substrates, (c) 3D PMMA substrates and (d) 3D glucose-gelatin scaffolds.

4.7. REPRODUCIBILITY OF SERS MEASUREMENTS

Spectral reproducibility is a major problem in SERS measurements due to heterogenic structure of biological systems coupled with chaotic distribution of AgNPs over a biofilm. In order to understand the degree of reproducibility of the spectra obtained from the mapped areas on the studied biofilms, CV of the spectra obtained from different mapped areas on the same sample (spot-to-spot) and different samples (sample-to-sample) with increasing incubation times of each microorganism were calculated on agar plates, 2D and

3D PMMA substrates and 3D glucose-gelatin scaffolds. An average of 36 spectra from each mapped area was used to calculate the spot-to-spot reproducibility, and the average spectra from each of three-mapped area were used to calculate the sample-to-sample reproducibility. The results of reproducibility study are provided in Table 4.2-4.13 for each microorganism on four different substrates, respectively. Although inconsistency was observed in CV values of some sample sets, we can say that in general, the CV values for sample-to-sample are relatively higher than the CV values for the spot-to-spot. Furthermore, there is no observed correlation with incubation times and CV values. This suggests that the CV mainly depends on the distribution of AgNPs on the droplet area, which are responsible for their interaction with components expressed by microorganisms during biofilm formation.

Table 4.2. CV values of SERS measurements of *P. aeruginosa* on agar plates.

<i>P.aeruginosa</i>	1 st Experiment				2 nd Experiment				3 rd Experiment				Total Avg.
	1 st spot	2 nd spot	3 rd spot	Avg. 1 st Exp.	1 st spot	2 nd spot	3 rd spot	Avg. 2 nd Exp.	1 st spot	2 nd spot	3 rd spot	Avg. 3 rd Exp.	
4 h	35.54	36.55	36.78	23.51	30.58	43.85	31.74	17.67	39.98	36.62	36.88	13.20	42.06
8 h	35.75	41.25	44.55	24.04	34.46	32.14	29.97	20.69	43.67	40.01	42.56	15.24	36.64
12 h	30.61	42.68	46.51	14.89	32.59	32.72	34.50	25.15	41.98	43.54	41.13	17.77	40.11
24 h	36.22	36.19	37.42	14.12	34.03	31.98	34.51	10.67	53.38	37.27	32.60	24.21	29.49
48 h	28.64	36.08	31.48	20.25	24.77	33.49	23.98	27.20	28.71	32.13	32.73	22.93	49.53
72 h	28.06	27.06	14.64	95.08	31.84	32.04	25.46	11.67	38.78	30.20	39.40	15.68	41.50
96 h	27.29	27.85	22.19	15.45	23.60	117.81	21.54	30.36	27.81	29.25	33.71	10.57	38.84
120 h	25.41	24.88	26.85	7.53	21.53	26.11	23.24	20.95	25.62	22.10	27.76	19.85	43.14

Table 4.3. CV values of SERS measurements of *S. epidermidis* on agar plates.

<i>S. epidermidis</i>	1 st Experiment				2 nd Experiment				3 rd Experiment				Total Avg.
	1 st spot	2 nd spot	3 rd spot	Avg. 1 st Exp.	1 st spot	2 nd spot	3 rd spot	Avg. 2 nd Exp.	1 st spot	2 nd spot	3 rd spot	Avg. 3 rd Exp.	
4 h	32.09	35.55	52.74	14.16	43.57	45.13	41.97	40.97	52.14	51.32	41.89	13.35	30.65
8 h	39.56	46.01	50.41	20.24	51.93	58.53	51.20	38.76	38.66	32.86	51.49	29.44	34.27
12 h	54.52	44.08	53.13	18.71	60.33	37.32	54.03	51.64	56.28	49.24	59.61	25.88	18.51
24 h	42.23	53.72	53.89	29.88	51.90	55.54	55.50	33.97	45.99	51.00	46.27	21.64	22.49
48 h	42.83	50.49	44.64	24.82	72.64	36.94	42.36	77.93	51.33	44.57	39.24	18.33	23.97
72 h	41.07	46.78	48.94	20.33	49.52	35.22	36.06	22.00	46.75	40.71	55.15	14.56	37.09
96 h	45.84	59.92	47.44	29.64	33.58	34.57	32.18	16.27	37.84	45.71	40.51	26.63	38.15
120 h	55.45	46.55	32.65	46.68	51.85	40.53	43.63	17.51	39.59	40.87	48.83	15.18	39.08

Table 4.4. CV values of SERS measurements of *C. albicans* on agar plates.

<i>C. albicans</i>	1 st Experiment				2 nd Experiment				3 rd Experiment				Total Avg.
	1 st spot	2 nd spot	3 rd spot	Avg. 1 st Exp.	1 st spot	2 nd spot	3 rd spot	Avg. 2 nd Exp.	1 st spot	2 nd spot	3 rd spot	Avg. 3 rd Exp.	
4 h	30.37	33.37	31.86	10.06	38.93	39.15	50.16	22.00	29.38	32.26	36.44	20.69	66.14
8 h	34.23	36.25	31.12	10.08	44.28	49.32	54.03	46.27	29.77	33.48	34.97	23.53	76.81
12 h	35.00	29.48	40.71	23.31	43.14	57.96	50.23	35.19	30.91	34.92	29.52	28.94	83.85
24 h	33.28	31.27	27.79	21.47	35.02	33.19	26.74	32.77	33.34	31.64	31.00	10.18	21.93
48 h	29.73	29.26	32.18	6.46	27.17	20.83	26.08	16.10	25.13	31.04	31.68	27.10	35.70
72 h	35.73	29.58	37.65	9.21	42.37	47.25	46.21	31.78	33.74	35.77	34.97	13.16	20.50
96 h	42.73	45.22	36.36	14.34	36.15	35.43	34.97	12.43	30.10	33.43	44.29	29.18	35.19
120 h	39.60	38.90	36.80	19.43	34.50	86.69	48.53	11.93	37.54	32.81	37.67	32.73	33.91

Table 4.5. CV values of SERS measurements of *P. aeruginosa* on 2D PMMA substrates.

<i>P.aeruginosa</i>	1 st Experiment				2 nd Experiment				3 rd Experiment				Total Avg.
	1 st spot	2 nd spot	3 rd spot	Avg. 1 st Exp.	1 st spot	2 nd spot	3 rd spot	Avg. 2 nd Exp.	1 st spot	2 nd spot	3 rd spot	Avg. 3 rd Exp.	
4 h	47.51	45.97	41.33	24.22	36.39	51.43	32.60	14.19	43.49	44.07	44.07	12.52	34.76
8 h	54.11	54.96	36.46	42.27	48.97	56.63	40.52	23.18	37.67	39.87	49.53	25.18	18.38
12 h	37.66	38.86	35.77	14.33	40.26	40.82	41.22	20.79	47.64	42.99	42.71	11.21	56.11
24 h	51.13	51.01	54.51	11.46	69.59	60.54	74.08	24.75	97.57	35.12	39.51	36.55	132.66
48 h	37.43	59.79	46.19	31.81	38.78	36.89	34.93	16.82	56.68	65.82	41.64	40.09	41.66
72 h	67.74	31.23	38.29	33.77	43.74	50.65	69.45	14.31	29.45	46.21	27.98	17.95	28.50
96 h	27.04	41.08	34.00	17.34	55.38	54.92	52.43	17.11	49.34	49.88	86.23	22.67	19.44
120 h	52.32	59.91	25.78	33.07	60.83	52.96	58.28	13.57	52.45	56.80	40.00	41.28	28.02

Table 4.6. CV values of SERS measurements of *S. epidermidis* on 2D PMMA substrates.

<i>S.epidermidis</i>	1 st Experiment				2 nd Experiment				3 rd Experiment				Total Avg.
	1 st spot	2 nd spot	3 rd spot	Avg. 1 st Exp.	1 st spot	2 nd spot	3 rd spot	Avg. 2 nd Exp.	1 st spot	2 nd spot	3 rd spot	Avg. 3 rd Exp.	
4 h	38.74	42.64	37.94	8.094	50.85	52.43	18.99	98.02	45.56	46.36	52.29	24.45	62.87
8 h	42.64	42.45	35.87	13.87	40.43	25.32	27.06	20.17	50.22	52.44	52.44	11.43	66.44
12 h	54.38	66.66	62.43	19.46	56.26	54.45	78.84	40.57	46.04	69.34	65.79	31.95	41.36
24 h	66.97	66.10	63.85	33.97	53.78	52.24	65.13	20.28	66.87	53.86	58.27	21.59	22.13
48 h	50.39	54.96	51.79	25.30	58.28	57.26	63.44	25.01	65.38	62.80	60.65	25.24	30.92
72 h	61.08	51.06	58.39	18.48	66.22	47.12	41.19	22.05	53.87	53.12	48.90	20.71	34.74
96 h	68.91	57.227	58.31	14.946	58.648	55.44	57.50	25.70	55.67	54.49	57.73	24.58	24.52
120 h	53.36	46.13	47.24	17.48	56.86	55.69	60.39	20.96	45.47	47.01	58.59	39.10	27.09

Table 4.7. CV values of SERS measurements of *C. albicans* on 2D PMMA substrates.

<i>C.albicans</i>	1 st Experiment				2 nd Experiment				3 rd Experiment				Total Avg.
	1 st spot	2 nd spot	3 rd spot	Avg. 1 st Exp.	1 st spot	2 nd spot	3 rd spot	Avg. 2 nd Exp.	1 st spot	2 nd spot	3 rd spot	Avg. 3 rd Exp.	
4 h	31.23	37.43	37.68	10.14	52.05	68.10	67.88	14.20	51.03	31.29	31.57	9.80	34.89
8 h	77.55	75.50	78.07	22.35	46.71	45.66	73.97	24.87	51.93	45.29	34.07	30.36	25.73
12 h	43.73	39.67	53.26	46.70	53.02	38.52	36.51	15.12	49.07	47.13	47.23	42.97	35.04
24 h	66.71	62.33	43.70	28.96	44.08	64.58	59.83	29.78	51.42	39.59	40.21	51.55	28.57
48 h	42.19	40.72	38.99	38.35	60.61	40.01	41.14	18.05	53.21	68.39	56.38	44.25	25.50
72 h	40.51	40.82	28.47	32.78	57.22	47.34	56.07	29.07	37.54	48.43	58.92	26.07	29.64
96 h	61.44	50.49	55.22	30.95	40.98	38.59	50.49	26.32	56.97	62.12	40.65	22.82	27.68
120 h	46.55	50.34	62.66	41.86	45.06	49.45	37.32	27.62	56.62	50.71	57.47	22.82	41.57

Table 4.8. CV values of SERS measurements of *P. aeruginosa* on 3D PMMA substrates.

<i>P.aeruginosa</i>	1 st Experiment				2 nd Experiment				3 rd Experiment				Total Avg.
	1 st spot	2 nd spot	3 rd spot	Avg. 1 st Exp.	1 st spot	2 nd spot	3 rd spot	Avg. 2 nd Exp.	1 st spot	2 nd spot	3 rd spot	Avg. 3 rd Exp.	
4 h	30.64	16.72	12.87	22.36	34.06	32.38	32.40	31.04	29.63	30.58	39.00	25.13	100.36
8 h	58.66	40.26	42.98	33.76	40.69	37.58	38.42	8.39	33.96	33.32	34.21	36.22	22.59
12 h	29.25	34.74	70.54	49.66	50.60	37.80	52.18	25.83	37.31	37.98	41.59	21.50	22.27
24 h	38.45	38.13	36.75	13.38	36.91	35.76	37.66	12.50	41.40	38.26	39.10	19.13	17.44
48 h	35.03	38.87	52.14	31.43	39.58	38.33	37.96	12.00	36.57	38.35	46.53	12.30	16.03
72 h	60.87	46.79	59.38	10.72	58.29	42.88	39.23	46.87	49.53	76.79	44.00	51.08	27.27
96 h	36.36	66.62	37.12	37.95	35.41	79.36	41.19	28.82	52.42	36.89	39.50	18.77	22.29
120 h	74.11	38.20	68.23	43.57	53.73	77.17	65.05	19.93	38.54	36.96	46.10	19.57	31.58

Table 4.9. CV values of SERS measurements of *S. epidermidis* on 3D PMMA substrates.

<i>S.epidermidis</i>	1 st Experiment				2 nd Experiment				3 rd Experiment				Total Avg.
	1 st spot	2 nd spot	3 rd spot	Avg. 1 st Exp.	1 st spot	2 nd spot	3 rd spot	Avg. 2 nd Exp.	1 st spot	2 nd spot	3 rd spot	Avg. 3 rd Exp.	
4 h	33.18	38.39	33.50	16.73	28.80	88.58	29.61	31.42	40.58	35.02	36.63	25.12	39.04
8 h	52.20	58.94	52.70	23.08	40.86	39.95	38.35	11.98	38.51	36.18	38.34	14.76	27.77
12 h	59.93	36.13	37.05	29.15	32.79	35.52	12.20	67.97	38.70	80.77	58.61	27.62	44.07
24 h	34.75	36.75	35.60	49.28	54.25	53.08	35.90	24.86	54.76	56.80	59.82	27.13	21.59
48 h	40.09	51.11	36.08	23.22	38.22	57.34	63.75	28.14	67.81	57.26	51.53	29.82	33.10
72 h	37.45	39.07	38.56	28.21	59.45	55.47	59.12	46.84	105.17	58.47	53.73	16.88	30.73
96 h	38.52	35.99	42.93	35.82	35.91	52.65	33.52	18.02	42.44	71.41	37.84	48.82	26.80
120 h	70.26	58.01	37.76	45.72	89.89	78.09	78.83	10.42	80.19	57.51	48.26	24.26	12.88

Table 4.10. CV values of SERS measurements of *C. albicans* on 3D PMMA substrates.

<i>C.albicans</i>	1 st Experiment				2 nd Experiment				3 rd Experiment				Total Avg.
	1 st spot	2 nd spot	3 rd spot	Avg. 1 st Exp.	1 st spot	2 nd spot	3 rd spot	Avg. 2 nd Exp.	1 st spot	2 nd spot	3 rd spot	Avg. 3 rd Exp.	
4 h	32.11	33.75	35.88	23.22	35.17	35.48	34.91	6.816	43.70	56.92	26.18	23.71	84.60
8 h	30.28	43.34	28.11	22.93	39.65	34.43	47.84	16.64	37.77	29.98	31.13	34.76	61.95
12 h	46.43	53.23	31.99	15.79	38.12	34.15	31.43	16.14	33.93	48.31	31.52	14.49	72.79
24 h	37.79	38.27	32.14	19.90	41.64	32.93	34.68	95.25	46.15	46.72	48.13	15.43	56.86
48 h	31.92	42.38	37.43	32.09	38.01	36.52	30.96	25.30	40.89	30.99	32.49	12.85	20.97
72 h	42.92	36.25	35.37	31.30	48.35	40.03	51.99	23.43	35.73	34.56	35.04	27.49	40.90
96 h	60.47	28.06	44.30	62.30	37.48	43.17	36.95	6.14	36.56	36.15	57.43	33.81	62.30
120 h	35.99	43.87	35.21	8.23	37.48	37.44	35.59	22.11	46.56	45.76	57.68	19.02	20.87

Table 4.11. CV values of SERS measurements of *P. aeruginosa* on 3D glucose-gelatin scaffolds.

<i>P.aeruginosa</i>	1 st Experiment				2 nd Experiment				3 rd Experiment				Total Avg.
	1 st spot	2 nd spot	3 rd spot	Avg. 1 st Exp.	1 st spot	2 nd spot	3 rd spot	Avg. 2 nd Exp.	1 st spot	2 nd spot	3 rd spot	Average 3 rd Exp.	
4 h	35.41	34.55	35.19	6.67	43.49	33.77	35.05	15.66	38.96	40.29	44.35	36.15	21.00
8 h	32.89	32.86	32.78	7.14	36.21	38.59	35.69	15.10	37.25	34.75	35.27	6.52	11.83
12 h	35.68	35.87	34.39	7.86	34.47	33.39	33.26	7.35	32.70	34.59	34.59	7.52	7.86
24 h	45.98	31.79	55.98	40.68	29.77	27.32	38.22	31.18	20.68	43.24	33.19	23.04	18.45
48 h	24.58	24.16	29.56	19.94	24.73	26.45	26.80	19.02	23.95	28.87	24.55	15.93	10.08
72 h	28.51	30.27	30.67	18.11	30.62	30.48	31.48	15.95	33.29	32.14	28.17	14.92	16.90
96 h	31.38	31.56	31.33	17.14	29.99	32.50	33.10	17.49	33.12	30.62	34.78	15.82	17.76
120 h	38.60	30.21	31.92	28.96	30.75	32.28	32.26	22.77	32.42	35.02	30.57	20.51	15.46

Table 4.12. CV values of SERS measurements of *S. epidermidis* on 3D glucose-gelatin scaffolds.

<i>S.epidermidis</i>	1 st Experiment				2 nd Experiment				3 rd Experiment				Total Avg.
	1 st spot	2 nd spot	3 rd spot	Avg. 1 st Exp.	1 st spot	2 nd spot	3 rd spot	Avg. 2 nd Exp.	1 st spot	2 nd spot	3 rd spot	Avg. 3 rd Exp.	
4 h	44.10	48.24	36.55	10.79	38.69	45.80	46.18	23.83	38.28	40.13	77.42	19.23	34.38
8 h	40.74	35.79	36.67	9.55	32.01	29.12	32.55	20.01	61.26	28.38	29.43	18.86	21.57
12 h	39.19	40.36	37.82	54.02	43.89	28.74	45.60	53.65	38.30	44.75	34.60	30.63	40.62
24 h	53.01	38.40	39.30	51.69	33.74	35.09	42.22	18.77	33.07	39.42	39.14	49.72	23.08
48 h	60.55	42.67	42.17	55.59	33.24	58.69	31.40	71.30	29.93	50.61	49.64	61.24	46.95
72 h	43.64	35.63	38.03	18.53	39.98	40.04	35.81	29.91	48.07	35.72	38.11	32.38	76.36
96 h	40.44	57.27	35.98	18.02	47.19	39.67	37.46	27.78	38.27	43.80	40.42	37.19	29.69
120 h	34.66	31.09	37.10	15.04	63.46	55.86	41.63	13.98	45.48	52.33	38.49	22.99	79.77

Table 4.13. CV values of SERS measurements of *C. albicans* on 3D glucose-gelatin scaffolds.

<i>C.albicans</i>	1 st Experiment				2 nd Experiment				3 rd Experiment				Total Avg.
	1 st spot	2 nd spot	3 rd spot	Avg. 1 st Exp.	1 st spot	2 nd spot	3 rd spot	Avg. 2 nd Exp.	1 st spot	2 nd spot	3 rd spot	Avg. 3 rd Exp.	
4 h	36.19	34.93	36.36	132.87	50.34	37.47	36.28	58.09	30.55	34.72	35.94	33.40	144.98
8 h	43.37	32.73	34.78	57.09	31.14	30.58	33.27	27.72	35.14	35.03	33.44	8.78	63.88
12 h	44.34	47.95	36.67	30.83	33.41	57.74	54.29	28.92	43.60	40.14	43.85	37.16	50.99
24 h	53.35	41.76	43.59	38.07	38.36	49.36	62.29	65.35	51.60	47.19	43.13	39.46	17.06
48 h	42.60	37.32	33.72	19.53	56.53	36.01	48.04	13.53	42.67	49.78	41.68	19.88	48.86
72 h	35.19	34.67	36.95	6.03	35.65	35.46	34.48	6.93	48.89	45.32	35.42	40.96	22.09
96 h	57.28	42.21	36.11	20.54	39.82	35.10	47.34	9.32	32.94	36.69	38.52	14.10	33.42
120 h	34.22	33.25	34.87	6.62	35.15	41.17	32.41	33.03	36.82	41.74	34.68	15.69	26.95

5. CONCLUSIONS AND OUTLOOK

Biofilm formation monitoring and discrimination of clinically relevant microorganisms *P. aeruginosa*, *S. epidermidis* and *C. albicans* on different host surfaces from 4 to 120 h incubation times were studied using SERS in this thesis. The model microorganisms were grown under four different conditions, on an agar plate, on 2D and 3D polymeric substrates used for construction of medical devices, and a 3D scaffold built from glucose-gelatin mixture. On an agar plate, the microorganisms can freely grow and multiply under almost no stress conditions. On 2D and 3D polymeric surfaces, they are under stress due to scarce amount of nutrients but on a 3D polymeric surface the fibrous structure can enhance proliferation of microorganisms. On a 3D scaffold built from glucose and gelatin, the scaffold components can be used as nutrients but the surface structure can cause stress on them. Thus, the metabolic activity of microorganisms is expected to be varied and these variations reflected on the SERS spectra. The obtained spectral data can be both used for biofilm formation monitoring and discrimination of formed biofilms to identify the biofilm forming microorganism.

Agar plates were used as a substrate to evaluate the metabolic activities of microorganisms on their natural conditions. From the spectral analysis; *P. aeruginosa* was found to be the most metabolically active microorganism that its spectral pattern changed significantly after 24 h incubation. Protein synthesis was increased significantly with increasing incubation time and also pyocyanin expression was identified after 8 h incubation, which can be assigned as a biomarker for *P. aeruginosa* [250]. The biofilm formation process of *S. epidermidis* was slower compared to *P. aeruginosa*, such that a slight increase in concentration of proteins and lipids were observed after 48 h incubation. *C. albicans* behaved differently from the other bacteria during biofilm production. The time points of 24 and 48 h were distinct, when carbohydrate, protein and lipid synthesis increased and provided a unique spectral pattern.

Biofilm formation on 2D PMMA substrates altered the metabolic activity processes of microorganisms as a result of hydrophobic polymeric host surface. In general, microorganisms tend to attach themselves onto hydrophobic surfaces [149, 153]. *P. aeruginosa* produced sticky polymeric shell after 72 h on PMMA substrate. The sticky

shell covered the whole cells, thus the intensity of the peak attributed purine bases decreased significantly at this time point. High levels of carbohydrate, protein and pyocyanin synthesis were also observed with the maturation of *P. aeruginosa* biofilm. Although biofilm formation of *S. epidermidis* occurred at 96 h on the hydrophobic host surface, a significant polymeric carbohydrate and protein synthesis could be observed. For *C. albicans*, polysaccharides and eDNA were determined as the main ingredients of the mature biofilm.

Rough surface can enhance the adhesion of microorganisms through providing a large surface area. The prepared fibrous 3D PMMA substrates facilitated the adhesion and accelerated formation of EPS for all three model microorganisms. The non-smooth surface of the substrate caused irregular fluctuations from time point to time point in *P. aeruginosa* biofilm. Nevertheless, EPS production could be identified after 72 h incubation. Furthermore, the fibrous structure enhanced the adhesion of *S. epidermidis* compared to the 2D flat polymeric substrate. The microorganisms entered early maturation phase within 24 h incubation on 2D surfaces. The PMMA surface increased the adaptation period of *C. albicans* compared to the agar plates. The microorganisms entered the maturation phase at 48 and 72 h on polymeric substrates, whereas on agar plates the main spectral pattern change was observed at 24 h. On the other hand, when the 2D and 3D PMMA substrates were compared among themselves; the fibrous structure enhanced the assembly of microorganisms and enriched the biofilm structure. Based on these findings, it is found that smooth polymeric surfaces decrease the biofilm formation rate of microorganisms significantly. Normally polymeric medical implants have smooth surfaces but their surface topography changes and become porous due to degradation of these devices in human body. The stability of polymeric devices in human body has to be consider to prevent alterations on polymeric surfaces and decrease the biofilm formation. It was also find out that *P. aeruginosa* and *C. albicans* have tendency to form biofilm on both 2D and 3D polymeric surfaces while *S. epidermidis* slowed down its metabolic activity and did not proliferate very effectively.

3D glucose-gelatin scaffold was prepared as a representative host surface that could be used as an energy source by microorganisms in the environment. Because *P. aeruginosa* and *C. albicans* can express gelatinase enzyme, they used the scaffold as an energy source, which altered their metabolic activities. As a very aggressive species, *P. aeruginosa*

digested all the scaffold in 24 h incubation and increased the expression of protein, lipid and pyocyanin remarkably with increasing incubation time. *C. albicans* could not use the scaffold as efficient as *P. aeruginosa* but the scaffold also helped to diversify the content of the biofilm structure as nutrient source. Different from these two microorganisms, *S. epidermidis* showed a slow adaptation process that only carbohydrate and protein synthesis was observed after 96 h incubation.

One of the main objectives of this study was to discriminate the different microorganisms from the SERS spectral data combined with PC-LDA multivariate statistical analysis. With this aim, the effective PCs were determined, which showed fluctuations in intensities of nucleic acids, amino acids, carbohydrates, proteins and lipids for all microorganisms and significantly pyocyanin was identified as a unique spectral signature for *P. aeruginosa*. From the thorough analysis with PC-LDA, three model microorganisms could be discriminated successfully on both substrates based on their distinct spectral profiles.

It may be thought that discriminating the microorganism biofilms inoculated on different substrates separately can be relatively easy but in a multi-species biofilm that is more relevant to the clinical cases can be challenging. For this, a multi-species biofilm sample was prepared and examined on an agar plate. The evaluation of the SERS spectral data revealed that the surviving species in the complex biofilm was *P. aeruginosa*, which was also verified with other microscopic techniques. As an aggressive species, *P. aeruginosa*, suppressed the proliferation of *S. epidermidis* and *C. albicans* in 48 h incubation and became the dominant species in the biofilm.

This study is an exploratory in nature to exploit the full potential of SERS. The band assignments on the SERS spectra were made from the previous studies reported in the literature and needs conformation to fully understand attributed changes due to that of molecular species. Thus, other spectroscopic techniques such as mass spectroscopy to identify the EPS components in detail can provide much satisfactory information about the metabolic profiles of microorganisms during the process. Furthermore, evaluating the biofilm formation using SERS under external conditions such as heat shock and antibiotic treatment can provide valuable information for discovery of novel medical treatments.

This study has also revealed that the host surface and surface structure can play an important role as it was found out from the metabolic profiles of the important model

microorganisms. In addition, the possibility of using SERS for discrimination of microorganisms in heterogenic biofilms was demonstrated indicating the potential of the technique for novel applications in clinics.

This study can be further extended into evaluation of real biofilm samples obtained from medical implants. In clinics, the aim is to identify the microorganisms forming the biofilm quickly. As this study suggests, SERS is a potential technique for rapid identification of the microorganisms forming a biofilm. The simplicity and speed of the technique is the real advantage in a clinical setting. The examination of the real biofilm samples from several implants with SERS and conventional approaches can really help to explore the real potential of the technique.

REFERENCES

1. Madigan MT, Martinko JM, Stahl AD, Clark PD. *Brock biology of microorganisms*. San Francisco: Pearson Benjamin-Cummings; 2010.
2. Ingraham JL, Maaløe O, Neidhart FC. "Growth rate as a variable," in *growth of the bacterial cell*. Sunderland, MA: Sinauer Associates; 1983.
3. Costerton JW, Cheng KJ, Geesey GG, Ladd TI, Nickel JC, Dasgupta M, Marrie TJ. Bacterial biofilms in nature and disease. *Annual Review of Microbiology*. 1987;41:435-64.
4. Vu B, Chen M, Crawford RJ, Ivanova EP. Bacterial extracellular polysaccharides involved in biofilm formation. *Molecules*. 2009;14(7):2535-54.
5. Heukelekian H, Heller A. Relation between food concentration and surface for bacterial growth. *Journal of Bacteriology*. 1940;40(4):547-58.
6. Zobell CE. The effect of solid surfaces upon bacterial activity. *Journal of Bacteriology*. 1943;46(1):39-56.
7. Jones HC, Roth IL, Sanders WM, 3rd. Electron microscopic study of a slime layer. *Journal of Bacteriology*. 1969;99(1):316-25.
8. Costerton JW, Geesey GG, Cheng KJ. How bacteria stick. *Scientific American*. 1978;238(1):86-95.
9. Donlan RM. Biofilms: Microbial life on surfaces. *Emerging Infectious Diseases*. 2002;8(9):881-90.
10. Costerton JW, Lewandowski Z, Caldwell DE, Korber DR, Lappin-Scott HM. Microbial biofilms. *Annual Review of Microbiology*. 1995;49:711-45.

11. Costerton JW, Irvin RT, Cheng KJ. The bacterial glycocalyx in nature and disease. *Annual Review of Microbiology*. 1981;35:299-324.
12. Sauer K, Cullen MC, Rickard AH, Zeef LA, Davies DG, Gilbert P. Characterization of nutrient-induced dispersion in *pseudomonas aeruginosa* pao1 biofilm. *Journal of Bacteriology*. 2004;186(21):7312-26.
13. Gjermansen M, Ragas P, Sternberg C, Molin S, Tolker-Nielsen T. Characterization of starvation-induced dispersion in *pseudomonas putida* biofilms. *Environmental Microbiology*. 2005;7(6):894-906.
14. Ahimou F, Semmens MJ, Haugstad G, Novak PJ. Effect of protein, polysaccharide, and oxygen concentration profiles on biofilm cohesiveness. *Applied and Environmental Microbiology*. 2007;73(9):2905-10.
15. Palmer RJ, Jr., White DC. Developmental biology of biofilms: Implications for treatment and control. *Trends in Biotechnology*. 1997;5(11):435-40.
16. Sutherland IW. The biofilm matrix an immobilized but dynamic microbial environment. *Trends in Biotechnology*. 2001;9(5):222-7.
17. Davey ME, O'Toole G A. Microbial biofilms: From ecology to molecular genetics. *Microbiology and Molecular Biology Reviews*. 2000;64(4):847-67.
18. Whiteley M, Bangerla MG, Bumgarner RE, Parsek MR, Teitzel GM, Lory S, Greenberg EP. Gene expression in *pseudomonas aeruginosa* biofilms. *Nature*. 2001;413(6858):860-4.
19. Davies DG, Geesey GG. Regulation of the alginate biosynthesis gene *algC* in *pseudomonas aeruginosa* during biofilm development in continuous culture. *Applied and Environmental Microbiology*. 1995;61(3):860-7.

20. Patel JD, Colton E, Ebert M, Anderson JM. Gene expression during *S. epidermidis* biofilm formation on biomaterials. *Journal of Biomedical Materials Research A*. 2012;100(11):2863-9.
21. Wang L, Li M, Dong D, Bach TH, Sturdevant DE, Vuong C, Otto M, Gao Q. Sarz is a key regulator of biofilm formation and virulence in *staphylococcus epidermidis*. *The Journal of Infectious Diseases*. 2008;197(9):1254-62.
22. Nobile CJ, Mitchell AP. Genetics and genomics of *candida albicans* biofilm formation. *Cellular Microbiology*. 2006;8(9):1382-91.
23. Miller MB, Bassler BL. Quorum sensing in bacteria. *Annual Review of Microbiology*. 2001;55:165-99.
24. Kociolek MG. Quorum-sensing inhibitors and biofilm. *Anti-Infective Agents in Medicinal Chemistry*. 2009;8: 315-26.
25. Alem MA, Oteef MD, Flowers TH, Douglas LJ. Production of tyrosol by *candida albicans* biofilms and its role in quorum sensing and biofilm development. *Eukaryotic Cell*. 2006;5(10):1770-9.
26. Govan JR, Deretic V. Microbial pathogenesis in cystic fibrosis: Mucoid *pseudomonas aeruginosa* and *burkholderia cepacia*. *Microbiological Reviews*. 1996;60(3):539-74.
27. Jung GB, Nam SW, Choi S, Lee GJ, Park HK. Evaluation of antibiotic effects on *pseudomonas aeruginosa* biofilm using Raman spectroscopy and multivariate analysis. *Biomedical Optics Express*. 2014;5(9):3238-51.
28. O'Toole G, Kaplan HB, Kolter R. Biofilm formation as microbial development. *Annual Review of Microbiology*. 2000;54:49-79.

29. Rybtke MT, Jensen PO, Hoiby N, Givskov M, Tolker-Nielsen T, Bjarnsholt T. The implication of *pseudomonas aeruginosa* biofilms in infections. *Inflammation & Allergy Drug Targets*. 2011;10(2):141-57.
30. Giltner CL, van Schaik EJ, Audette GF, Kao D, Hodges RS, Hassett DJ, Irvin RT. The *pseudomonas aeruginosa* type iv pilin receptor binding domain functions as an adhesin for both biotic and abiotic surfaces. *Molecular Microbiology*. 2006;59(4):1083-96.
31. O'Toole GA, Kolter R. Flagellar and twitching motility are necessary for *pseudomonas aeruginosa* biofilm development. *Molecular Microbiology*. 1998;30(2):295-304.
32. Vallet I, Olson JW, Lory S, Lazdunski A, Filloux A. The chaperone/usher pathways of *pseudomonas aeruginosa*: Identification of fimbrial gene clusters (cup) and their involvement in biofilm formation. *Proceedings of the National Academy of Sciences*. 2001;98(12):6911-6.
33. Jackson KD, Starkey M, Kremer S, Parsek MR, Wozniak DJ. Identification of psl, a locus encoding a potential exopolysaccharide that is essential for *pseudomonas aeruginosa* pao1 biofilm formation. *Journal of Bacteriology*. 2004;186(14):4466-75.
34. Ma L, Conover M, Lu H, Parsek MR, Bayles K, Wozniak DJ. Assembly and development of the *pseudomonas aeruginosa* biofilm matrix. *PLOS Pathogens*. 2009;5(3):e1000354.
35. Whitchurch CB, Tolker-Nielsen T, Ragas PC, Mattick JS. Extracellular DNA required for bacterial biofilm formation. *Science*. 2002;295(5559):1487.
36. Molin S, Tolker-Nielsen T. Gene transfer occurs with enhanced efficiency in biofilms and induces enhanced stabilisation of the biofilm structure. *Current Opinion in Biotechnology*. 2003;14(3):255-61.

37. Friedman L, Kolter R. Genes involved in matrix formation in *pseudomonas aeruginosa* pa14 biofilms. *Molecular Microbiology*. 2004;51(3):675-90.
38. Yang L, Nilsson M, Gjermansen M, Givskov M, Tolker-Nielsen T. Pyoverdine and pqs mediated subpopulation interactions involved in *pseudomonas aeruginosa* biofilm formation. *Molecular Microbiology*. 2009;74(6):1380-92.
39. Pamp SJ, Gjermansen M, Tolker-Nielsen T. The biofilm matrix: A sticky framework. *The biofilm mode of life: Mechanisms and adaptations*. 2007; 37-69.
40. Keith RC, Keith LM, Hernandez-Guzman G, Uppalapati SR, Bender CL. Alginate gene expression by *pseudomonas syringae* pv. Tomato dc3000 in host and non-host plants. *Microbiology*. 2003;149(Pt 5):1127-38.
41. Penaloza-Vazquez A, Kidambi SP, Chakrabarty AM, Bender CL. Characterization of the alginate biosynthetic gene cluster in *pseudomonas syringae* pv. *syringae*. *Journal of Bacteriology*. 1997;179(14):4464-72.
42. Laue H, Schenk A, Li H, Lambertsen L, Neu TR, Molin S, Ullrich MS. Contribution of alginate and levan production to biofilm formation by *pseudomonas syringae*. *Microbiology*. 2006;152(Pt 10):2909-18.
43. Osman SF, Fett WF, Fishman ML. Exopolysaccharides of the phytopathogen *pseudomonas syringae* pv. *Glycinea*. *Journal of Bacteriology*. 1986;166(1):66-71.
44. Ryder C, Byrd M, Wozniak DJ. Role of polysaccharides in *pseudomonas aeruginosa* biofilm development. *Current Opinion in Microbiology*. 2007;10(6):644-8.
45. Govan JR, Deretic V. Microbial pathogenesis in cystic fibrosis: Mucoid *pseudomonas aeruginosa* and *burkholderia cepacia*. *Microbiol Rev*. 1996;60(3):539-74.

46. Hentzer M, Teitzel GM, Balzer GJ, Heydorn A, Molin S, Givskov M, Parsek MR. Alginate overproduction affects *pseudomonas aeruginosa* biofilm structure and function. *Journal of Bacteriology*. 2001;183(18):5395-401.
47. Sutherland I. Biofilm exopolysaccharides: A strong and sticky framework. *Microbiology*. 2001;147(Pt 1):3-9.
48. Tielen P, Strathmann M, Jaeger KE, Flemming HC, Wingender J. Alginate acetylation influences initial surface colonization by mucoid *pseudomonas aeruginosa*. *Microbiological Research*. 2005;160(2):165-76.
49. Ma L, Jackson KD, Landry RM, Parsek MR, Wozniak DJ. Analysis of *pseudomonas aeruginosa* conditional psl variants reveals roles for the psl polysaccharide in adhesion and maintaining biofilm structure postattachment. *Journal of Bacteriology*. 2006;188(23):8213-21.
50. Overhage J, Schemionek M, Webb JS, Rehm BH. Expression of the psl operon in *pseudomonas aeruginosa* pao1 biofilms: Psla performs an essential function in biofilm formation. *Applied and Environmental Microbiology*. 2005;71(8):4407-13.
51. Allesen-Holm M, Barken KB, Yang L, Klausen M, Webb JS, Kjelleberg S, Molin S, Givskov M, Tolker-Nielsen T. A characterization of DNA release in *pseudomonas aeruginosa* cultures and biofilms. *Molecular Microbiology*. 2006;59(4):1114-28.
52. Alipour M, Suntres ZE, Omri A. Importance of dnase and alginate lyase for enhancing free and liposome encapsulated aminoglycoside activity against *pseudomonas aeruginosa*. *Journal of Antimicrobial Chemotherapy*. 2009;64(2):317-25.
53. Borlee BR, Goldman AD, Murakami K, Samudrala R, Wozniak DJ, Parsek MR. *Pseudomonas aeruginosa* uses a cyclic-di-gmp-regulated adhesin to reinforce the biofilm extracellular matrix. *Molecular Microbiology*. 2010;75(4):827-42.

54. Diggle SP, Stacey RE, Dodd C, Camara M, Williams P, Winzer K. The galactophilic lectin, leca, contributes to biofilm development in *pseudomonas aeruginosa*. *Environmental Microbiology*. 2006;8(6):1095-104.
55. Johansson EM, Crusz SA, Kolomiets E, Buts L, Kadam RU, Cacciarini M, Bartels KM, Diggle SP, Camara M, Williams P, Loris R, Nativi C, Rosenau F, Jaeger KE, Darbre T, Reymond JL. Inhibition and dispersion of *pseudomonas aeruginosa* biofilms by glycopeptide dendrimers targeting the fucose-specific lectin lecb. *Chemistry & Biology*. 2008;15(12):1249-57.
56. Tielker D, Hacker S, Loris R, Strathmann M, Wingender J, Wilhelm S, Rosenau F, Jaeger KE. *Pseudomonas aeruginosa* lectin lecb is located in the outer membrane and is involved in biofilm formation. *Microbiology*. 2005;151(Pt 5):1313-23.
57. Abel MH, Bass FG, Krane EJ, Thomas AL, Liggins GC. Pituitary stalk-section and some of its effects on endocrine function in the fetal lamb. *Quarterly Journal of Experimental Physiology and Cognate Medical Sciences*. 1978;63(3):211-9.
58. Lequette Y, Greenberg EP. Timing and localization of rhamnolipid synthesis gene expression in *pseudomonas aeruginosa* biofilms. *Journal of Bacteriology*. 2005;187(1):37-44.
59. Pamp SJ, Tolker-Nielsen T. Multiple roles of biosurfactants in structural biofilm development by *pseudomonas aeruginosa*. *Journal of Bacteriology*. 2007;189(6):2531-9.
60. Boles BR, Thoendel M, Singh PK. Rhamnolipids mediate detachment of *pseudomonas aeruginosa* from biofilms. *Molecular Microbiology*. 2005;57(5):1210-23.
61. Schleheck D, Barraud N, Klebensberger J, Webb JS, McDougald D, Rice SA, Kjelleberg S. *Pseudomonas aeruginosa* pao1 preferentially grows as aggregates in liquid batch cultures and disperses upon starvation. *PLoS One*. 2009;4(5):e5513.

62. Barraud N, Hassett DJ, Hwang SH, Rice SA, Kjelleberg S, Webb JS. Involvement of nitric oxide in biofilm dispersal of *pseudomonas aeruginosa*. *Journal of Bacteriology*. 2006;188(21):7344-53.
63. Banin E, Brady KM, Greenberg EP. Chelator-induced dispersal and killing of *pseudomonas aeruginosa* cells in a biofilm. *Applied and Environmental Microbiology*. 2006;72(3):2064-9.
64. Yang L, Barken KB, Skindersoe ME, Christensen AB, Givskov M, Tolker-Nielsen T. Effects of iron on DNA release and biofilm development by *pseudomonas aeruginosa*. *Microbiology*. 2007;153(Pt 5):1318-28.
65. Davey ME, Caiazza NC, O'Toole GA. Rhamnolipid surfactant production affects biofilm architecture in *pseudomonas aeruginosa* pao1. *Journal of Bacteriology*. 2003;185(3):1027-36.
66. Goodman AL, Kulasekara B, Rietsch A, Boyd D, Smith RS, Lory S. A signaling network reciprocally regulates genes associated with acute infection and chronic persistence in *pseudomonas aeruginosa*. *Developmental Cell*. 2004;7(5):745-54.
67. Hengge R. Principles of c-di-gmp signalling in bacteria. *Nature Reviews Microbiology*. 2009;7(4):263-73.
68. Vuong C, Otto M. *Staphylococcus epidermidis* infections. *Microbes and Infection*. 2002;4(4):481-9.
69. Gottenbos B, van der Mei HC, Busscher HJ. Initial adhesion and surface growth of *staphylococcus epidermidis* and *pseudomonas aeruginosa* on biomedical polymers. *Journal of Biomedical Materials Research*. 2000;50(2):208-14.

70. Mazmanian SK, Ton-That H, Schneewind O. Sortase-catalysed anchoring of surface proteins to the cell wall of *staphylococcus aureus*. *Molecular Microbiology*. 2001;40(5):1049-57.
71. Nilsson M, Frykberg L, Flock JI, Pei L, Lindberg M, Guss B. A fibrinogen-binding protein of *staphylococcus epidermidis*. *Infection and Immunity*. 1998;66(6):2666-73.
72. Pei L, Flock JI. Lack of fbe, the gene for a fibrinogen-binding protein from *staphylococcus epidermidis*, reduces its adherence to fibrinogen coated surfaces. *Microbial Pathogenesis*. 2001;31(4):185-93.
73. Pei L, Flock JI. Functional study of antibodies against a fibrogenin-binding protein in *staphylococcus epidermidis* adherence to polyethylene catheters. *The Journal of Infectious Diseases*. 2001;184(1):52-5.
74. McCrea KW, Hartford O, Davis S, Eidhin DN, Lina G, Speziale P, Foster TJ, Hook M. The serine-aspartate repeat (sdr) protein family in *staphylococcus epidermidis*. *Microbiology*. 2000;146 (Pt 7):1535-46.
75. Hussain M, Herrmann M, von Eiff C, Perdreau-Remington F, Peters G. A 140-kilodalton extracellular protein is essential for the accumulation of *staphylococcus epidermidis* strains on surfaces. *Infection and Immunity*. 1997;65(2):519-24.
76. Mack D, Fischer W, Krokotsch A, Leopold K, Hartmann R, Egge H, Laufs R. The intercellular adhesin involved in biofilm accumulation of *staphylococcus epidermidis* is a linear beta-1,6-linked glucosaminoglycan: Purification and structural analysis. *Journal of Bacteriology*. 1996;178(1):175-83.
77. McKenney D, Pouliot K, Wang Y, Murthy V, Ulrich M, Doring G, Lee JC, Goldmann DA, Pier GB. Vaccine potential of poly-1-6 beta-d-n-succinylglucosamine, an immunoprotective surface polysaccharide of *staphylococcus aureus* and *staphylococcus epidermidis*. *Journal of Biotechnology*. 2000;83(1-2):37-44.

78. Heilmann C, Schweitzer O, Gerke C, Vanittanakom N, Mack D, Gotz F. Molecular basis of intercellular adhesion in the biofilm-forming *staphylococcus epidermidis*. *Molecular Microbiology*. 1996;20(5):1083-91.
79. McKenney D, Hubner J, Muller E, Wang Y, Goldmann DA, Pier GB. The ica locus of *staphylococcus epidermidis* encodes production of the capsular polysaccharide/adhesin. *Infection and Immunity*. 1998;66(10):4711-20.
80. Fey PD, Ulphani JS, Gotz F, Heilmann C, Mack D, Rupp ME. Characterization of the relationship between polysaccharide intercellular adhesin and hemagglutination in *staphylococcus epidermidis*. *The Journal of Infectious Diseases*. 1999;179(6):1561-4.
81. Vuong C, Voyich JM, Fischer ER, Braughton KR, Whitney AR, DeLeo FR, Otto M. Polysaccharide intercellular adhesin (pia) protects *staphylococcus epidermidis* against major components of the human innate immune system. *Cellular Microbiology*. 2004;6(3):269-75.
82. Kocianova S, Vuong C, Yao Y, Voyich JM, Fischer ER, DeLeo FR, Otto M. Key role of poly-gamma-dl-glutamic acid in immune evasion and virulence of *staphylococcus epidermidis*. *The Journal of Clinical Investigation*. 2005;115(3):688-94.
83. Fey PD, Olson ME. Current concepts in biofilm formation of *staphylococcus epidermidis*. *Future Microbiology*. 2010;5(6):917-33.
84. Sun D, Accavitti MA, Bryers JD. Inhibition of biofilm formation by monoclonal antibodies against *staphylococcus epidermidis* rp62a accumulation-associated protein. *Clinical and Diagnostic Laboratory Immunology*. 2005;12(1):93-100.
85. Tormo MA, Knecht E, Gotz F, Lasa I, Penades JR. Bap-dependent biofilm formation by pathogenic species of *staphylococcus*: Evidence of horizontal gene transfer? *Microbiology*. 2005;151(Pt 7):2465-75.

86. Degnan BA, Fontaine MC, Doebereiner AH, Lee JJ, Mastroeni P, Dougan G, Goodacre JA, Kehoe MA. Characterization of an isogenic mutant of *streptococcus pyogenes manfredo* lacking the ability to make *streptococcal* acid glycoprotein. *Infection and Immunity*. 2000;68(5):2441-8.
87. Degnan BA, Palmer JM, Robson T, Jones CE, Fischer M, Glanville M, Mellor GD, Diamond AG, Kehoe MA, Goodacre JA. Inhibition of human peripheral blood mononuclear cell proliferation by *streptococcus pyogenes* cell extract is associated with arginine deiminase activity. *Infection and Immunity*. 1998;66(7):3050-8.
88. Chandra J, Kuhn DM, Mukherjee PK, Hoyer LL, McCormick T, Ghannoum MA. Biofilm formation by the fungal pathogen *candida albicans*: Development, architecture, and drug resistance. *Journal of Bacteriology*. 2001;183(18):5385-94.
89. Pierce CG, Vila T, Romo JA, Montelongo-Jauregui D, Wall G, Ramasubramanian A, Lopez-Ribot JL. The *candida albicans* biofilm matrix: Composition, structure and function. *Journal of Fungi (Basel)*. 2017;3(1).
90. Nobile CJ, Nett JE, Hernday AD, Homann OR, Deneault JS, Nantel A, Andes DR, Johnson AD, Mitchell AP. Biofilm matrix regulation by *candida albicans zap1*. *PLoS Biology*. 2009;7(6):e1000133.
91. Zarnowski R, Westler WM, Lacmbouh GA, Marita JM, Bothe JR, Bernhardt J, Lounes-Hadj Sahraoui A, Fontaine J, Sanchez H, Hatfield RD, Ntambi JM, Nett JE, Mitchell AP, Andes DR. Novel entries in a fungal biofilm matrix encyclopedia. *MBio*. 2014;5(4):e01333-14.
92. Chaffin WL, Lopez-Ribot JL, Casanova M, Gozalbo D, Martinez JP. Cell wall and secreted proteins of *candida albicans*: Identification, function, and expression. *Microbiology and Molecular Biology Reviews*. 1998;62(1):130-80.

93. Nobile CJ, Johnson AD. *Candida albicans* biofilms and human disease. *Annual Review of Microbiology*. 2015;69:71-92.
94. Zhao X, Daniels KJ, Oh SH, Green CB, Yeater KM, Soll DR, Hoyer LL. *Candida albicans* als3p is required for wild-type biofilm formation on silicone elastomer surfaces. *Microbiology*. 2006;152(Pt 8):2287-99.
95. Martins M, Uppuluri P, Thomas DP, Cleary IA, Henriques M, Lopez-Ribot JL, Oliveira R. Presence of extracellular DNA in the *candida albicans* biofilm matrix and its contribution to biofilms. *Mycopathologia*. 2010;169(5):323-31.
96. Martins M, Henriques M, Lopez-Ribot JL, Oliveira R. Addition of dnase improves the in vitro activity of antifungal drugs against *candida albicans* biofilms. *Mycoses*. 2012;55(1):80-5.
97. Nett J, Lincoln L, Marchillo K, Massey R, Holoyda K, Hoff B, VanHandel M, Andes D. Putative role of beta-1,3 glucans in *candida albicans* biofilm resistance. *Antimicrobial Agents and Chemotherapy*. 2007;51(2):510-20.
98. Xie Z, Thompson A, Sobue T, Kashleva H, Xu H, Vasilakos J, Dongari-Bagtzoglou A. *Candida albicans* biofilms do not trigger reactive oxygen species and evade neutrophil killing. *The Journal of Infectious Diseases*. 2012;206(12):1936-45.
99. Granger BL. Insight into the antiadhesive effect of yeast wall protein 1 of *candida albicans*. *Eukaryotic Cell*. 2012;11(6):795-805.
100. Granger BL, Flenniken ML, Davis DA, Mitchell AP, Cutler JE. Yeast wall protein 1 of *candida albicans*. *Microbiology*. 2005;151(Pt 5):1631-44.
101. Robbins N, Uppuluri P, Nett J, Rajendran R, Ramage G, Lopez-Ribot JL, Andes D, Cowen LE. Hsp90 governs dispersion and drug resistance of fungal biofilms. *PLOS Pathogens*. 2011;7(9):e1002257.

102. Uppuluri P, Chaturvedi AK, Srinivasan A, Banerjee M, Ramasubramaniam AK, Kohler JR, Kadosh D, Lopez-Ribot JL. Dispersion as an important step in the *candida albicans* biofilm developmental cycle. *PLOS Pathogens*. 2010;6(3):e1000828.
103. Uppuluri P, Pierce CG, Thomas DP, Bubeck SS, Saville SP, Lopez-Ribot JL. The transcriptional regulator *nrg1p* controls *candida albicans* biofilm formation and dispersion. *Eukaryotic Cell*. 2010;9(10):1531-7.
104. Thompson DS, Carlisle PL, Kadosh D. Coevolution of morphology and virulence in *candida* species. *Eukaryotic Cell*. 2011;10(9):1173-82.
105. Gow NA. Growth and guidance of the fungal hypha. *Microbiology*. 1994;140(12):3193-205.
106. Sudbery P, Gow N, Berman J. The distinct morphogenic states of *candida albicans*. *Trends in Biotechnology*. 2004;12(7):317-24.
107. Barelle CJ, Bohula EA, Kron SJ, Wessels D, Soll DR, Schafer A, Brown AJ, Gow NA. Asynchronous cell cycle and asymmetric vacuolar inheritance in true hyphae of *candida albicans*. *Eukaryotic Cell*. 2003;2(3):398-410.
108. Gow NA, Gooday GW. A model for the germ tube formation and mycelial growth form of *candida albicans*. *Sabouraudia*. 1984;22(2):137-44.
109. Yokoyama K, Takeo K. Differences of asymmetrical division between the pseudomycelial and yeast forms of *candida albicans* and their effect on multiplication. *Archives of Microbiology*. 1983;134(3):251-3.
110. Chabasse D, Bouchara JP, de Gentile L, Chennebault JM. *Candida albicans* chlamydospores observed in vivo in a patient with aids. *Annales De Biologie Clinique*. 1988;46(10):817-8.

111. Cole GT, Seshan KR, Phaneuf M, Lynn KT. Chlamyospore-like cells of *candida albicans* in the gastrointestinal tract of infected, immunocompromised mice. *Canadian Journal of Microbiology*. 1991;37(8):637-46.
112. Staib P, Morschhauser J. Chlamyospore formation in *candida albicans* and *candida dubliniensis*--an enigmatic developmental programme. *Mycoses*. 2007;50(1):1-12.
113. Jong AY, Stins MF, Huang SH, Chen SH, Kim KS. Traversal of *candida albicans* across human blood-brain barrier in vitro. *Infection and Immunity*. 2001;69(7):4536-44.
114. Korting HC, Hube B, Oberbauer S, Januschke E, Hamm G, Albrecht A, Borelli C, Schaller M. Reduced expression of the hyphal-independent *candida albicans* proteinase genes *sap1* and *sap3* in the *efg1* mutant is associated with attenuated virulence during infection of oral epithelium. *Journal of Medical Microbiology*. 2003;52(Pt 8):623-32.
115. Kumamoto CA, Vines MD. Contributions of hyphae and hypha-co-regulated genes to *candida albicans* virulence. *Cellular Microbiology*. 2005;7(11):1546-54.
116. Gonzalez-Novo A, Correa-Bordes J, Labrador L, Sanchez M, Vazquez de Aldana CR, Jimenez J. Sep7 is essential to modify septin ring dynamics and inhibit cell separation during *candida albicans* hyphal growth. *Molecular Biology of the Cell*. 2008;19(4):1509-18.
117. Sinha I, Wang YM, Philp R, Li CR, Yap WH, Wang Y. Cyclin-dependent kinases control septin phosphorylation in *candida albicans* hyphal development. *Developmental Cell*. 2007;13(3):421-32.
118. Wang A, Raniga PP, Lane S, Lu Y, Liu H. Hyphal chain formation in *candida albicans*: Cdc28-hgc1 phosphorylation of *efg1* represses cell separation genes. *Molecular Biology of the Cell*. 2009;29(16):4406-16.

119. Wang Y. Cdks and the yeast-hyphal decision. *Current Opinion in Microbiology*. 2009;12(6):644-9.
120. Zheng XD, Lee RT, Wang YM, Lin QS, Wang Y. Phosphorylation of rga2, a cdc42 gap, by cdk/hgc1 is crucial for *candida albicans* hyphal growth. *The EMBO Journal*. 2007;26(16):3760-9.
121. Carlisle PL, Banerjee M, Lazzell A, Monteagudo C, Lopez-Ribot JL, Kadosh D. Expression levels of a filament-specific transcriptional regulator are sufficient to determine *candida albicans* morphology and virulence. *Proceedings of the National Academy of Sciences*. 2009;106(2):599-604.
122. Bendaoud M, Vinogradov E, Balashova NV, Kadouri DE, Kachlany SC, Kaplan JB. Broad-spectrum biofilm inhibition by *kingella kingae* exopolysaccharide. *Journal of Bacteriology*. 2011;193(15):3879-86.
123. Mottola C, Seixas R, Tavares L, Oliveira M. Bacterial biofilms: Impact on aquatic ecosystems. *Perspectives in animal ecology and reproduction*. 2015; 1-11.
124. Lee JW, Nam JH, Kim YH, Lee KH, Lee DH. Bacterial communities in the initial stage of marine biofilm formation on artificial surfaces. *The Journal of Microbiology*. 2008;46(2):174-82.
125. Dongari-Bagtzoglou A. Pathogenesis of mucosal biofilm infections: Challenges and progress. *Expert Review of Anti-Infective Therapy*. 2008;6(2):201-8.
126. Post JC, Hiller NL, Nistico L, Stoodley P, Ehrlich GD. The role of biofilms in otolaryngologic infections: Update 2007. *Current Opinion in Otolaryngology & Head and Neck Surgery*. 2007;15(5):347-51.

127. Post JC, Stoodley P, Hall-Stoodley L, Ehrlich GD. The role of biofilms in otolaryngologic infections. *Current Opinion in Otolaryngology & Head and Neck Surgery*. 2004;12(3):185-90.
128. Singh PK, Parsek MR, Greenberg EP, Welsh MJ. A component of innate immunity prevents bacterial biofilm development. *Nature*. 2002;417(6888):552-5.
129. Chole RA, Faddis BT. Evidence for microbial biofilms in cholesteatomas. *Archives of Otolaryngology Head and Neck Surgery*. 2002;128(10):1129-33.
130. Coticchia J, Zuliani G, Coleman C, Carron M, Gurrola J, Hauptert M, Berk R. Biofilm surface area in the pediatric nasopharynx: Chronic rhinosinusitis vs obstructive sleep apnea. *Archives of Otolaryngology Head and Neck Surgery*. 2007;133(2):110-4.
131. Domingue PA, Sadhu K, Costerton JW, Bartlett K, Chow AW. The human vagina: Normal flora considered as an in situ tissue-associated, adherent biofilm. *Genitourinary Medicine*. 1991;67(3):226-31.
132. Jansen AM, Lockatell V, Johnson DE, Mobley HL. Mannose-resistant proteus-like fimbriae are produced by most proteus mirabilis strains infecting the urinary tract, dictate the in vivo localization of bacteria, and contribute to biofilm formation. *Infection and Immunity*. 2004;72(12):7294-305.
133. Mladina R, Poje G, Vukovic K, Ristic M, Music S. Biofilm in nasal polyps. *Rhinology*. 2008;46(4):302-7.
134. Donlan RM, Costerton JW. Biofilms: Survival mechanisms of clinically relevant microorganisms. *Clinical Microbiology Reviews*. 2002;15(2):167-93.
135. Braunwald E. Valvular heart disease. *Heart disease*. 1997; 1007-76.

136. Illingworth BL, Tweden K, Schroeder RE, Cameron JD. In vivo efficacy of silver-coated (silzone (tm)) infection-resistant polyester fabric against a biofilm-producing bacteria, *staphylococcus epidermidis*. *Journal of Heart Valve Disease*. 1998;7(5):524-30.
137. Karchmer AW, Gibbons GW. Infections of prosthetic heart valves and vascular grafts. *Infections associated with indwelling medical devices*. 1994; 213–49.
138. Elliott TS, Moss HA, Tebbs SE, Wilson IC, Bonser RS, Graham TR, Burke LP, Faroqui MH. Novel approach to investigate a source of microbial contamination of central venous catheters. *European Journal of Clinical Microbiology & Infectious Diseases*. 1997;16(3):210-3.
139. Raad I. Intravascular-catheter-related infections. *Lancet*. 1998;351(9106):893-8.
140. Stickler DJ, Morris NS, McLean RJ, Fuqua C. Biofilms on indwelling urethral catheters produce quorum-sensing signal molecules in situ and in vitro. *Applied and Environmental Microbiology*. 1998;64(9):3486-90.
141. Dart JKG. Contact lens and prosthesis infections. *Duane's foundations of clinical ophthalmology*. 1996; 1–30.
142. Marrie TJ, Costerton JW. A scanning and transmission electron microscopic study of the surfaces of intrauterine contraceptive devices. *American Journal of Obstetrics & Gynecology*. 1983;146(4):384-94.
143. Wolf AS, Krieger D. Bacterial colonization of intrauterine devices (iuds). *Archives of Gynecology and Obstetrics*. 1986;239(1):31-7.
144. Song F, Koo H, Ren D. Effects of material properties on bacterial adhesion and biofilm formation. *Journal of Dental Research*. 2015;94(8):1027-34.

145. Flemming HC, Wingender J. The biofilm matrix. *Nature Reviews Microbiology*. 2010;8(9):623-33.
146. Katsikogianni MG, Missirlis YF. Interactions of bacteria with specific biomaterial surface chemistries under flow conditions. *Acta Biomater*. 2010;6(3):1107-18.
147. Soni KA, Balasubramanian AK, Beskok A, Pillai SD. Zeta potential of selected bacteria in drinking water when dead, starved, or exposed to minimal and rich culture media. *Current Microbiology*. 2008;56(1):93-7.
148. Bullitt E, Makowski L. Structural polymorphism of bacterial adhesion pili. *Nature*. 1995;373(6510):164-7.
149. Pringle JH, Fletcher M. Influence of substratum wettability on attachment of freshwater bacteria to solid surfaces. *Applied and Environmental Microbiology*. 1983;45(3):811-7.
150. Carson J, Allsopp D. The enumeration of marine periphytic bacteria from a temperol sampling series. *Biodeterioration: Proceedings of the fourth international biodeterioration symposium*. 1980; 193-8.
151. Dexter SC. Influence of substratum critical surface tension on bacterial adhesion—in situ studies. *Journal of Colloid and Interface Science*. 1979;70(2):346-54.
152. Absolom DR, Lamberti FV, Policova Z, Zingg W, van Oss CJ, Neumann AW. Surface thermodynamics of bacterial adhesion. *Applied and Environmental Microbiology*. 1983;46(1):90-7.
153. Ista LK, Fan H, Baca O, Lopez GP. Attachment of bacteria to model solid surfaces: Oligo(ethylene glycol) surfaces inhibit bacterial attachment. *FEMS Microbiology Letters*. 1996;142(1):59-63.

154. Renner LD, Weibel DB. Physicochemical regulation of biofilm formation. *MRS Bulletin*. 2011;36(5):347-55.
155. Epstein AK, Wong TS, Belisle RA, Boggs EM, Aizenberg J. Liquid-infused structured surfaces with exceptional anti-biofouling performance. *Proceedings of the National Academy of Sciences*. 2012;109(33):13182-7.
156. Bosker WTE, Patzsch K, Stuart MAC, Norde W. Sweet brushes and dirty proteins. *Soft Matter*. 2007;3(6):754-62.
157. Patel JD, Ebert M, Ward R, Anderson JM. S. *Epidermidis* biofilm formation: Effects of biomaterial surface chemistry and serum proteins. *Journal of Biomedical Materials Research A*. 2007;80(3):742-51.
158. Haldar J, An D, Alvarez de Cienfuegos L, Chen J, Klibanov AM. Polymeric coatings that inactivate both influenza virus and pathogenic bacteria. *Proceedings of the National Academy of Sciences*. 2006;103(47):17667-71.
159. Wong SY, Li Q, Veselinovic J, Kim BS, Klibanov AM, Hammond PT. Bactericidal and virucidal ultrathin films assembled layer by layer from polycationic n-alkylated polyethylenimines and polyanions. *Biomaterials*. 2010;31(14):4079-87.
160. Cheng G, Xue H, Zhang Z, Chen S, Jiang S. A switchable biocompatible polymer surface with self-sterilizing and nonfouling capabilities. *Angewandte Chemie International Edition in English*. 2008;47(46):8831-4.
161. Denkhaus E, Meisen S, Telgheder U, Wingender J. Chemical and physical methods for characterisation of biofilms. *Microchimica Acta*. 2007;158(1-2):1-27.
162. Beyenal H, Donovan C, Lewandowski Z, Harkin G. Three-dimensional biofilm structure quantification. *Journal of Microbiological Methods*. 2004;59(3):395-413.

163. Mueller LN, de Brouwer JF, Almeida JS, Stal LJ, Xavier JB. Analysis of a marine phototrophic biofilm by confocal laser scanning microscopy using the new image quantification software phlip. *BMC Ecolgy*. 2006;6:1.
164. Neu TR, Woelfl S, Lawrence JR. Three-dimensional differentiation of photoautotrophic biofilm constituents by multi-channel laser scanning microscopy (single-photon and two-photon excitation). *Journal of Microbiological Methods*. 2004;56(2):161-72.
165. Strathmann M, Wingender J, Flemming HC. Application of fluorescently labelled lectins for the visualization and biochemical characterization of polysaccharides in biofilms of *pseudomonas aeruginosa*. *Journal of Microbiological Methods*. 2002;50(3):237-48.
166. Cortizo MC, de Mele MFL. Microstructural characteristics of thin biofilms through optical and scanning electron microscopy. *World Journal of Microbiology & Biotechnology*. 2003;19(8):805-10.
167. Hansma HG, Pietrasanta LI, Auerbach ID, Sorenson C, Golan R, Holden PA. Probing biopolymers with the atomic force microscope: A review. *Journal of Biomaterials Science, Polymer Edition*. 2000;11(7):675-83.
168. Lawrence JR, Swerhone GD, Leppard GG, Araki T, Zhang X, West MM, Hitchcock AP. Scanning transmission x-ray, laser scanning, and transmission electron microscopy mapping of the exopolymeric matrix of microbial biofilms. *Applied and Environmental Microbiology*. 2003;69(9):5543-54.
169. Lattner D, Flemming HC, Mayer C. ¹³c-nmr study of the interaction of bacterial alginate with bivalent cations. *International Journal of Biological Macromolecules*. 2003;33(1-3):81-8.

170. Mayer C, Lattner D, Schurks N. ¹³C nuclear magnetic resonance studies on selectively labeled bacterial biofilms. *Journal of Industrial Microbiology and Biotechnology*. 2001;26(1/2):62-9.
171. Schurks N, Wingender J, Flemming HC, Mayer C. Monomer composition and sequence of alginates from *pseudomonas aeruginosa*. *International Journal of Biological Macromolecules*. 2002;30(2):105-11.
172. Majors PD, McLean JS, Pinchuk GE, Fredrickson JK, Gorby YA, Minard KR, Wind RA. Nmr methods for in situ biofilm metabolism studies. *Journal of Microbiological Methods*. 2005;62(3):337-44.
173. Reschiglian P, Zattoni A, Roda B, Michelini E, Roda A. Field-flow fractionation and biotechnology. *Trends in Biotechnology*. 2005;23(9):475-83.
174. Aoi Y. In situ identification of microorganisms in biofilm communities. *Journal of Bioscience and Bioengineering*. 2002;94(6):552-6.
175. Lay JO, Jr. Maldi-tof mass spectrometry of bacteria. *Mass Spectrometry Reviews*. 2001;20(4):172-94.
176. Meays CL, Broersma K, Nordin R, Mazumder A. Source tracking fecal bacteria in water: A critical review of current methods. *Journal of Environmental Management*. 2004;73(1):71-9.
177. Wuertz S, Okabe S, Hausner M. Microbial communities and their interactions in biofilm systems: An overview. *Water Science & Technology*. 2004;49(11-12):327-36.
178. Boyce JD, Cullen PA, Adler B. Genomic-scale analysis of bacterial gene and protein expression in the host. *Emerging Infectious Diseases*. 2004;10(8):1357-62.

179. Lahm HW, Langen H. Mass spectrometry: A tool for the identification of proteins separated by gels. *Electrophoresis*. 2000;21(11):2105-14.
180. Ram RJ, Verberkmoes NC, Thelen MP, Tyson GW, Baker BJ, Blake RC, Shah M, Hettich RL, Banfield JF. Community proteomics of a natural microbial biofilm. *Science*. 2005;308(5730):1915-20.
181. Boualam M, Mathieu L, Fass S, Cavard J, Gatel D. Relationship between coliform culturability and organic matter in low nutritive waters. *Water Research*. 2002;36(10):2618-26.
182. Choo-Smith LP, Maquelin K, van Vreeswijk T, Bruining HA, Puppels GJ, Ngo Thi NA, Kirschner C, Naumann D, Ami D, Villa AM, Orsini F, Doglia SM, Lamfarraj H, Sockalingum GD, Manfait M, Allouch P, Endtz HP. Investigating microbial (micro)colony heterogeneity by vibrational spectroscopy. *Applied and Environmental Microbiology*. 2001;67(4):1461-9.
183. Suci PA, Siedlecki KJ, Palmer RJ, White DC, Geesey GG. Combined light microscopy and attenuated total reflection fourier transform infrared spectroscopy for integration of biofilm structure, distribution, and chemistry at solid-liquid interfaces. *Applied and Environmental Microbiology*. 1997;63(11):4600-3.
184. Venkata HNN, Nomura N, Shigeto S. Leucine pools in *escherichia coli* biofilm discovered by Raman imaging. *Journal of Raman Spectroscopy*. 2011;42(11):1913-5.
185. Chao Y, Zhang T. Surface-enhanced raman scattering (sers) revealing chemical variation during biofilm formation: From initial attachment to mature biofilm. *Analytical and Bioanalytical Chemistry*. 2012;404(5):1465-75.
186. Efeoglu E, Culha M. In situ-monitoring of biofilm formation by using surface-enhanced Raman scattering. *Applied Spectroscopy*. 2013;67(5):498-505.

187. Ivleva NP, Wagner M, Horn H, Niessner R, Haisch C. In situ surface-enhanced Raman scattering analysis of biofilm. *Analytical Chemistry*. 2008;80(22):8538-44.
188. Kelestemur S, Culha M. Understanding and discrimination of biofilms of clinically relevant microorganisms using surface-enhanced Raman scattering. *Applied Spectroscopy*. 2017;71(6):1180-8.
189. Pearman WF, Lawrence-Snyder M, Angel SM, Decho AW. Surface-enhanced Raman spectroscopy for in situ measurements of signaling molecules (autoinducers) relevant to bacteria quorum sensing. *Applied Spectroscopy*. 2007;61(12):1295-300.
190. Nakamoto K. *Infrared and raman spectra of inorganic and coordination compounds, fifth edition, part a*. New York: John Wiley & Sons Inc; 1997.
191. Herzberg G. *Molecular spectra and molecular structure: Ii, infrared and Raman spectra of polyatomic molecules*. New York: Van Nostrand Reinhold; 1945.
192. Nakamoto K. *Infrared and raman spectra of inorganic and coordination compounds, fifth edition, part b*. New York: John Wiley & Sons Inc; 1997.
193. Stuart B. *Infrared spectroscopy: Fundamentals and applications*. USA: John Wiley & Sons, Ltd; 2004.
194. Smith ED, G. *Modern raman spectroscopy – a practical approach*. England: John Wiley & Sons Ltd; 2005.
195. Skoog DA, Leary JJ. *Principles of instrumental analysis*. Fort Worth: Saunders College Pub; 1992.
196. Smekal. A. The quantum theory of dispersion. *Naturwissenschaften*. 1923;11:873.

197. Landsberg G, Mandelstam L. A novel effect of light scattering in crystals. *Naturwissenschaften*. 1928;16:557–8.
198. Raman CV, Krishnan KS. A new type of secondary radiation. *Nature*. 1928;121:501-2.
199. Ferraro JR, Nakamoto K, Brown CW. *Introductory Raman spectroscopy USA*: Elsevier; 2003.
200. Catherine EH, Alan GS. *Inorganic chemistry*. England: Pearson; 2008.
201. Nivaldo JT. *Chemistry a molecular approach custom edition*. U.S.A: Pearson; 2008.
202. Albrecht MG, Creighton JA. Anomalously intense Raman spectra of pyridine at a silver electrode. *Journal of the American Chemical Society*. 1977;99:5215-7.
203. Jeanmaire DL, Duyn RPV. Surface Raman spectroelectrochemistry part I. Heterocyclic, aromatic, and aliphatic amines adsorbed on the anodized silver electrode. *Journal of Electroanalytical Chemistry*. 1977;84(1):1-20.
204. Shafer-Peltier KE, Haynes CL, Glucksberg MR, Van Duyne RP. Toward a glucose biosensor based on surface-enhanced Raman scattering. *Journal of the American Chemical Society*. 2003;125(2):588-93.
205. Yonzon CR, Haynes CL, Zhang X, Walsh JT, Jr., Van Duyne RP. A glucose biosensor based on surface-enhanced Raman scattering: Improved partition layer, temporal stability, reversibility, and resistance to serum protein interference. *Analytical Chemistry*. 2004;76(1):78-85.
206. Fleischmann M, Hendra PJ, Mcquillan AJ. Raman spectra of pyridine adsorbed at a silver electrode. *Chemical Physics Letters*. 1974;26:163-6.

207. Duyne RPV. Applications of Raman spectroscopy in electrochemistry. *Le Journal de Physique Colloques*. 1977;38:239-52.
208. Duyne VRP. *Laser excitation of Raman scattering from adsorbed molecules on electrode surfaces*. New York: Academic Press; 1979.
209. Vo-Dinh T, Wang HN, Scaffidi J. Plasmonic nanoprobe for SERS biosensing and bioimaging. *Journal of Biophotonics*. 2010;3(1-2):89-102.
210. Moskovits M. Surface roughness and the enhanced intensity of Raman scattering by molecules adsorbed on metals. *The Journal of Chemical Physics*. 1978;69:4159.
211. Maier SAA, H. A. Plasmonics: Localization and guiding of electromagnetic energy in metal/dielectric structures. *Journal of Applied Physics*. 2005;98(1):10.
212. Haes AJ, Haynes CL, McFarland AD, Schatz GC, Van Duyne RR, Zou SL. Plasmonic materials for surface-enhanced sensing and spectroscopy. *MRS Bulletin*. 2005;30(5):368-75.
213. Lu XM, Rycenga M, Skrabalak SE, Wiley B, Xia YN. Chemical synthesis of novel plasmonic nanoparticles. *Annual Review of Physical Chemistry*. 2009;60:167-92.
214. Rycenga M, Cobley CM, Zeng J, Li W, Moran CH, Zhang Q, Qin D, Xia Y. Controlling the synthesis and assembly of silver nanostructures for plasmonic applications. *Chemical Reviews*. 2011;111(6):3669-712.
215. Radziuk D, Moehwald H. Prospects for plasmonic hot spots in single molecule SERS towards the chemical imaging of live cells. *Phys Chem Chem Phys*. 2015;17(33):21072-93.

216. Kolesov R, Grotz B, Balasubramanian G, Stohr RJ, Nicolet AAL, Hemmer PR, Jelezko F, Wrachtrup J. Wave-particle duality of single surface plasmon polaritons. *Nature Physics*. 2009;5(7):470-4.
217. Fan JA, Wu CH, Bao K, Bao JM, Bardhan R, Halas NJ, Manoharan VN, Nordlander P, Shvets G, Capasso F. Self-assembled plasmonic nanoparticle clusters. *Science*. 2010;328(5982):1135-8.
218. Prodan E, Radloff C, Halas NJ, Nordlander P. A hybridization model for the plasmon response of complex nanostructures. *Science*. 2003;302(5644):419-22.
219. Wiley B, Sun Y, Xia Y. Synthesis of silver nanostructures with controlled shapes and properties. *Accounts of Chemical Research*. 2007;40(10):1067-76.
220. Ru EL, Etchegoin P. *Principles of surface enhanced Raman spectroscopy*. Oxford: Elsevier; 2009.
221. Hao E, Schatz GC. Electromagnetic fields around silver nanoparticles and dimers. *Journal of Chemical Physics*. 2004;120(1):357-66.
222. Kelly KL, Coronado E, Zhao LL, Schatz GC. The optical properties of metal nanoparticles: The influence of size, shape, and dielectric environment. *Journal of Physical Chemistry B*. 2003;107(3):668-77.
223. Chung T, Lee SY, Song EY, Chun H, Lee B. Plasmonic nanostructures for nano-scale bio-sensing. *Sensors*. 2011;11(11):10907-29.
224. Picorel R, Holt RE, Cotton TM, Seibert M. Surface-enhanced resonance Raman scattering spectroscopy of bacterial photosynthetic membranes. The carotenoid of *rhodospirillum rubrum*. *The Journal of Biological Chemistry*. 1988;263(9):4374-80.

225. Efrima S, Bronk BV. Silver colloids impregnating or coating bacteria. *The Journal of Physical Chemistry B*. 1998;102(31):5947-50.
226. Zeiri L, Bronk BV. Physicochemical. And engineering aspects silver metal. Induced surface enhanced raman of bacteria. *Colloids and Surfaces A*. 2002;208:357-62.
227. Zeiri L, Efrima S. Surface-enhanced Raman spectroscopy of bacteria: The effect of excitation wavelength and chemical. Modification of the colloidal. Milieu. *Journal of Raman Spectroscopy*. 2005;36:667-75.
228. Premasiri WR, Moir DT, Klempner MS, Krieger N, Jones G, Ziegler LD. Characterization of the surface enhanced Raman scattering (SERS) of bacteria. *The Journal of Physical Chemistry B*. 2005;109(1):312-20.
229. Sengupta A, Mujacic M, Davis EJ. Detection of bacteria by surface-enhanced Raman spectroscopy. *Analytical and Bioanalytical Chemistry*. 2006;386(5):1379-86.
230. Kahraman M, Yazici MM, Sahin F, Bayrak OF, Culha M. Reproducible surface-enhanced Raman scattering spectra of bacteria on aggregated silver nanoparticles. *Applied Spectroscopy*. 2007;61(5):479-85.
231. Kahraman M, Yazici MM, Sahin F, Culha M. Convective assembly of bacteria for surface-enhanced Raman scattering. *Langmuir*. 2008;24(3):894-901.
232. Kahraman M, Zamaleeva AI, Fakhrullin RF, Culha M. Layer-by-layer coating of bacteria with noble metal nanoparticles for surface-enhanced Raman scattering. *Analytical and Bioanalytical Chemistry*. 2009;395(8):2559-67.
233. Cheng WT, Liu MT, Liu HN, Lin SY. Micro-Raman spectroscopy used to identify and grade human skin pilomatrixoma. *Microscopy Research and Technique*. 2005;68(2):75-9.

234. Ivleva NP, Wagner M, Horn H, Niessner R, Haisch C. Raman microscopy and surface-enhanced Raman scattering (SERS) for in situ analysis of biofilms. *Journal of Biophotonics*. 2010;3(8-9):548-56.
235. Ivleva NP, Wagner M, Szkola A, Horn H, Niessner R, Haisch C. Label-free in situ SERS imaging of biofilms. *The Journal of Physical Chemistry B*. 2010;114(31):10184-94.
236. Jarvis RM, Brooker A, Goodacre R. Surface-enhanced Raman spectroscopy for bacterial discrimination utilizing a scanning electron microscope with a Raman spectroscopy interface. *Analytical Chemistry*. 2004;76(17):5198-202.
237. Jarvis RM, Goodacre R. Characterisation and identification of bacteria using SERS. *Chemical Society Reviews*. 2008;37(5):931-6.
238. Maquelin K, Kirschner C, Choo-Smith LP, van den Braak N, Endtz HP, Naumann D, Puppels GJ. Identification of medically relevant microorganisms by vibrational spectroscopy. *Journal of Microbiological Methods*. 2002;51(3):255-71.
239. Shanmukh S, Jones L, Zhao YP, Driskell JD, Tripp RA, Dluhy RA. Identification and classification of respiratory syncytial virus (rsv) strains by surface-enhanced Raman spectroscopy and multivariate statistical techniques. *Analytical and Bioanalytical Chemistry*. 2008;390(6):1551-5.
240. Jarvis RM, Law N, Shadi IT, O'Brien P, Lloyd JR, Goodacre R. Surface-enhanced Raman scattering from intracellular and extracellular bacterial locations. *Analytical Chemistry*. 2008;80(17):6741-6.
241. Kahraman M, Keseroglu K, Culha M. On sample preparation for surface-enhanced Raman scattering (SERS) of bacteria and the source of spectral features of the spectra. *Applied Spectroscopy*. 2011;65(5):500-6.

242. Premasiri WR, Lee JC, Sauer-Budge A, Theberge R, Costello CE, Ziegler LD. The biochemical origins of the surface-enhanced Raman spectra of bacteria: A metabolomics profiling by sers. *Analytical and Bioanalytical Chemistry*. 2016;408(17):4631-47.
243. Ramya S, George RP, Rao RVS, Dayal RK. Detection of algae and bacterial biofilms formed on titanium surfaces using micro-Raman analysis. *Applied Surface Science*. 2010;256(16):5108-15.
244. Masyuko RN, Lanni EJ, Driscoll CM, Shrout JD, Sweedler JV, Bohn PW. Spatial organization of *pseudomonas aeruginosa* biofilms probed by combined matrix-assisted laser desorption ionization mass spectrometry and confocal Raman microscopy. *Analyst*. 2014;139(22):5700-8.
245. Efeoglu E, Culha M. Surface-enhanced Raman scattering for biofilm characterization. *Spectroscopy*. 2013;28(11):36-41.
246. Chen PY, Cui L, Zhang KS. Surface-enhanced Raman spectroscopy monitoring the development of dual-species biofouling on membrane surfaces. *Journal of Membrane Science*. 2015;473:36-44.
247. Bodelon G, Montes-Garcia V, Lopez-Puente V, Hill EH, Hamon C, Sanz-Ortiz MN, Rodal-Cedeira S, Costas C, Celiksoy S, Perez-Juste I, Scarabelli L, La Porta A, Perez-Juste J, Pastoriza-Santos I, Liz-Marzan LM. Detection and imaging of quorum sensing in *pseudomonas aeruginosa* biofilm communities by surface-enhanced resonance Raman scattering. *Nature Materials*. 2016;15(11):1203-11.
248. Poliseti S, Baig NF, Morales-Soto N, Shrout JD, Bohn PW. Spatial mapping of pyocyanin in *pseudomonas aeruginosa* bacterial communities using surface enhanced Raman scattering. *Applied Spectroscopy*. 2017;71(2):215-23.
249. Lee PC, Meisel D. Adsorption and surface-enhanced Raman of dyes on silver and gold sols. *Journal of Physical Chemistry*. 1982;86(17):3391-5.

250. Wu X, Chen J, Li X, Zhao Y, Zughaier SM. Culture-free diagnostics of *pseudomonas aeruginosa* infection by silver nanorod array based SERS from clinical sputum samples. *Nanomedicine*. 2014;10(8):1863-70.
251. Jarvis RM, Brooker A, Goodacre R. Surface-enhanced Raman scattering for the rapid discrimination of bacteria. *Faraday Discussions*. 2006;132:281-92.
252. Kneipp K, Kneipp H, Itzkan I, Dasari RR, Feld MS. Surface-enhanced Raman scattering and biophysics. *Journal of Physics-Condensed Matter*. 2002;14(18):R597-R624.
253. Movasaghi Z, Rehman S, Rehman IU. Raman spectroscopy of biological tissues. *Applied Spectroscopy Reviews*. 2007;42(5):493-541.
254. Neugebauer U, Schmid U, Baumann K, Ziebuhr W, Kozitskaya S, Deckert V, Schmitt M, Popp J. Towards a detailed understanding of bacterial metabolism - spectroscopic characterization of *staphylococcus epidermidis*. *Chemphyschem*. 2007;8(1):124-37.
255. Notingher I, Verrier S, Haque S, Polak JM, Hench LL. Spectroscopic study of human lung epithelial cells (A549) in culture: Living cells versus dead cells. *Biopolymers*. 2003;72(4):230-40.
256. Harz M, Rosch P, Peschke KD, Ronneberger O, Burkhardt H, Popp J. Micro-Raman spectroscopic identification of bacterial cells of the genus *staphylococcus* and dependence on their cultivation conditions. *Analyst*. 2005;130(11):1543-50.
257. Schkolnik G, Schmidt M, Mazza MG, Harnisch F, Musat N. In situ analysis of a silver nanoparticle-precipitating *shewanella* biofilm by surface enhanced confocal Raman microscopy. *PLoS One*. 2015;10(12).

258. Carey PR, Gibson BR, Gibson JF, Greenberg ME, Heidari-Torkabadi H, Pusztai-Carey M, Weaver ST, Whitmer GR. Defining molecular details of the chemistry of biofilm formation by Raman microspectroscopy. *Biochemistry*. 2017;56(17):2247-50.
259. Malini R, Venkatakrishna K, Kurien J, Pai KM, Rao L, Kartha VB, Krishna CM. Discrimination of normal, inflammatory, premalignant, and malignant oral tissue: A Raman spectroscopy study. *Biopolymers*. 2006;81(3):179-93.
260. Binoy J, Abraham JP, Joe IH, Jayakumar VS, Pettit GR, Nielsen OF. NIR-FT Raman and FT-IR spectral studies and ab initio calculations of the anti-cancer drug combretastatin-a4. *Journal of Raman Spectroscopy*. 2004;35(11):939-46.
261. Laucks ML, Sengupta A, Junge K, Davis EJ, Swanson BD. Comparison of psychro-active arctic marine bacteria and common mesophilic bacteria using surface-enhanced Raman spectroscopy. *Applied Spectroscopy*. 2005;59(10):1222-8.
262. Sandt C, Smith-Palmer T, Pink J, Brennan L, Pink D. Confocal Raman microspectroscopy as a tool for studying the chemical heterogeneities of biofilms in situ. *Journal of Applied Microbiology*. 2007;103(5):1808-20.
263. Pelton JT, McLean LR. Spectroscopic methods for analysis of protein secondary structure. *Analytical Biochemistry*. 2000;277(2):167-76.
264. Schmid T, Messmer A, Yeo BS, Zhang WH, Zenobi R. Towards chemical analysis of nanostructures in biofilms ii: Tip-enhanced Raman spectroscopy of alginates. *Analytical and Bioanalytical Chemistry*. 2008;391(5):1907-16.
265. Kives J, Orgaz B, SanJose C. Polysaccharide differences between planktonic and biofilm-associated EPS from *pseudomonas fluorescens* b52. *Colloids and Surfaces B-Biointerfaces*. 2006;52(2):123-7.

266. Coulon C, Vinogradov E, Filloux A, Sadovskaya I. Chemical analysis of cellular and extracellular carbohydrates of a biofilm-forming strain *pseudomonas aeruginosa* pa14. *PLoS One*. 2010;5(12).
267. Southey-Pillig CJ, Davies DG, Sauer K. Characterization of temporal protein production in *pseudomonas aeruginosa* biofilms. *Journal of Bacteriology*. 2005;187(23):8114-26.
268. Decker R, Burdelski C, Zobiak M, Buttner H, Franke G, Christner M, Sass K, Zobiak B, Henke HA, Horswill AR, Bischoff M, Bur S, Hartmann T, Schaeffer CR, Fey PD, Rohde H. An 18 kda scaffold protein is critical for *staphylococcus epidermidis* biofilm formation. *PLOS Pathogens*. 2015;11(3):e1004735.
269. Ramage G, Vandewalle K, Wickes BL, Lopez-Ribot JL. Characteristics of biofilm formation by *candida albicans*. *Revista Iberoamericana de Micología*. 2001;18(4):163-70.
270. Balan SS, Nethaji R, Sankar S, Jayalakshmi S. Production of gelatinase enzyme from bacillus spp isolated from the sediment sample of porto novo coastal sites. *Asian Pacific Journal of Tropical Biomedicine*. 2012:1811-6.
271. Costerton JW, Stewart PS, Greenberg EP. Bacterial biofilms: A common cause of persistent infections. *Science*. 1999;284(5418):1318-22.
272. Adam B, Baillie GS, Douglas LJ. Mixed species biofilms of *candida albicans* and *staphylococcus epidermidis*. *Journal of Medical Microbiology*. 2002;51(4):344-9.
273. Bandara HM, Yau JY, Watt RM, Jin LJ, Samaranayake LP. *Pseudomonas aeruginosa* inhibits in-vitro *candida* biofilm development. *BMC Microbiology*. 2010;10:125.
274. Hogan DA, Kolter R. *Pseudomonas-candida* interactions: An ecological role for virulence factors. *Science*. 2002;296(5576):2229-32.

275. Kerr JR. Suppression of fungal growth exhibited by *pseudomonas aeruginosa*. *Journal of Clinical Microbiology*. 1994;32(2):525-7.
276. Nseir S, Jozefowicz E, Cavestri B, Sendid B, Di Pompeo C, Dewavrin F, Favory R, Roussel-Delvallez M, Durocher A. Impact of antifungal treatment on *candida-pseudomonas* interaction: A preliminary retrospective case-control study. *Intensive Care Medicine*. 2007;33(1):137-42.
277. Thein ZM, Samaranayake YH, Samaranayake LP. Effect of oral bacteria on growth and survival of *candida albicans* biofilms. *Archives of Oral Biology*. 2006;51(8):672-80.
278. Federle MJ, Bassler BL. Interspecies communication in bacteria. *The Journal of Clinical Investigation*. 2003;112(9):1291-9.
279. Wu X, Liu Y, Li X, Wen P, Zhang Y, Kong Y, Wang X, Guo Y, Xing F, Gao J. Preparation of aligned porous gelatin scaffolds by unidirectional freeze-drying method. *Acta Biomaterialia*. 2010;6:1167-77.